VOLUME 36 FEBRUARY 1958 NUMBER 2

Canadian Journal of Physics

Editor: H. E. DUCKWORTH

Associate Editors:

L. G. ELLIOTT, *Atomic Energy of Canada, Ltd., Chalk River*
J. S. FOSTER, *McGill University*
G. HERZBERG, *National Research Council of Canada*
L. LEPRINCE-RINGUET, *Ecole Polytechnique, Paris*
B. W. SARGENT, *Queen's University*
G. M. VOLKOFF, *University of British Columbia*
W. H. WATSON, *University of Toronto*
G. A. WOONTON, *McGill University*

Published by THE NATIONAL RESEARCH COUNCIL

OTTAWA CANADA

CANADIAN JOURNAL OF PHYSICS

(*Formerly Section A, Canadian Journal of Research*)

Under the authority of the Chairman of the Committee of the Privy Council on Scientific and Industrial Research, the National Research Council issues THE CANADIAN JOURNAL OF PHYSICS and five other journals devoted to the publication, in English or French, of the results of original scientific research. Matters of general policy concerning these journals are the responsibility of a joint Editorial Board consisting of: members representing the National Research Council of Canada; the Editors of the Journals; and members representing the Royal Society of Canada and four other scientific societies.

EDITORIAL BOARD

Representatives of the National Research Council

R. B. Miller, *University of Alberta*
H. G. Thode, *McMaster University*
D. L. Thomson, *McGill University*
W. H. Watson (Chairman), *University of Toronto*

Editors of the Journals

D. L. Bailey, *University of Toronto*
T. W. M. Cameron, *Macdonald College*
H. E. Duckworth, *McMaster University*
K. A. C. Elliott, *Montreal Neurological Institute*
Léo Marion, *National Research Council*
R. G. E. Murray, *University of Western Ontario*

Representatives of Societies

D. L. Bailey, *University of Toronto*
Royal Society of Canada
T. W. M. Cameron, *Macdonald College*
Royal Society of Canada
H. E. Duckworth, *McMaster University*
Royal Society of Canada
Canadian Association of Physicists
K. A. C. Elliott, *Montreal Neurological Institute*
Canadian Physiological Society
R. G. E. Murray, *University of Western Ontario*
Canadian Society of Microbiologists
H. G. Thode, *McMaster University*
Chemical Institute of Canada
T. Thorvaldson, *University of Saskatchewan*
Royal Society of Canada

Ex officio

Léo Marion (Editor-in-Chief), *National Research Council*
J. B. Marshall (Administration and Awards), *National Research Council*

Manuscripts for publication should be submitted to Dr. H. E. Duckworth, Editor, Canadian Journal of Physics, Hamilton College, McMaster University, Hamilton, Ontario.

(For instructions on preparation of copy, see **Notes to Contributors** (inside back cover).)

Proof, correspondence concerning proof, and orders for reprints should be sent to the Manager, Editorial Office (Research Journals), Division of Administration and Awards, National Research Council, Ottawa 2, Canada.

Subscriptions, renewals, requests for single or back numbers, and all remittances should be sent to Division of Administration and Awards, National Research Council, Ottawa 2, Canada. Remittances should be made payable to the Receiver General of Canada, credit National Research Council.

The journals published, frequency of publication, and prices are:

Canadian Journal of Biochemistry and Physiology	Monthly	$3.00 a year
Canadian Journal of Botany	Bimonthly	$4.00 a year
Canadian Journal of Chemistry	Monthly	$5.00 a year
Canadian Journal of Microbiology	Bimonthly	$3.00 a year
Canadian Journal of Physics	Monthly	$4.00 a year
Canadian Journal of Zoology	Bimonthly	$3.00 a year

The price of regular single numbers of all journals is 75 cents.

Canadian Journal of Physics

Issued by THE NATIONAL RESEARCH COUNCIL OF CANADA

VOLUME 36 FEBRUARY 1958 NUMBER 2

ON POSSIBLE REALIZATIONS OF MACH'S PROGRAM[1]

F. A. KAEMPFFER

ABSTRACT

By "Mach's Program" is meant the intention to understand all inertial effects as being caused by gravitational interaction. Within the framework of a simplified theory of gravitation, based upon ideas by Hund and Sciama, it is easy to invent primitive cosmological models for which Mach's Program is realized. In particular, it is possible to understand the inertia of a linearly accelerated body as being due to radiative gravitational interaction with all other masses in the universe. If it is true that anti-matter has negative gravitational mass, as has been suggested by Morrison and Gold, then one may look upon Newton's second law as a manifestation of the preponderance of matter over anti-matter in our universe.

1. INTRODUCTION

Newton's second law is certainly one of the most obscure of all the understandable relations underlying our description of the physical world in which we find ourselves. Anyone who has ever tried to explain this law to a person who insisted on asking questions will know the difficulty of giving good reasons for the two facts embodied in it, namely, that production of an acceleration, rather than some other derivative of the position, requires a force exerted on the body to be accelerated, and that this so-called law is true only if the acceleration to be produced takes place with respect to certain mysterious coordinate systems, called "inertial frames".

It is curious that the existence of inertial frames is usually demonstrated for the kinematically more complicated case of central acceleration, like in Newton's famous rotating bucket experiment, instead of for the simple case of linear acceleration.

For later reference let us state here an experimental definition of what is meant by an inertial frame in the case of rotational motion. Suppose two observers O and O' are fixed to their respective coordinate systems S and S', which are in rotation with respect to each other around a common axis (see Fig. 1). Then the motion of O' in S can be described by angular velocity $\boldsymbol{\omega}$, position $\mathbf{r}$, and velocity $\mathbf{v} = (\boldsymbol{\omega} \times \mathbf{r})$. Elementary kinematics tells us then that

[1]Manuscript received September 20, 1957.
Contribution from the Department of Physics, The University of British Columbia, Vancouver 8, B.C.

the acceleration of O' in S consists of two terms, Coriolis acceleration $\mathbf{c} = 2(\boldsymbol{\omega}\times\mathbf{v})$ and centrifugal acceleration $\mathbf{f} = -(\boldsymbol{\omega}\times(\boldsymbol{\omega}\times\mathbf{r}))$, which add up to the central acceleration

$$\mathbf{a} = 2(\boldsymbol{\omega}\times\mathbf{v}) - (\boldsymbol{\omega}\times(\boldsymbol{\omega}\times\mathbf{r})) = (\boldsymbol{\omega}\times(\boldsymbol{\omega}\times\mathbf{r})). \tag{1}$$

Similarly, O has in S' angular velocity $\boldsymbol{\omega}' = -\boldsymbol{\omega}$, position $\mathbf{r}'$, velocity $\mathbf{v}' = (\boldsymbol{\omega}'\times\mathbf{r}') = -\mathbf{v}$, and therefore a central acceleration

$$\mathbf{a}' = (\boldsymbol{\omega}'\times(\boldsymbol{\omega}'\times\mathbf{r}')). \tag{1'}$$

The remarkable experimental fact is that there exist observers who can maintain central accelerations, as described above, without requiring any forces to do so. The coordinate system tied to such an observer will then be called an inertial frame. Only if the rotational motion of an observer takes place with respect to an inertial frame will the production of the corresponding central acceleration require a force $\mathbf{F}$ according to Newton's second law $\mathbf{F} = m\mathbf{a}$.

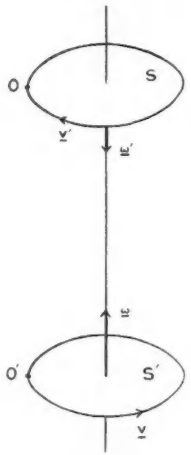

FIG. 1.

The only clue we have regarding the reason for the existence of inertial frames is the astronomical observation that all inertial frames coincide with those frames in which the observable universe as a whole appears to be in a state of unaccelerated motion. Newton himself apparently did not recognize this coincidence as a link, and it remains a psychological puzzle why so few physicists have been attracted by the almost obvious suggestion made by Berkeley and, more emphatically, by Mach, who stated clearly that the distribution of matter in the universe ought to be considered as the cause of the inertia of all bodies embedded in it.

Imagine that throughout human history our earth, by some freak of climate,

had been covered with thick clouds, so that yesterday we were without astronomical experience but in possession of the laws of mechanics, including knowledge of the disturbing and quite mysterious existence of inertial frames, which are not tied to any obviously simple state of motion on this earth. Imagine further that last night another freak of climate had dissipated for a few hours all clouds and for the first time we were seeing the stars around us. A few simple measurements, quickly done, would have revealed that the system of stars and the inertial frames coincide. It is hard not to believe that even the most soberminded of witnesses would have agreed that here might be a possibility to at last understand what so far had to be accepted as one of those facts.

Faced thus with the suggestion of a causal relationship between the universal distribution of matter and the inertia of a body immersed in it, one is led to search for an interaction that may be made responsible for this conjectured state of affairs. Since gravitation is apparently the only interaction that indiscriminately affects all bodies having inertia, regardless of whether the bodies have or have not additional properties like mesonic charge, electric charge, Fermi charge, etc., it is extremely tempting to adopt and to attempt a realization of Mach's Program. Adopting Mach's Program means to declare one's intention to understand all inertial effects in terms of the gravitational interaction between the masses in the universe and the body that exhibits inertia. Realizing Mach's Program means to derive Newton's second law from a suitable theory of gravitation.

2. THEORY OF GRAVITATION

It has been known for a long time that the very existence of Coriolis and centrifugal forces cannot be understood from the point of view of Mach's Program within the framework of a scalar field theory of gravitation, and it was precisely this insufficiency of Newton's theory of gravitation that was one of the motivations for Einstein's attempt to describe gravitation in terms of a tensor field. Unfortunately, it turned out that the various versions of Einstein's theory do not by themselves constitute realizations of Mach's Program, and it seems that to date not even any special cosmological model has been found, formulated in terms of general relativity theory, that fully realizes this program (see Bondi 1952).

Therefore, for the present discussion, let us cast aside all those cosmological models that require Riemann geometry, and let us simplify the description of the probably rather complicated phenomenon of gravitation, by devising a vector field theory analogous to electromagnetic theory, which combines ideas due to Hund (1948) and Sciama (1953, 1957) with a formal procedure by Gupta (1954), and which enables one to demonstrate how Mach's Program may be realized in principle within primitive Euclidean models of the universe.

In analogy to the electromagnetic field, described by a polar electric vector $\mathbf{E}$ and an axial magnetic vector $\mathbf{H}$, which act upon any charge e with the force

$$\mathbf{F} = e[\mathbf{E}+(1/c)(\mathbf{v}\times\mathbf{H})],$$

it will now be assumed that it is possible to describe the gravitational field in

terms of a polar vector $\mathbf{f}$ and an axial vector $\mathbf{g}$, which act upon any gravitational mass m with the force

$$\mathbf{F} = m[\mathbf{f}+(1/c)(\mathbf{v}\times\mathbf{g})]. \tag{2}$$

The fields $\mathbf{f}$ and $\mathbf{g}$ are supposed to be produced by gravitating masses and currents, analogous to the production of the fields $\mathbf{E}$ and $\mathbf{H}$ by electric charges and currents, but with the important additional requirement that all forms of energy, including the field energy of $\mathbf{f}$ and $\mathbf{g}$ itself, are considered as sources of gravitation. This means that those terms in the field equations which correspond to the source terms in Maxwell's equations are from the outset to be considered as functions of the fields $\mathbf{f}$ and $\mathbf{g}$ themselves, and it becomes necessary to use a description by successive approximations, similar to the method employed by Gupta (1954).

It is clear that in zero approximation, i.e. if one neglects both the effects of $\mathbf{g}$ and the gravitational effect of the field energy itself, the description must revert to Newton's theory of gravitation, where there is just a polar vector $\mathbf{f}^{(0)}$ which satisfies for given gravitational mass density ρ the equation

$$\operatorname{div}\mathbf{f}^{(0)} = -4\pi\gamma\rho \quad (\gamma = \text{gravitational constant}) \tag{3$^{(0)}$}$$

and which acts upon any gravitational mass m according to Newton's law of gravitation with the force

$$\mathbf{F}_{\text{Newton}} = m\mathbf{f}^{(0)}. \tag{2$^{(0)}$}$$

If in first approximation one does take into account the effect of $\mathbf{g}$, but considers only fields that are sufficiently weak, so that the gravitational effect of the field energy itself may still be neglected, one will have a description in terms of $\mathbf{f}^{(1)}$ and $\mathbf{g}^{(1)}$, which is the complete analogue to Maxwell's equations, namely

$$\operatorname{div}\mathbf{f}^{(1)} = -4\pi\gamma\rho, \qquad \operatorname{curl}\mathbf{g}^{(1)} = -\frac{4\pi}{c}\gamma\rho\mathbf{v} + \frac{1}{c}\frac{\partial\mathbf{f}^{(1)}}{\partial t}. \tag{3$^{(1)}$}$$

The equations enabling one to consider $\mathbf{f}$ and $\mathbf{g}$ as derivable from four-potentials,

$$\operatorname{div}\mathbf{g} = 0, \qquad \operatorname{curl}\mathbf{f} = -\frac{1}{c}\frac{\partial\mathbf{g}}{\partial t}, \tag{4}$$

can be required to hold in all approximations. One may thus introduce, as is usual in electromagnetic theory, potentials by

$$\mathbf{g} = \operatorname{curl}\mathbf{A}, \qquad \mathbf{f} = -\operatorname{grad}\phi - \frac{1}{c}\frac{\partial\mathbf{A}}{\partial t}. \tag{5}$$

It turns out that this first approximation is already sufficient for the derivation of Newton's second law in the case of a body accelerated linearly, and for the understanding of Coriolis force in the case of a body accelerated centrally with respect to the universe. However, in order to understand the centrifugal force experienced by a body rotating with respect to the universe one has to go to the next approximation, in which the gravitational contribution from the

energy of the fields in first approximation, namely $u^{(1)} = -(1/8\pi\gamma)(\mathbf{f}^{(1)2}+\mathbf{g}^{(1)2})$, is added to the gravitational mass density ρ by putting $\rho^{(1)} = \rho+(1/c^2)u^{(1)}$, so that, for example, the equation governing the production of $\mathbf{f}$ by gravitating sources reads in second approximation

$$(3^{(2)}) \qquad \text{div } \mathbf{f}^{(2)} = -4\pi\gamma[\rho+(1/c^2)u^{(1)}],$$

with a similar equation, containing the gravitational contribution from the energy flux density vector $\mathbf{s}^{(1)} = -(c/4\pi\gamma)(\mathbf{f}^{(1)}\times\mathbf{g}^{(1)})$, namely $(1/c^2)\mathbf{s}^{(1)}$, added to the current in the equation governing the production of $\mathbf{g}$.

One may thus proceed by successive approximations to a more and more accurate formal description of gravitational phenomena. This procedure can be written down more concisely in terms of the Lagrangian formalism. One starts in first approximation with a Lagrangian density

$$(6^{(1)}) \qquad L^{(1)} = -\frac{1}{2\gamma}\frac{\partial A_\nu}{\partial x_\mu}\frac{\partial A_\nu}{\partial x_\mu} - 4\pi A_\nu j_\nu^{(0)}$$

with a given, field independent, current four-vector $j_\nu^{(0)}$, so that the corresponding field equations are

$$(7^{(1)}) \qquad \delta L^{(1)}/\delta A_\nu = 0, \qquad \text{i.e. } \Box A_\nu = 4\pi\gamma j_\nu^{(0)}.$$

The equations in second approximation are obtained by adding to the source $j_\nu^{(0)}$ the gravitational contribution from the energy momentum density, namely $(1/c^2)T_{\nu 0}^{(1)}$, so that

$$(7^{(2)}) \qquad \Box A_\nu = 4\pi\gamma j_\nu^{(1)} = 4\pi\gamma[j_\nu^{(0)}+(1/c^2)T_{\nu 0}^{(1)}]$$

where

$$(8^{(1)}) \qquad T_{\nu 0}^{(1)} = -\frac{\partial A_\mu}{\partial x_0}\frac{\partial L^{(1)}}{\partial(\partial A_\mu/\partial x_\nu)} + L^{(1)}\delta_{\nu 0}.$$

These equations $(7^{(2)})$ are in turn derivable from a Lagrangian density $L^{(2)}$ so that they become identical with $\delta L^{(2)}/\delta A_\nu = 0$. In general, the equations in nth approximation are identical with

$$(7^{(n)}) \qquad \delta L^{(n-1)}/\delta A_\nu = (4\pi\gamma/c^2)T_{\nu 0}^{(n-1)}.$$

It is an interesting and open question whether one can derive expressions for the field equations in the limit $n\to\infty$ in closed form. The pursuit of this problem is outside the scope of the present discussion.

3. NEWTON'S SECOND LAW FOR LINEAR ACCELERATION

Turning our attention now to the equations $(7^{(1)})$ describing the field in first approximation, let us consider the case of a body of gravitational mass m accelerated linearly with respect to the other masses constituting the universe. From the point of view of an observer tied to m, a mass element ρdV at distance $\mathbf{r}$ will be moving with velocity $\mathbf{v}$ and linear acceleration $\dot{\mathbf{v}}$ (see Fig. 2). According to the field equations this element ρdV will produce at distance $\mathbf{r}$ a gravitational

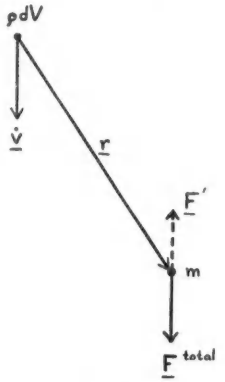

FIG. 2.

field, analogous to the static plus radiation field in electrodynamics, which, taking only terms of lowest order in v/c, has the form

$$(9)\qquad \begin{cases} \mathbf{f}^{(1)} = \dfrac{\gamma}{r^3}\left\{-\mathbf{r}+\dfrac{1}{c^2}(\mathbf{r}\times(\mathbf{r}\times\dot{\mathbf{v}}))\right\}\rho dV, \\ \mathbf{g}^{(1)} = \dfrac{1}{r}(\mathbf{f}^{(1)}\times\mathbf{r}). \end{cases}$$

This field will then, according to equation (2), exert a force, again taking consistently only terms of lowest order in v/c,

$$(10)\qquad \mathbf{F} = m\mathbf{f}^{(1)}.$$

Now let us replace the actual universe by a primitive model, consisting of a sphere of radius R and constant mass density ρ, with m being located at the center. Then the total force exerted on m will be obtained by the integration

$$(11)\qquad \mathbf{F}_{\text{total}} = m\int\mathbf{f}^{(1)}dV$$

which is elementary and yields the interesting result that the total force is parallel and proportional to the acceleration $\dot{\mathbf{v}}$,

$$(12)\qquad \mathbf{F}_{\text{total}} = (4\pi\gamma\rho R^2/3c^2)m\dot{\mathbf{v}}$$

with all other components averaging to zero. It is clear that this force will be experienced by m as a drag, proportional to $\dot{\mathbf{v}}$, and will have to be compensated by a force $\mathbf{F}'$ equal and opposite to it if the state of acceleration $\dot{\mathbf{v}}' = -\dot{\mathbf{v}}$ is to be maintained. Thus Newton's second law in the case of linear acceleration can be understood as being due to the radiative gravitational interaction of the universe with the mass to be accelerated.

In order to obtain numerical agreement with experience one requires in the approximation considered here the relation, obtained by inspection from (12),

$$(13)\qquad 4\pi\gamma\rho R^2/3c^2 = 1,$$

which is familiar from cosmology (see Bondi 1952) and which seems in reasonable order-of-magnitude agreement with the observational data available for ρ and R in this model.

4. NEWTON'S SECOND LAW FOR ROTATIONAL MOTION

Consider next a body of gravitational mass m moving with respect to the inertial frame on a circular path of radius r. Seen from an observer tied to m the universe will be revolving around an axis going through $r = 0$ with angular velocity $\boldsymbol{\omega}$. The inertial forces experienced by m are then Coriolis force $-2m(\mathbf{v}\times\boldsymbol{\omega})$ and centrifugal force $-m(\boldsymbol{\omega}\times(\boldsymbol{\omega}\times\mathbf{r}))$. If the fields $\mathbf{f}$ and $\mathbf{g}$ produced by the rotating universe are considered as the cause of these forces according to equation (2), they must have the form

$$\mathbf{f} = \omega^2\mathbf{r}, \tag{14a}$$

$$\mathbf{g} = -2c\boldsymbol{\omega}. \tag{14b}$$

The field equations in first order ($3^{(1)}$) can be solved easily in this case, if again a model universe of radius R and constant density ρ is taken. By symmetry $\mathbf{f}^{(1)}$ will vanish at the center, but for $\mathbf{g}^{(1)}$ one obtains, in complete analogy with the magnetic field produced at the center of a rotating homogeneously charged sphere,

$$\mathbf{g}^{(1)} = -(2\pi\gamma\rho R^2/3c^2)\,2c\boldsymbol{\omega}. \tag{15}$$

By comparison with (14b) it is thus found that in order to yield the observed Coriolis force the model under consideration must be subject to the relation

$$2\pi\gamma\rho R^2/3c^2 = 1, \tag{16}$$

which up to a factor 2 is identical with the order-of-magnitude relation (13) obtained in the preceding section from quite different considerations.

It was Hund (1948) who first observed that the very large negative energy density corresponding to $\mathbf{g}^{(1)}$,

$$u^{(1)} = -(1/8\pi\gamma)g^{(1)2} = -\omega^2c^2/2\pi\gamma, \tag{17}$$

is sufficient to account for the centrifugal force by virtue of the equations in second order ($3^{(2)}$). Indeed, $u^{(1)}$ corresponds to a negative mass density

$$\rho^{(1)} = -\omega^2/2\pi\gamma \tag{18}$$

which by gravitational repulsion, as demanded by the field equation

$$\operatorname{div}\mathbf{f}^{(2)} = -4\pi\gamma\rho^{(1)} = 2\omega^2, \tag{19}$$

gives rise to the observed centrifugal force

$$\mathbf{f}^{(2)} = \omega^2\mathbf{r}. \tag{20}$$

(Note that, because of cylindrical symmetry, $\operatorname{div}\mathbf{r} = 2$.)

It should be stressed that from the point of view of this model the inertial forces are caused mainly by the distant masses, since the solutions of the field

equations always contain an integral $\int_0^R r dr$. It is instructive to compute the $\mathfrak{g}$-field produced by the rotation of a single galaxy near its center. Let R', ρ', and ω' be radius, mean density, and angular velocity with respect to the inertial frame of a typical galaxy. Then one should expect near its center an additional $\mathfrak{g}$-field of the order

$$g' \cong \gamma \rho' R'^2 \omega'/c \tag{21}$$

corresponding to a negative mass density

$$\mu \cong -\gamma \rho'^2 R'^4 \omega'^2/c^4. \tag{22}$$

Using the reasonable values $\rho' \sim 10^{-21}$ g./cm.^{3}, $R' \sim 10^{22}$ cm., $\omega' \sim 10^{-16}$ sec.$^{-1}$ one finds

$$-\mu \cong 10^{-36} \text{ g./cm.}^3, \tag{23}$$

which appears to be quite beyond observation at the present time. In fact, such a negative mass density would cause gravitationally an effect equal to the inertial forces observed on a rotating system revolving with angular velocity Ω, where

$$\Omega^2 = -2\pi\gamma\mu \cong 10^{-43} \text{ sec.}^{-2}. \tag{24}$$

The corresponding effective centrifugal acceleration even near the rim of the galaxy would still have the exceedingly small value

$$\Omega^2 R' \cong 10^{-21} \text{ cm. sec.}^{-2}, \tag{25}$$

which is 11 orders of magnitude smaller than the ordinary centrifugal acceleration due to the rotation with angular velocity ω'.

5. REMARKS ON THE PRINCIPLE OF EQUIVALENCE

In the preceding discussion it has been assumed that all forms of matter and energy are sources of a universal gravitational field, which is attractive for resting matter. This amounts to assuming the validity of the so-called principle of equivalence, which states that any form of matter which exhibits inertia is at the same time source of a gravitational field of a strength proportional to its inertia and may therefore be assigned a gravitational mass, which is always taken to be positive and proportional to its inertia. In particular, any piece of anti-matter in our universe has been assumed to have positive gravitational mass, because there is no experimental evidence to date which would indicate any difference between the inertias experienced by a particle and by its anti-particle. Within the framework of the model theory discussed above it is thus in principle possible to assume that any fraction of the universe consists of anti-matter without changing any of the conclusions that have been reached so far.

Any tampering with the principle of equivalence would require a drastic change in the field equations to make realization of Mach's Program feasible, and would entail a radically different approach. Recently Morrison and Gold (1956) have put forward the interesting hypothesis that anti-matter has negative gravitational mass, and have envisaged a universe in which the

number of galaxies made up out of anti-matter is equal to the number of galaxies made up out of matter. It is clear that one cannot realize Mach's Program on the basis of the field theory of gravitation used here if the model of Morrison and Gold is adopted, since, except for tiny local fluctuations of the order of magnitude of the contribution to the inertia by a single galaxy, there will be cancellation of the gravitational effects of matter and anti-matter contributed by the distant galaxies whose influence dominates local inertial behavior. One may thus say, on the basis of the gravitational theory used here, that if anti-matter has indeed negative gravitational mass, then the very existence of inertia and the facts incorporated in Newton's second law are manifestations of the preponderance of matter over anti-matter in our universe.

Morrison (1957) has suggested that in addition to the positive gravitational "rest" mass of matter and the negative gravitational "rest" mass of anti-matter there is a third kind of gravitational mass which has the same sign for both matter and anti-matter and which is "kinetic" in origin so that it vanishes for resting matter or anti-matter. Upon adoption of Mach's Program one may then attempt to account for the inertia of both matter and anti-matter by interaction with the "kinetic" mass of the universe, to which the universal recessive motion of distant galaxies may conceivably make a dominant contribution. One can, of course, not rule out such possibilities, but it appears that to this end a theory of gravitation is required which leaves the realm of invariance under Lorentz transformations, and for which therefore the laws of conservation of energy, momentum, and angular momentum are put into question as far as the gravitational field is concerned.

ACKNOWLEDGMENTS

The author is indebted to Professor P. Morrison for a clarifying discussion. The financial aid of the National Research Council in the form of a Research Associateship is gratefully acknowledged.

REFERENCES

BONDI, H. 1952. Cosmology (Cambridge University Press).
GUPTA, S. N. 1954. Phys. Rev. **96**, 1683.
HUND, F. 1948. Z. Physik, **124**, 742.
MORRISON, P. 1957. Private communication.
MORRISON, P. and GOLD, T. 1956. Private print. (See also TIME, Can. ed., June 10, 1957, p. 70.)
SCIAMA, D. 1953. Monthly Notices Roy. Astron. Soc. **113**, 34.
——— 1957. Sci. American, **196**, No. 2, 99.

HORIZONTAL MOVEMENTS OF AURORA[1]

J. S. Kim and B. W. Currie

ABSTRACT

Measurements on the drifts of auroral forms at three stations to the south of the auroral zone in West-Central Canada failed to show evidence of a motion due to the earth's rotation relative to fixed excitation patterns in space. The distribution and the magnitude of the speed of auroral structures parallel and normal to the geomagnetic meridians are substantially the same as for non-luminous ionic irregularities observed by radio methods. The speed of an auroral arc or band parallel to the geomagnetic meridian is apparently constant. Speeds increase with geomagnetic activity, particularly in an east–west direction. There is no definite indication of a reversal of the east–west motions close to local midnight. Speeds and directions show no characteristic variations with the time of night.

INTRODUCTION

Numerous radio investigations in recent years have demonstrated the existence and movement of ionic irregularities in the upper atmosphere (Ratcliffe 1955). The origins of these irregularities are still uncertain. Some are unquestionably due to the impacts of extraterrestrial matter such as meteors, particles ejected from the sun, and galactic dust attracted towards the sun. Some may originate from turbulence—the turbulence causing electronic distributions that are normally uniform to become irregular, or producing irregular distributions of air density that become apparent when the air is ionized. Some may be due to electrical discharge processes within the atmosphere such as discharges upward into the ionosphere from thunderstorms. The causes of the observed movements are even less certain. They may result from the movement of the surrounding neutral air through meteorological processes, or the action of electric fields in combination with the steady magnetic field of the earth, or wave-motions in the distributions of electrons, or a combination of these causes. For these reasons, it is of interest to investigate the horizontal motions of aurora to see what features, if any, they may have in common with the motions of ionic irregularities that are observed by radio methods.

The movements of auroral ionization, as observed visually, may be divided into two types. One is generally very rapid and takes place within the body of the display. The other is relatively slow and involves displacements of displays as a whole. The first is often more apparent than real, auroral structures appearing and disappearing in rapid succession and thus giving the impression of waves of luminosity travelling either horizontally or toward the observer's zenith. The second is evident most frequently as a displacement of an arc or band normal to its lateral extent. To the south of the zone of maximum auroral occurrence, an arc or band will often appear in the

[1]Manuscript received October 7, 1957.
Contribution from the Institute of Upper Atmospheric Physics, University of Saskatchewan, Saskatoon, Sask., Canada.

observer's northern sky and then gradually move southward without any marked change in its configuration. This may be followed by a succession of slow retreats and advances. Sometimes the arc or band disappears as it approaches the observer's zenith, and is followed by the appearance of a new arc or band in the north that moves southward. Similar motions are observed to the north of the auroral zone, the primary movement now appearing to be northward. Motions parallel to the lateral extent of a display also occur, but these are difficult to detect. Detection depends on the presence of persistent convolutions and structures that cannot be confused with the more transient features that characterize the first type of movement. Slow rotations of a display, clockwise or counterclockwise, are also occasionally observed. These again may be more apparent than real, variations in the lateral direction of an arc as it moves eastward or westward being interpreted as rotations. It is movements of the second type that are considered in this paper.

Quantitative investigations of these movements have only recently become possible through the development of all-sky cameras (Meinel and Schulte 1953; Stoffregen 1955; Meek 1955; Park 1957). The sky is imaged in a convex or parabolic mirror with its axis vertical. This image is photographed (usually once every minute) by a movie camera placed directly above the mirror. A clock or a digital counter controlled by a clock is located in the field of view of the movie camera to give the time. Because exposure times are seldom long enough to record the star background, altitudes and azimuths of points on a photograph are obtained from suitably-located markers or lamps placed in the field of view of the mirror and photographed along with the sky. The markers sometimes consist of a hemispherical grid of wires placed symmetrically about the mirror. Often they consist of nothing more than the rods supporting the camera and short crosspieces attached to them at heights corresponding to selected angular altitudes as imaged by the camera. For the accurate determination of angular altitudes and azimuths of auroral points, the photographs must be projected onto a grid of concentric circles and radial lines. The grid is constructed usually by reference to star photographs taken with the camera so as to eliminate errors due to aberrations in the optical systems. The images of the markers serve to adjust the magnification of the projector, and to locate the projected image properly on the grid.

The movements of an auroral display are seen readily by running the film from an all-sky camera at a moderate rate through a projector. This is particularly necessary for east–west motions. An observer looking directly at an auroral display seldom recognizes these motions, possibly because persistent features that serve as indicators of the motions are confused with the more transient features of the display. Because of the relatively long exposure times required (20 seconds for some types of cameras), the transient features either do not appear or are smeared by the auroral motions into a picture that shows only the limiting edges of the auroral display.

Certain assumptions are necessary in order to measure horizontal displacements and the rates at which they take place. One is that the lower edge of

arcs and bands occurs at a constant height above the earth. Numerous parallactic measurements of auroral heights indicate that this is generally the case, and that a height of 100 km. is a reasonable one to assume (Currie 1955; Jensen and Currie 1953). Another is that the components of the displacements most likely to be of value for comparative purposes are ones parallel and normal respectively to the geomagnetic meridians, since auroral characteristics such as the isolines of occurrence and the lateral extent in an east–west sense coincide more closely with the geomagnetic than the geographic lines of latitude (Jones and Currie 1941). Only displacements of arcs and bands parallel to a meridian, either geographic or geomagnetic, can be measured with any considerable frequency; and to a first approximation these are normal to the arcs and bands in West-Central Canada.

OBSERVATIONAL DETAILS

Motions parallel to the geomagnetic meridians were measured on all-sky photographs taken at Saskatoon, Flin Flon, and Uranium City during January, February, and March, 1956. The geographic latitude and longitude (ϕ, λ), the geomagnetic latitude and longitude (Φ, Λ), and the angle between the geographic and the geomagnetic meridian (ψ) for each station are given in Table I. Uranium City is on the southern edge of the zone of maximum auroral occurrence for the Northern Hemisphere. The photographs were

TABLE I

GEOGRAPHIC LATITUDE AND LONGITUDE (ϕ, λ), GEOMAGNETIC LATITUDE AND LONGITUDE (Φ, Λ), AND THE ANGLE ψ BETWEEN THE GEOGRAPHIC AND GEOMAGNETIC MERIDIANS FOR SASKATOON, FLIN FLON, AND URANIUM CITY

Station	ϕ, °N.	λ, °W.	Φ, °N.	Λ, °W.	ψ, °
Saskatoon	52.1	106.6	60.5	48.9	13.8
Flin Flon	54.8	101.8	63.8	43.5	13.6
Uranium City	59.6	108.8	67.7	55.6	19.1

taken on 16-mm. film at 1-minute intervals with about 20-second exposure times. The period covered by the photographs was one with a predominance of arc and band-like structures. Comparison of the relative occurrences of auroras at each station (number of nights with aurora expressed as a percentage of the number of nights when aurora could have been photographed if present) showed that the data were approximately representative of the region and of the time of year. Auroral occurrence increased with geomagnetic latitude at about the expected rate (Vestine 1944). Auroral occurrence at all three stations was substantially greater for January than for February, contrary to long-time averages for regions to the south of the auroral zone. However, auroral occurrence increased rapidly during March in accordance with the approach to the usual spring maximum.

Motions normal to the geomagnetic meridians were measured on all-sky photographs taken at Flin Flon throughout 1956. Owing apparently to in-

creased solar activity, the character of the displays changed during the later part of 1956, structures suitable for detecting lateral motions occurring more frequently. The additional months of data provided sufficient measurements to be of some value for statistical purposes.

The photographs were projected onto a special grid for each station. This consisted of a system of geographic latitude and longitude lines, centered on the station and extending outward to cover the region over which auroras were photographed. The lines were spaced according to the assumption that the lower edge of all auroral forms is at a height of 100 km. above the earth. The latitude and longitude of the point directly below any selected point on the lower edge of an auroral form could be read directly from the grid. Absolute displacements could then be computed from the latitude and longitude readings corresponding to the positions of the selected auroral point on successive photographs. Actually, the grids were used largely to check on the direction and uniformity of motion of the auroral forms. A line corresponding to the geomagnetic meridian for the station was placed on its grid. It was marked with a scale of distances from the station. Measurements of displacements parallel to the geomagnetic meridians were made only on arcs and bands that were above the geomagnetic meridian for the station and that moved so that their positions on successive photographs were substantially parallel to each other. The grid as a whole was necessary to check this point. Measurements of displacements normal to the geomagnetic meridians were more complicated, since computations of the displacements had to be made from the latitude and longitude readings.

Displacements were ordinarily measured for 4-minute intervals, and in most cases on auroral structures at least 20 degrees above the horizon. While shorter time intervals and lower altitudes could have been used, the errors would have been appreciable because of the small size of the photographs and the rapid decrease in magnification of horizontal distances toward the edges of the photographs.

RESULTS

1. Motions Parallel to the Geomagnetic Meridians

Several general features of the motions of arcs and bands parallel to the geomagnetic meridians, and hence approximately normal to their lateral extent, are indicated by the measurements. The speed of each arc or band is constant to within the accuracy with which the measurements could be made. An arc or band is rarely stationary, although the direction of motion of some reverses. Motions in a northward or southward sense are not related to the time of night. The higher speeds, especially in a southward sense, occur generally at times of considerable magnetic disturbance.

The deduction concerning the constancy of the speed of particular arcs and bands parallel to the geomagnetic meridian was based on measurements for 77 independent arcs and bands as photographed from Saskatoon, 587 from Flin Flon, and 502 from Uranium City. Of these, 49, 335, and 328 respectively were moving southward. For all except the fastest moving forms, the

speeds were measured for at least two successive 4-minute intervals; and in numerous cases for five or more. One persistent arc moved slowly enough for 19 such measurements to be made; another for 15 measurements.

About one-third of the arcs and bands reversed their direction of motion. Whether or not they came to rest and remained so for a short period of time before starting in the opposite direction is uncertain. A gradual slowing before and speeding up after the reversal was not observed, but this may have been because of the 1-minute intervals between photographs. Very occasionally a series of photographs showed an arc that was apparently stationary, but these were for low altitudes where small displacements were difficult to detect.

The percentage occurrences of arcs moving southward, northward, and reversing direction at each of the three stations for the period before midnight were approximately the same as for the period after midnight. There was some indication that auroras during the hour or so immediately after sunset and again before sunrise have motions that are predominantly southward. The data were insufficient to be certain about this point. The speeds also showed no significant differences for different periods of the night, although they were usually greater at times close to sunset and sunrise than at other times.

The largest speeds invariably occurred at times with much magnetic disturbance. A correlation of speeds with magnetic disturbance indices would have required considerably more data, since the number of arcs and bands suitable for measuring displacements parallel to the geomagnetic meridians decreases as the magnetic activity increases. Rayed and other structures which change their form rapidly with time begin to predominate, and the number of reliable measurements of displacements that can be made gets small.

Table II gives a tabulation of the observed speeds parallel to the geomagnetic meridians, grouped according to 3-km./min. intervals of speed. Because of the small number of cases with speeds above 39 km./min., these are shown as a single group. The highest observed speed was about 50 km./min., once southward at Saskatoon and twice northward at Flin Flon. It is evident from the table that the number of cases with southward motion exceeds the number with northward motion for all ranges of speed except the one for speeds less than 3 km./min. Obviously, there is a resultant displacement of auroral ionization southward. The average southward speeds of arcs and bands at Saskatoon, Flin Flon, and Uranium City from these observations are respectively 10.6, 9.4, and 10.4 km./min., and average northward speeds, 8.5, 8.0, and 9.3 km./min. Averages computed using the 4-minute values, irrespective of the arcs or bands on which they were made, give approximately the same speeds, namely 9.7, 8.0, and 9.3 km./min. southward, and 8.8, 6.3, and 8.9 km./min. northward. Apparently there is no systematic variation of speeds with latitude. Applying the usual statistical tests, the differences between the southward and northward speeds are significant for each station. The differences are appreciably smaller than would be expected for an excita-

TABLE II

SPEEDS OF AURORAL ARCS AND BANDS PARALLEL TO THE GEOMAGNETIC MERIDIANS AS OBSERVED AT SASKATOON, FLIN FLON, AND URANIUM CITY

The observations are grouped according to 3-km./min. ranges of speed. Each row includes occurrences of the highest indicated speed for the range but not the lowest. The first quantity in the columns under the names of the stations gives the number of 4-minute occurrences of the indicated speed; the second quantity, which is in brackets, the number of independent arcs and bands with the indicated speed.

Speed, km./min.	Saskatoon		Flin Flon		Uranium City	
	South	North	South	North	South	North
0–3	3(1)	11(2)	149(45)	188(46)	78(20)	51(17)
3–6	47(11)	11(4)	235(82)	150(71)	187(62)	83(44)
6–9	18(7)	15(9)	134(61)	98(49)	142(63)	77(33)
9–12	28(9)	11(4)	95(51)	66(38)	141(66)	63(33)
12–15	21(10)	2(1)	77(37)	31(21)	102(43)	24(16)
15–18	5(3)	0	42(21)	16(8)	73(36)	14(10)
18–21	7(2)	3(2)	18(11)	17(9)	25(16)	17(12)
21–24	2(2)	2(2)	18(11)	6(4)	17(10)	8(3)
24–27	2(1)	1(1)	13(9)	2(2)	2(2)	3(2)
27–30	2(2)	1(1)	3(1)	2(1)	4(4)	9(3)
30–33		1(1)	5(4)		1(1)	
33–36					2(2)	1(1)
36–39				1(1)	2(2)	
39	1(1)	2(1)	3(2)	3(2)	2(1)	
Totals	136(49)	60(28)	792(335)	580(252)	778(328)	350(174)

tion pattern fixed in space relative to the earth. For arcs and bands lying along the geomagnetic parallels of latitude, the expected speeds southward due to the earth's rotation are respectively 4.1, 3.8, and 4.6 km./min. at Saskatoon, Flin Flon, and Uranium City. If the random portions of the speeds southward and northward have the same average values for a large number of observations the resultant drift southward along the geomagnetic meridian at each station is obtained by dividing the observed differences by two. These are about 1.0, 0.7, and 0.6 km./min. respectively.

2. Motions Normal to the Geomagnetic Meridians

Several general features of the motions of auroral structures normal to the geomagnetic meridians were indicated by the measurements. These are less certain than ones for the motions parallel to the geomagnetic meridians because of the limited number of cases. When structures suitable for measuring absolute displacement occur, the motions are predominantly in an east–west sense and occur at much greater speeds than for the south–north motions. Motions in an east–west sense are rarely detected except at times of considerable magnetic disturbance; and the more disturbed the magnetic field, the larger are the speeds. Speeds are apparently independent of the time of night, and on an average are the same for eastward and westward motions. Westward motions occur more frequently before midnight and eastward motions after midnight. The speed of particular structures appears to remain constant; but this is difficult to verify because of their relatively short durations.

Measurements were made on 90 independent auroral structures, 35 exhibiting eastward motion and 55 westward motion. The average duration of each

structure was about 5 minutes. The average speed eastward of the structures was 28.9 km./min., and westward, 28.7 km./min. Average speeds computed from the total displacements and the total durations were 26.3 km./min. eastward and 26.4 km./min. westward. Again the observations show no evidence of an excitation pattern fixed in space relative to the earth.

Table III shows a tabulation of the average departures from normal of the magnetic field intensity at Flin Flon corresponding to various ranges of speed. The magnetic values were computed from the average values of ΔX, ΔY, and ΔZ (X, Y, and Z are the components northward, eastward, and downward of the earth's field as recorded by a three-component magnetic vario-

TABLE III

AVERAGE DEPARTURES FROM NORMAL OF THE MAGNETIC FIELD INTENSITY AT FLIN FLON CORRESPONDING TO VARIOUS RANGES OF SPEEDS OF AURORAL STRUCTURES NORMAL TO THE GEOMAGNETIC MERIDIANS

Ranges of speed, km./min.	Number of cases	Average speed, km./min.	Average departure field intensity, gammas
0–10	5	5.4	24
10–20	21	14.5	102
20–30	19	25.4	142
30–40	17	34.1	145
40–50	8	46.6	182
50–60	8	53.7	173
60–70	2	64.6	125
70–80	1	71.0	113

meter), for the time intervals during which the displacements occurred. Nine of the 90 cases are not included because of incomplete magnetic records. Fig. 1 shows a plot of the average speeds as abscissae against the average

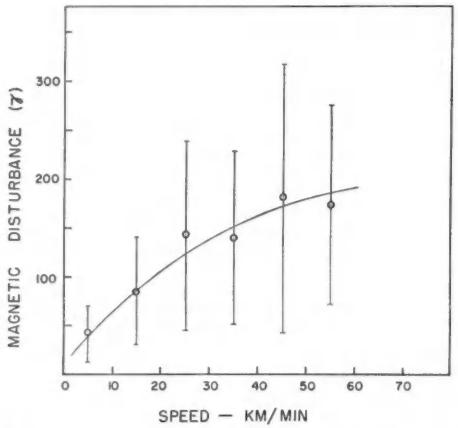

FIG. 1. Plot of the average departures from normal of the magnetic field intensity during the east–west motions of auroras for 10 km./min. ranges of speed. The vertical lines show the extreme variation of the magnetic values included in each average value.

departures of the magnetic field intensity as ordinates. Although the variance is large, there is unquestionably an increase of speed as the magnetic disturbance increases. A relationship between the direction of motion and the magnitude of the disturbance was not evident.

Table IV shows the numbers of occurrences of eastward and westward motions and the corresponding average speeds for different hours of the night. Westward motions were characteristic of the early morning hours, eastward motions of the late morning hours, and motions in both directions of about a 4-hour period centered on midnight. The speeds do not indicate a gradual slowing down of the westward motions prior to a change to eastward motions, as might be expected if motions in the evening hours are generally opposite to those for the morning hours.

TABLE IV

THE DIURNAL OCCURRENCES AND SPEEDS OF EAST–WEST MOTIONS OF AURORAL STRUCTURES AT FLIN FLON

Time, M.S.T.	Occurrences		Speeds, km./min.	
	East	West	East	West
18–19		1		23.0
19–20		1		34.3
20–21		4		26.0
21–22		8		38.7
22–23	4	9	22.6	23.4
23–24	6	15	32.3	30.6
00–01	13	10	27.0	29.8
01–02	5	7	35.3	20.0
02–03	4		28.3	
03–04	3		35.4	
04–05				

DISCUSSION

Auroras are assumed generally to be excited by charged particles that travel in streams from the sun and penetrate into the earth's atmosphere. Because of the interaction between the charged particles and the earth's magnetic field, the latitudes where auroras occur depend on the speed of the particles. Variations in speeds of the particles in the solar streams, and the distortions of the earth's magnetic field by the ring current that is assumed to develop outside the earth and in its equatorial plane during geomagnetic storms, are presumably responsible for the sporadic occurrence of auroras over regions in high latitudes, and the apparently random ways in which displays move. The only systematic motions that should be observed are ones superimposed on these due to the earth's rotation relative to the streams of exciting particles. The failure of these observations to show any definite indication of a motion due to the earth's rotation confirms the earlier and less extensive observations on east–west motions at Yerkes Observatory (Meinel and Schulte 1953) and at Saskatoon (Meek 1954). It is unlikely that the small resultant drift southward of the auroral ionization along the geomagnetic meridians is due to sampling and errors in measuring the speeds.

The average orientation of arcs and bands in West-Central Canada (Jensen and Currie 1953) is such as to have given appreciably greater values of the southward drift, if it had been due to the earth's rotation.

It is of some interest to compare the motions of the auroral luminosities with those of the non-luminous ionic irregularities detected in the E and F regions by radio methods. The speeds of auroral forms and structures are of the same order of magnitude as the speeds of the ionic irregularities (Chapman 1953; Briggs and Spencer 1954; Toman 1955; Maxwell 1955; Dagg 1957; Harang and Pedersen 1957). Histograms of the frequencies of occurrence of the speeds tabulated in Table II (see Fig. 2) would approximate in many cases to the corresponding histograms for the ionic irregularities, for example,

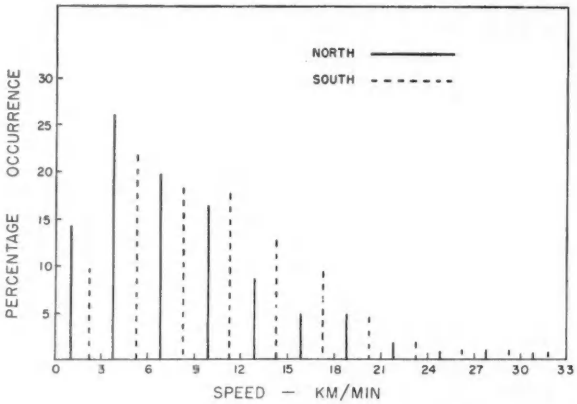

FIG. 2. Histograms of the percentage occurrences of 3-km./min. ranges of speed of northward and southward moving auroras. The larger speeds are more frequent for southward moving auroras.

Fig. 16 by Toman for F-region drifts. The directions of the E and F region drifts, observed by radio methods, are usually more regular and change systematically with the time of day and the season. This may be because the motions of the ionic irregularities can be followed continuously, and some of the radio methods permit more exact determinations of direction of motion. The ionic irregularities also experience sudden changes of direction of motion, for example, Fig. 1 by Briggs and Spencer. Recent observations on E-layer drifts at Kjeller, Norway, by Harang and Pedersen, indicate a prevailing motion toward the southeast in winter, the southward component of which is about the same as for the drift of the auroral arcs and bands toward the south. Since aurora occurs predominantly in the E region, it might be anticipated that the aurora would be subject to any relatively-constant drifts characteristic of the E region. On the other hand, if aurora is due to a discharge mechanism due to electrical fields that develop between the E and F regions, the auroral drifts might well be influenced by drifts in the F region. While it is difficult to see how the discharge fields could develop because of the high electrical

conductivity along the lines of the earth's magnetic field, meridional winds deduced for the *F* region are southward to the south of latitude 60° N. (approximately the position of the auroral zone in West-Central Canada), and northward to the north of latitude 60° N. (Pant 1956). Visual observations made to the north of the auroral zone during 1932–33 at Chesterfield, Coppermine, and Cape Hope's Advance indicate that an investigation of auroral drifts, similar to this one, would show a northward drift over latitudes to the north of the auroral zone. While confirmation of the visual observations by all-sky camera studies could not be taken as positive proof of a control on auroral drifts by processes taking place in the *F* region, it would suggest a relationship between winds of meteorological origin and the average drifts of auroras.

The increase in speed of the non-luminous ionic irregularities with increasing magnetic activity is now a well-established phenomenon, especially for the *F* region. For example, see Fig. 2 by Maxwell and Fig. 1 by Dagg for *F*-region drift speeds plotted against geomagnetic *K* indices. Since the auroral speeds (especially of structures which usually extend upward beyond the *E* region) also show an increase with geomagnetic activity, the possibility exists that the same mechanism controls the speeds of both the ionic irregularities and the aurora.

The observations by Meinel and Schulte at Yerkes indicated that the motion was westward in the evening, reversed during the midnight hours, and was eastward in the morning. Meek's observations at Saskatoon showed eastward motions taking place at various times throughout the night, westward motions up to 2:00 a.m., and no evidence of a reversal. In general, the Flin Flon observations agree with the ones made by Meek. While only westward motions were observed in the early evening and eastward motions in the late morning, motions in one direction were relatively as frequent as in the other for the four hours centered on midnight and showed no evidence of a slowing down close to midnight. The failure of the Saskatoon and Flin Flon observations to agree with the ones at Yerkes is disappointing, since investigations by Chapman, Vestine, Martyn, and others of geomagnetic disturbance features indicate the possibility of current systems flowing at ionospheric levels and reversing direction near midnight, the current systems being induced by winds at ionospheric levels through a dynamo action.

Three distinct types of clouds of abnormal ionization occur in auroral and polar regions as observed by ionosonde equipment (Hagg and Hanson 1954). Two of these, clouds of sporadic *E* and clouds accompanied by radio blackouts, appear to be associated with aurora. The first has speeds and speed distributions comparable to those for aurora, but occurs more frequently at Resolute Bay (74.7° N.) than at Baker Lake (64.3° N.). The frequency of occurrence of aurora at the former is very much less than at the latter station. The diurnal distribution of the first also differs notably from that for aurora. The second type is observed at stations close to the auroral zone, and has a diurnal distribution comparable to that for aurora. It has average speeds of 75 km./min., and maximum speeds of the order of 250 km./min. Radio blackouts are often an aftermath of such occurrences, and these may be wide-

spread and persist for many hours. The second type is apparently associated with the penetration of ionizing particles into the atmosphere, and is usually accompanied by auroral displays, but the speed, the extent of the clouds, and the persistence indicate that it is not aurora. Again it is interesting to speculate whether or not widespread ionization can occur at and below auroral levels with visual aurora taking place intermittently only at particular locations.

It is believed that these observations on auroral motions, and the discussion of their possible relationships to other phenomena involving ionic irregularities in the upper atmosphere, are sufficient to show that studies of auroral motions by sequences of all-sky camera photographs are worth while. Eighteen of these cameras, including nine 35-mm. cameras designed by the National Research Council that make possible more accurate measurements on aurora than the usual 16-mm. camera, are operating in Canada during the International Geophysical Year. While they are intended primarily to record the occurrence of aurora and the development of auroral displays, an investigation of auroral movements both inside and outside the zone of maximum auroral occurrence from their photographs may contribute significantly toward an explanation of the process by which aurora is excited.

ACKNOWLEDGMENTS

The assistance of Mr. B. Morrison in operating a camera and magnetic variometers at Flin Flon, of Mr. D. Bekolay and Mr. D. Markowsky in operating a camera at Uranium City, and of Mr. F. Hector in operating a camera and magnetic variometers at Saskatoon is gratefully acknowledged. Financial assistance through a contract with the Radio Physics Laboratory of the Defence Research Board of Canada for auroral investigations is also acknowledged. Dr. J. Meek was largely responsible for starting the network of camera stations, and this investigation of auroral motions.

REFERENCES

Briggs, B. H. and Spencer, M. 1954. Repts. Progr. in Phys. **17**, 245.
Chapman, H. J. 1953. Can. J. Phys. **31**, 120.
Currie, B. W. 1955. Can. J. Phys. **33**, 773.
Dagg, M. 1957. J. Atmospheric and Terrest. Phys. **10**, 194.
Hagg, E. L. and Hanson, G. H. 1954. Can. J. Phys. **32**, 790.
Harang, L. and Pedersen, K. 1957. J. Geophys. Research, **62**, 183.
Jensen, R. E. and Currie, B. W. 1953. J. Geophys. Research, **58**, 201.
Jones, C. K. and Currie, B. W. 1941. Terrestrial Magnetism and Atmospheric Elec. **46**, 269.
Maxwell, A. 1955. Physics of the Ionosphere. Repts. Phys. Soc. Conf. Part II, 166.
Meek J. H. 1954. Astrophys. J. **120**, 602.
——— 1955. Spec. Publ. Phys. Dept. Univ. Sask., Saskatoon, Sask.
Meinel, A. B. and Schulte, O. H. 1953. Astrophys. J. **117**, 454.
Pant, P. S. 1956. J. Geophys. Research, **61**, 459.
Park, F. R. 1957. Bull. Radio and Elect. Eng. Div., National Research Council, Ottawa, **7**, 1.
Ratcliffe, J. A. 1955. Physics of the Ionosphere. Repts. Phys. Soc. Conf. Part II, 88.
Stoffregen, W. 1955. Spec. Publ. Upsala Ionospheric Laboratory, Sweden.
Toman, K. 1955. J. Geophys. Research, **60**, 57.
Vestine, F. H. 1944. Terrestrial Magnetism and Atmospheric Elec. **49**, 77.

ROTATIONAL SPECTRA OF RbF BY THE ELECTRIC RESONANCE METHOD[1]

H. LEW, D. MORRIS,[2] F. E. GEIGER, JR.,[3] AND J. T. EISINGER[4]

ABSTRACT

Transitions between the $J = 0$ and $J = 1$ rotational states of RbF have been measured by means of the molecular beam electric resonance method. The following rotational constants have been determined (all frequencies in Mc./sec.):

	$Rb^{85}F$	$Rb^{87}F$
$Y_{01} = B_e$	6315.543±0.009	6289.002±0.010
$-Y_{11} = \alpha_e$	45.638±0.017	45.350±0.017
$Y_{21} = \gamma_e$	0.094±0.007	0.094±0.007
B_e	6315.639±0.036	6289.098±0.036

The quadrupole interaction constants $-eqQ/h$ in the $J = 1$ state are found to be

$Rb^{85}F$	$v = 0$	70.340±0.030 Mc./sec.
	$v = 1$	69.543±0.060 Mc./sec.
$Rb^{87}F$	$v = 0$	34.024±0.040 Mc./sec.
$eqQ^{85}/eqQ^{87} = 2.0673 \pm 0.0030$		

The equilibrium internuclear distance is $r_e = (2.26554 \pm 0.00005) \times 10^{-8}$ cm. The electric dipole moment of $Rb^{85}F$ in the $v = 0$ state is $\mu = (8.80 \pm 0.10) \times 10^{-18}$ e.s.u. The mass ratio of the Rb isotopes is $M_{85}/M_{87} = 0.9770148 \pm 0.0000052$.

I. INTRODUCTION

Over the last few years, pure rotational spectra in almost all the alkali halides have been obtained either by microwave absorption spectroscopy at high temperatures (Honig, Mandel, Stitch, and Townes 1954) or by the molecular beam electric resonance method (e.g. Lee, Fabricand, Carlson, and Rabi 1953). From the extensive data general trends in such quantities as interatomic distances and electric dipole moments have been observed and empirical relations derived for them. As a step towards completing the picture for the alkali halides, it was decided to study RbF in the electric resonance apparatus of this laboratory. This molecule was one of the few that had been left undone by the microwave spectroscopists (Honig *et al.* 1954) because of experimental difficulties. The other alkali halides yet to be studied for rotational spectra are LiF, KF, NaF, and LiCl. Rubidium fluoride was chosen for the present study because the frequencies required would be the lowest among the molecules mentioned and because the necessary microwave equipment for the estimated transition frequencies was already on hand.

[1]Manuscript received October 30, 1957.
Contribution from the Division of Pure Physics, National Research Council, Ottawa, Canada.
Issued as N.R.C. No. 4600.
[2]National Research Laboratories Postdoctorate Fellow 1953–55; now with the Division of Applied Physics, National Research Council, Ottawa.
[3]National Research Laboratories Postdoctorate Fellow 1950–51; now with Naval Research Laboratories, Washington 25, D.C.
[4]Now with Bell Telephone Laboratories, Murray Hill, New Jersey.

Rubidium fluoride was first studied by the electric resonance method by Hughes and Grabner (1950), who observed transitions between Stark sublevels belonging to a given rotational level. They obtained values for the quadrupole interaction constant eqQ_{Rb} for different rotational states and different vibrational states and values for the so-called $I_F.J$ interaction constant where I_F is the spin of the fluorine nucleus. The present measurements, in addition to yielding quadrupole interaction constants which are in agreement with those of Hughes and Grabner, yield values for the molecular rotational constants B_e and α_e and a value for the electric dipole moment μ. The $I_F.J$ interaction, however, was not resolved.

Prior to a search for transitions an estimate of B_e was made through the use of internuclear distances tabulated by Honig *et al.* (1954). These authors give a calculated internuclear distance for RbF of 2.246 Å with a probable accuracy of about one per cent. Thus B_e should be around 6450 ± 125 Mc./sec. or the frequency of a $(J = 1) \leftarrow (J = 0)$ transition about 12900 ± 250 Mc./sec.

II. THEORY

For the analysis of the rotational spectra observed in the present experiment, aside from the hyperfine structure, Dunham's (1932) expressions for the energy levels of a vibrating rotator are used. In order to avoid excessive reference to the original or other papers, some of the appropriate relations are reproduced here. In terms of Dunham's coefficients the frequencies of a $(J = 1) \leftarrow (J = 0)$ transition for the first four vibrational states are (Lee *et al.* 1953)

$$\begin{aligned} f_0 &= 2Y_{01}+4Y_{02}+Y_{11}+(1/2)Y_{21}, \\ f_1 &= 2Y_{01}+4Y_{02}+3Y_{11}+(9/2)Y_{21}, \\ f_2 &= 2Y_{01}+4Y_{02}+5Y_{11}+(25/2)Y_{21}, \\ f_3 &= 2Y_{01}+4Y_{02}+7Y_{11}+(49/2)Y_{21}. \end{aligned} \tag{1}$$

The various Y_{lj} are related to more familiar molecular constants as follows:

$$Y_{01} \approx B_e, \qquad Y_{02} \approx -D_e, \qquad Y_{11} \approx -\alpha_e, \qquad Y_{21} \approx \gamma_e.$$

Since the determinant of the coefficients in (1) is of rank 3, only three coefficients may be determined even though more than three f_v may be available. The smallest of the coefficients, Y_{02}, is usually calculated from the relation $Y_{02} = -4B_e^3/\omega_e^2$ provided ω_e is known from other work.

Before Eq. 1 can be used to treat the experimental data, the hyperfine structure of the $J = 1$ state must be taken into account. The theory for this has been given by Hughes and Grabner (1950). These authors found that, in their study of transitions between various sublevels belonging to the $J = 1$ state, it was sufficient to assume two internal interactions in the molecule: one an interaction between the electric quadrupole moment of the Rb nucleus and the gradient of the electric field acting on it and the other a magnetic interaction between the fluorine nuclear magnetic moment and the field arising from the rotation of the molecule (the $I.J$ or spin–rotation interaction).

These two interactions split the $J = 1$ level into six components as shown in Figs. 1 and 2. In the figures, the various quantum numbers have the following significance: $F_1 = I_1 + J$ where I_1 is the spin of the Rb nucleus and

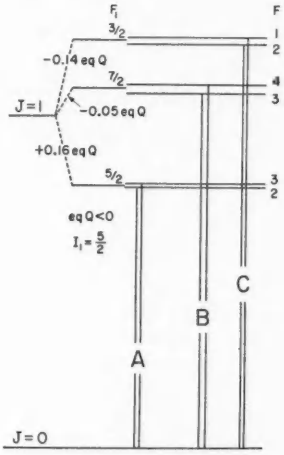

FIG. 1. Energy levels of $Rb^{85}F$.

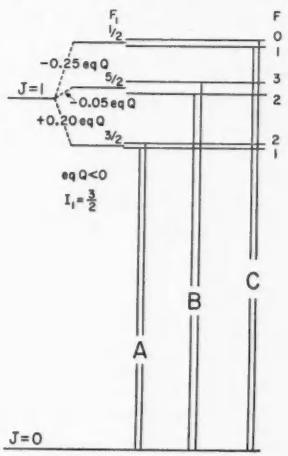

FIG. 2. Energy levels of $Rb^{87}F$.

$F = I_2 + F_1$ where I_2 is the spin of the F nucleus. There are theoretically six observable transitions between $J = 1$ and $J = 0$ but, since the $I_F.J$ splitting is not resolved in the present experiment, only three distinct lines are observed and these are labelled A, B, and C. The $I.J$ splittings are of the order of 10 kc./sec. (Hughes and Grabner 1950). The patterns shown in Figs. 1 and 2 are, of course, for zero external electric field.

The electric dipole moment μ of the molecule may be determined by observing the shift in a transition frequency on the application of a static electric field. For RbF the most convenient line for this purpose is line C. This line involves the levels ($J = 0$) and ($J = 1$, $F_1 = \frac{3}{2}$). By Eq. 2 of Hughes (1947) the shift in the $J = 0$ level for weak electric fields E is simply

$$\Delta W = -\tfrac{1}{6}\mu^2 E^2 / B_e. \tag{2}$$

By Eq. 13 of Fano (1948) or similar expressions elsewhere (e.g. Townes and Schawlow (1955), Eqs. 10–31) the upper level of line C splits into two components which are separated from the field-free level by

$$\Delta W = (\pm)\frac{1}{80}\frac{\mu^2 E^2}{B_e}, \tag{3}$$

where the upper sign applies for the substates $|M_{F_1}| = \frac{1}{2}$ and the lower sign for $|M_{F_1}| = \frac{3}{2}$. At sufficiently small fields these two Stark levels are unresolved and the equal and opposite shifts of the two substates result only in a broadening of the line. Hence the frequency shift in line C is simply

that given by Eq. 2. This very simple relationship between the electric dipole moment and easily measured quantities makes the line C particularly suitable for the determination of the dipole moment.

III. APPARATUS

The apparatus is of conventional design, basically that described by Hughes (1947) but in the modification first described by Lee *et al.* (1953). A diagram of the apparatus giving some of the important dimensions is shown in Fig. 3. The vacuum tank is of non-magnetic stainless steel plate, 0.475 cm. thick,

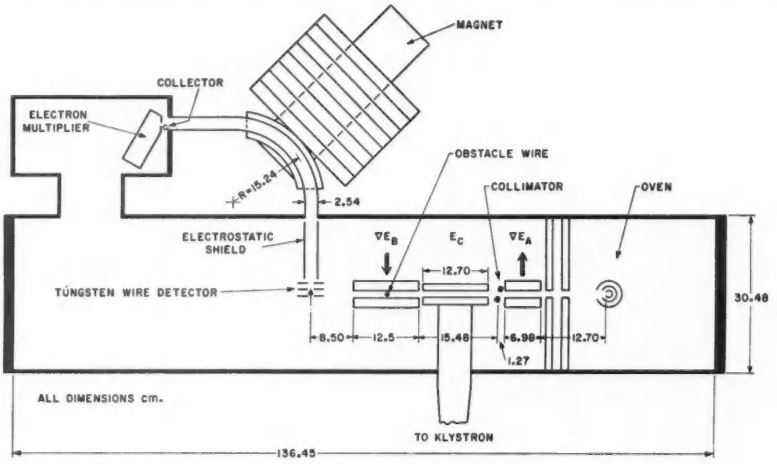

FIG. 3. Schematic plan view of apparatus.

rolled into a cylinder and welded. It is divided into the usual three chambers and evacuated by three oil-diffusion pumps.

The oven is a vertically mounted cylindrical steel tube closed at the bottom and provided with a plug at the top. It has an inside diameter of 1.59 cm. and a wall thickness of 0.025 cm. The total depth of the oven is 5 cm. and the center of the slit is located 3.2 cm. from the bottom. The width and height of the slit are respectively 0.0076 cm. and 1.27 cm. The heating elements for the oven are molybdenum coils enclosed in thin ceramic tubes mounted parallel to the axis of the oven and arranged in a circle around it. This assembly is surrounded by two radiation shields, the outer one of which is water cooled.

The brass pole-pieces of the A and B fields are of identical cross section but of different lengths. The cross section is as shown in Fig. 4. The various design constants are given in Table I. The beam position is exactly equidistant from the two outer faces of the pole pieces so that the latter may be reversed in their mount and hence the gradient reversed without a need for realignment of the system.

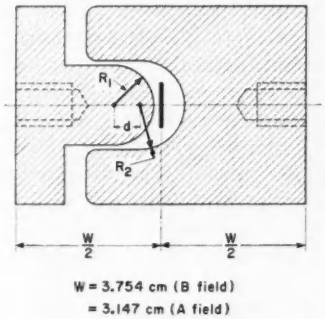

FIG. 4. Pole pieces of A and B fields, sectional view.

TABLE I

DESIGN CONSTANTS OF DEFLECTING FIELDS
(A and B fields of identical cross section)

Separation of equivalent parallel wires $2a$ = 1.000 cm.
Radius of convex piece R_1 = 0.508 cm.
Radius of concave piece R_2 = 0.564 cm.
Separation between centers of curvature d = 0.345 cm.
Beam position = 0.1 cm. from apex of convex piece
Field intensity/voltage = 2.888 (volt/cm.)/volt
Gradient/field = 1.981 cm.$^{-1}$

The C field consists of two parallel plates, one of which (Item 1 in Fig. 5) is of aluminum deposited on glass and the other (Item 2) of brass. The brass piece contains a slit 0.038 cm. high and 4.75 cm. long in the direction of the beam. Microwave energy is fed into the C region by way of this slit. The

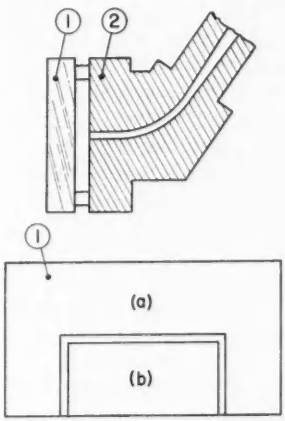

FIG. 5. C field.

slit couples to an external waveguide through a 55° bend and a taper section. The bend was necessitated by an obstacle in the side of the vacuum tank directly opposite the C field. Although the brass plate was ground optically flat prior to assembly it is not known how flat it remained after assembly. The microwave energy in the waveguide is in the TE_{01} mode.

The use of an aluminized glass plate as one of the surfaces of the C field was decided on because of the ease with which such a plate could be made flat and the ease of having the active surface divided into two mutually insulated regions as shown in the lower half of Fig. 5. The aluminum surface was merely scored with a pointed instrument. The purpose of this division was to permit low frequencies (a few megacycles) to be applied to the C region for the observation of ΔM_J transitions. The large contact potential between aluminum and brass, however, had been inadvertently overlooked and was not recognized until late in the measurements. Fortunately this potential introduced a negligible correction in the measurements at zero field, as will be shown.

The aluminized surface was coated with a thin film of silicon dioxide to protect it from abrasion. Quartz spacers between the plates provide a spacing of 0.69065 cm.

The collimator consists of two quartz semicylindrical jaws mounted at a fixed separation of 0.152 cm. between apexes. The radius of curvature of the jaws is 0.318 cm. By rotating the unit about an axis coincident with the mid-line of the opening between the jaws the effective slit width as presented to the beam can be varied from 0 to 0.152 cm. The usual width for the present experiments was 0.0076 cm.

The detector is a tungsten wire 0.0127 cm. in diameter with a slit in front of it of 0.010 cm. width. The ions that are formed by surface ionization are pulled off at right angles to the incident beam to a mass spectrometer. The ion optical system for this extraction is identical with that used by Braunstein and Trischka (1955). With this ion gun, although 80% of Rb ions formed on the tungsten wire could be pulled out of the gun, only 20% reached the collector of the mass spectrometer. The usual energy of the ions was about 1000 ev. No thorough attempt has been made to determine the exact cause for the loss of ions.

At the collector end of the mass spectrometer the ion current may be collected directly in a cage and measured on an electrometer circuit or it may be amplified by means of an electron multiplier and then measured on an electrometer circuit. The latter arrangement was the one usually used in the experiments.

The obstacle wire in the middle of the B field is a nylon filament of 0.051 cm. diameter. It is coated with colloidal graphite and maintained at a potential midway between those of the B field pole pieces.

IV. ELECTRONIC EQUIPMENT

In order to measure transitions to an accuracy of 1 part in 10^6 the microwave signal must be stable to about 1 part in 10^7 and its frequency purity

should be no worse than 1 in 10^6. A system fulfilling these requirements is shown in Fig. 6. Although this system is essentially the same as that used by Lee *et al.* (1953) and later by Stroke, Jaccarino, Edmonds, and Weiss (1957),

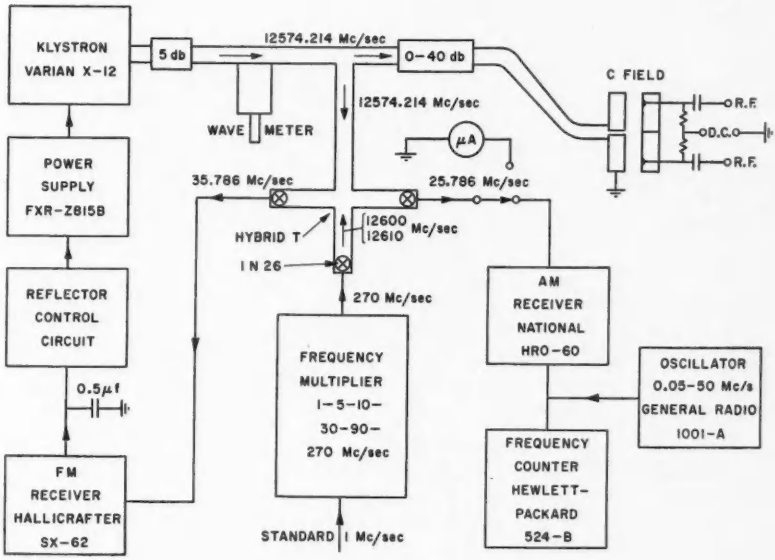

FIG. 6. The microwave system.

it is considered desirable to describe it here both for the sake of completeness and for the purpose of mentioning some details which may be of interest to anyone wishing to set up a similar system. The source of microwaves is a Varian X-12 klystron immersed in oil. For greater ease of understanding the operation of the system the klystron is shown generating a definite frequency of 12574.214 Mc./sec., which is actually the frequency of one of the lines observed. Part of the energy is fed to the C field through a series of attenuators, as shown. Part of the energy is fed into a hybrid tee where mixing with two reference frequencies takes place. The reference frequencies are obtained by crystal rectification of 270 Mc./sec. To obtain adequate power in the region of the 47th harmonic to permit operation of the negative feedback loop, a crystal current of about 10 ma. is necessary. The 270 Mc./sec. standard is obtained by mutiplications of a 1 Mc./sec. signal from a Primary Frequency Standard maintained by the Division of Applied Physics of this institution. The multiplier circuit is that given by Hedrick (1953). This circuit has provision for introducing sidebands into the output at 5, 10, 30, or 90 Mc./sec. from the 270 Mc./sec. Hence at the output of the crystal rectifier one can find the frequencies 12,600 Mc./sec. and 12,610 Mc./sec. With the former frequency the klystron signal produces a beat of 25.786

Mc./sec. and with the latter a beat of 35.786 Mc./sec. The 25.786 Mc./sec. signal is used simply for frequency measurement. That is, this beat frequency is measured precisely to yield the klystron frequency precisely. The 35.786 Mc./sec. signal is used for frequency control of the klystron. The FM receiver is tuned to this frequency and if the beat tends to drift from this frequency as a result of a drift in the klystron frequency an error voltage is produced which can be applied to the klystron reflector through the reflector control circuit to counteract the drift. The reflector control circuit is given in detail in Figure 8 of Stroke *et al.* (1957). With this circuit and a Hallicrafter SX-62 FM receiver it was found necessary to connect a 0.5 μf. condenser across the output of the FM discriminator in order to prevent the feedback system from oscillating.

The feedback system not only stabilizes the klystron frequency but also reduces its frequency spread. Without the feedback, the output of the Varian X-12 has a frequency spread of about 100 kc./sec.; with the feedback the spread is reduced to 15 kc./sec. The 100 kc./sec. spread cannot be ascribed to ripple in the power supply voltages; the heater of the klystron is operated from a storage battery and the 3 millivolt ripple in the beam and reflector voltages of the FXR Model Z 815B power supply is not sufficient to produce this spread. Furthermore the fundamental frequency of this noise is not 60 c./sec. but is variable between 65 and 70 c./sec.

It is difficult to determine just how stable a signal is which has a noise bandwidth of 15 kc./sec., but repeated measurements of a given signal have been found to yield results which agree to ±1 kc./sec. Thus the stability is at least 1 part in 10^7.

The 100 kc./sec. Primary Frequency Standard from which our 1 Mc./sec. standard is derived is always within 3 parts in 10^7 of the nominal frequency and is known to better than 1 in 10^8.

V. EXPERIMENT

Because RbF is highly deliquescent it was found necessary to dry it in an auxiliary vacuum system at 800°–900° K. before loading it in the oven. Even with this preliminary drying the substance was found to have a strong tendency to clog the slit, especially after the oven had been raised to the usual operating temperature of about 1030° K. The only way the writer found of avoiding the clogging was to load the oven very lightly. The usual charge was about 0.2 g. This was sufficient for several days' operation.

The beam intensities used in the measurements were about 4×10^{-10} amp. or 400,000 cm. of galvanometer deflection (1 cm. = 10^{-15} amp.). This was the intensity as measured at the tungsten wire detector and not at the end of the mass spectrometer. This intensity is considerably less than those used by others in similar experiments (cf. Lee *et al.* 1953; Fabricand *et al.* 1953; Trischka and Braunstein 1954). Attempts to increase the beam intensity were not very successful. Furthermore the attempts suggested that a thorough investigation into the reasons for the low intensities might be a long drawn-out affair. Hence, since transitions were already observable with the available

intensities, it was decided to proceed with the measurements and see how far one could get. It turned out that one could get most of the information desired but that the measurements would have been easier and the accuracy greater if greater intensities had been available.

Since the operating conditions of the tungsten wire have a direct bearing on the detected beam intensities, it is considered desirable to record them here. The tungsten wire was of commercial quality* 0.0127 cm. in diameter. Before being used for beam detection it was heated for several hours at around 890° C. in its normal mount in vacuum with a current of 1.0 amp. The above temperature and the 1500° C. mentioned below are temperatures as measured directly by means of an optical pyrometer and not corrected for emissivity. This gentle baking out removed most of the alkali impurities in the tungsten, as indicated by the ion current coming out of it, but did not remove more refractory impurities such as oxides. Then just prior to being used for beam detection the wire was flashed for a few seconds at 1500° C. with a current of 1.7 amp. and immediately returned to 890° C. at 1.0 amp. Immediately after flashing, the wire often showed a very high sensitivity, i.e. one in which over 1.2 million cm. of RbF was detected. The sensitivity usually dropped very rapidly after flashing and levelled off in about 20 minutes to a value roughly one-third the initial value. It was at this lower sensitivity that the experiment was done.† The flashing had to be repeated occasionally.

In the measurement of a line it was found difficult to plot a line shape because of fluctuations in the refocused beam. There were quiescent periods between fluctuations, however, which were of sufficient duration to permit a reasonably reliable determination of the peak of the transition. Hence all the results of the present work were obtained by repeated settings of the microwave oscillator on the peak of the line. Under the best of conditions and for the strongest lines, the signal-to-noise ratio was about 20 to 1. The line widths were estimated to be approximately 50 kc./sec. On the basis of the uncertainty principle the expected line width is 10 kc./sec. The large observed width probably arose partly from the inhomogeneity of the microwave signal and partly from the fact that perhaps more than the optimum power was required for the transitions.

VI. RESULTS AND DISCUSSION

A. *Observed Lines, Quadrupole Interaction*

In $Rb^{85}F$, rotational transitions belonging to three vibrational states $v = 0, 1, 2$ were observed, whereas in $Rb^{87}F$, lines belonging to the $v = 0$ state only were observed. These are all listed in Table II, without any correction for the contact potential of the C field. It is shown below that the correction amounts to only 400 c./sec. or well below the uncertainties of the measurements.

*"Elmet" brand by North American Philips Co., Lewiston, Maine.

†Experiments done after the measurements suggest that a thorough aging of the tungsten followed by oxidation may yield a detecting surface of constantly high sensitivity (Datz and Taylor 1956).

TABLE II

OBSERVED FREQUENCIES (MC./SEC.)
$(J = 1) \leftarrow (J = 0)$

Line	F_1 of $J = 1$ level	$v = 0$	$v = 1$	$v = 2$
		$Rb^{85}F$		
C	3/2	12595.316±0.005	12504.307±0.010	
B	7/2	12588.985±0.005	12498.054±0.010	
A	5/2	12574.214±0.005	12483.444±0.010	12393.058±0.010
		$Rb^{87}F$		
C	1/2	12541.181±0.010		
B	5/2	12534.381±0.010		
A	3/2	12525.870±0.010		

The quadrupole interaction constants in those cases in which all three of the hyperfine structure lines have been measured are given in Table III. For comparison the corresponding values found by Hughes and Grabner (1950) are also given. It is seen that these agree very well with our somewhat more accurate values.

TABLE III

VALUES OF $-eqQ/h$ FOR THE ROTATIONAL STATE $J = 1$ IN MC./SEC.

Molecule	Vibrational state	Present work	Hughes and Grabner
$Rb^{85}F$	0	70.340±0.030	70.31±0.10
	1	69.543±0.060	69.54±0.10
$Rb^{87}F$	0	34.024±0.040	34.00±0.06

$eqQ^{85}/eqQ^{87} = 2.0673 \pm 0.0030$.

From the ratio of the quadrupole interactions in the zeroth vibrational state in the two isotopic species we find for the ratio of the nuclear quadrupole moments of the Rb isotopes

$$Q^{85}/Q^{87} = 2.0673 \pm 0.0030.$$

This agrees with the more accurate value of 2.0669±0.0005 found by Trischka and Braunstein (1954) in their study of RbCl.

B. Rotational Constants

The positions of the rotational levels in the absence of hyperfine structure are easily determined in accordance with the patterns shown in Figs. 1 and 2. This can be done for the cases $v = 0$ and 1 in $Rb^{85}F$ and $v = 0$ in $Rb^{87}F$. For the vibrational state $v = 2$ of $Rb^{85}F$, however, since only one of the three hyperfine levels has been measured and the quadrupole interaction constant is not determinable, it is necessary to use Hughes and Grabner's value for this interaction constant, 68.71±0.10 Mc./sec. The rotational transition frequencies unperturbed by h.f.s. are then as shown in Table IV.

TABLE IV

CALCULATED ROTATIONAL TRANSITION FREQUENCIES IN THE ABSENCE OF HYPERFINE STRUCTURE (MC./SEC.)
$(J = 1) \leftarrow (J = 0)$

$Rb^{85}F$	$v = 0$	12585.468±0.010
	$v = 1$	12494.571±0.020
	$v = 2$	12404.052±0.026
$Rb^{87}F$	$v = 0$	12532.674±0.020

The various rotational constants calculated from the above frequencies are shown in Table V. The calculations required a knowledge of $Y_{10} \approx \omega_e$ and $Y_{20} \approx -\omega_e x_e$. From a study of the ultraviolet absorption spectra of

TABLE V

ROTATIONAL CONSTANTS (MC./SEC.)

	$Rb^{85}F$	$Rb^{87}F$
$Y_{01} \approx B_e$	6315.543±0.009	6289.002±0.010
$-Y_{11} \approx \alpha_e$	45.638±0.017	45.350±0.017
$Y_{21} \approx \gamma_e$	0.094±0.007	0.094±0.007
B_e	6315.639±0.036	6289.098±0.036

alkali halides, Barrow and Caunt (1953) give for RbF, $\omega_e = 390$ cm.$^{-1}$ and $\omega_e x_e = 1.3$ cm.$^{-1}$. Hence we find $Y_{02} = -4B_e^3/\omega_e^2 = -0.007$ Mc./sec. and, by formulae conveniently listed in Lee *et al.* (1953),

$$B_e = Y_{01} + (0.096 \pm 0.035) \text{ Mc./sec.}$$

The probable error in the added term above is based on an estimated 5% probable error in the spectroscopic value of ω_e and $\omega_e x_e$. Thus the quoted errors in B_e arise almost entirely from the errors in the vibrational constants.

In the case of $Rb^{87}F$, where only one vibrational state has been measured, it was necessary to assume $\alpha_e^{87} = (\mu_{85}/\mu_{87})^{3/2}\alpha_e^{85}$ and $Y_{21}^{87} = Y_{21}^{85}$, where the μ's are the reduced masses of the molecules.

C. Mass Ratio

The ratio of the masses of the Rb isotopes may be calculated from the relation (Fabricand *et al.* 1953)

$$\frac{M_{85}}{M_{87}} = \frac{(Y_{01}^{87}/Y_{01}^{85})(M_F/M_{87})}{1+(M_F/M_{87})-(Y_{01}^{87}/Y_{01}^{85})},$$

where M_F is the mass of the fluorine atom. Strictly speaking, in the above formula, the ratio of the Y_{01}'s should be replaced by the ratio of B_e's. However, these two ratios agree to within 1 part in 10^7 or well within the accuracy of our experiment. We find

$$M_{85}/M_{87} = 0.9770148 \pm 0.0000052.$$

For comparison, this and other measurements of the same ratio are shown

in Table VI. It seems the spectroscopic values are consistently lower than the mass spectroscopic value even though all the values overlap within the stated errors.

TABLE VI

MEASUREMENTS OF THE MASS RATIO OF THE Rb ISOTOPES

Method	Molecule	Ratio (M_{85}/M_{87})	Ref.*
Mass spectroscopy	—	0.9770191±0.0000022	(*a*)
Microwave absorption	RbI	0.9770177±0.0000045	(*b*)
	RbBr	0.9770146±0.0000055	(*b*)
Molecular beams	RbCl	0.9770163±0.0000045	(*c*)
	RbF	0.9770148±0.0000052	(*d*)

*(*a*) Collins, Nier, and Johnson (1951). (*b*) Honig *et al.* (1954). (*c*) Trischka and Braunstein (1954). (*d*) This work.

D. Internuclear Distance

The equilibrium internuclear distance of RbF calculated from B_e is

$$r_e = (2.26554 \pm 0.00005) \times 10^{-8} \text{ cm.},$$

where the uncertainty arises entirely from those in Planck's constant and the atomic mass unit (Cohen, Dumond, Layton, and Rollet 1955). This internuclear distance is somewhat larger than either of the values 2.225 and 2.246 given by Honig *et al.* (1954) on the basis of the simple additivity of ionic radii. However, the agreement is within the 1 or 2% accuracy claimed for the latter.

Honig *et al.* also give an empirical formula for internuclear distances involving the polarizabilities of the ions concerned and the electronegativities of the atoms. Using polarizabilities given by Rittner (1951) and electronegativities given by Pauling (1940) we obtain a value of 2.2545 Å. This is only $\frac{1}{2}$% lower than the experimental value. This agreement suggests that the empirical formula is a good one to use to predict the B_e values of alkali halides which have not yet been measured.

E. Electric Dipole Moment

For the determination of the electric dipole moment of RbF in the $v = 0$ state the Stark effect of the 12595.316 Mc./sec. line was studied. This line was chosen for reasons given in Section II. Static voltages of up to 20 volts were applied to the C field in which the gap was 0.69065 cm. The shift in the frequency of the line was measured with the static voltage first in one direction and then in the other. Typical shifts are, for $V_c = +20.00$ volts, $\Delta f = (0.461 \pm 0.006)$ Mc./sec. and for $V_c = -20.00$ volts, $\Delta f = (0.407 \pm 0.010)$ Mc./sec. The difference in the frequency shifts is of course due to the contact potential of the C field. From the measurements it is calculated that the contact potential of the aluminized surface coated with silicon dioxide relative to the brass surface is $+(0.61 \pm 0.05)$ volts. The electric dipole moment of $Rb^{85}F$ in the $v = 0$ state is then found to be, by Eq. 2,

$$\mu = (8.80 \pm 0.10) \times 10^{-18} \text{ e.s.u.}$$

Rittner gives an expression for the dipole moment of an alkali halide involving the polarizabilities of the ions. This relation yields a value of 7.96×10^{-18} e.s.u. The calculated value is thus lower than the experimental value, a relationship which is consistent with what is observed in all alkali halides for which the dipole moments are known.

It is easily seen that the contact potential of 0.61 volt introduces a negligible error in the measurements of the lines at "zero" C field. The energies of the Stark levels of a molecule in the $^1\Sigma$ state do not depend, to first order, on the electric field when this field is small. Among the levels with which we are concerned the one with the highest second-order dependence on the external field is the $J = 0$ level. At a field of 0.883 volt/cm. corresponding to a potential of 0.61 volt, the shift in the $J = 0$ level of RbF is only 0.0004 Mc./sec., which is well below the limit of detection in the present experiment.

ACKNOWLEDGMENTS

The authors wish to acknowledge with thanks the continued encouragement and assistance of Drs. G. Herzberg, A. E. Douglas, and C. C. Costain of this institution both during the construction of the apparatus and during the course of the experiment. Thanks are also due to Drs. R. O. Carlson and J. W. Trischka for helpful suggestions on the art of using a tungsten wire for the detection of alkali halides.

REFERENCES

BARROW, R. F. and CAUNT, A. D. 1953. Proc. Roy. Soc. (London), A, **219**, 120.
BRAUNSTEIN, R. and TRISCHKA, J. W. 1955. Phys. Rev. **98**, 1092.
COHEN, E. R., DUMOND, J. M. W., LAYTON, T. W., and ROLLET, J. S. 1955. Revs. Modern Phys. **27**, 363.
COLLINS, T. L., NIER, A. O., and JOHNSON, W. H. 1951. Phys. Rev. **84**, 717.
DATZ, S. and TAYLOR, E. H. 1956. J. Chem. Phys. **25**, 389, 395.
DUNHAM, J. L. 1932. Phys. Rev. **41**, 721.
FABRICAND, B. P., CARLSON, R. O., LEE, C. A., and RABI, I. I. 1953. Phys. Rev. **91**, 1403.
FANO, U. 1948. Natl. Bur. Standards (U.S.), J. Research, **40**, 215.
HEDRICK, L. C. 1953. Rev. Sci. Instr. **24**, 565.
HONIG, A., MANDEL, M., STITCH, M. L., and TOWNES, C. H. 1954. Phys. Rev. **96**, 629.
HUGHES, H. K. 1947. Phys. Rev. **72**, 614.
HUGHES, V. and GRABNER, L. 1950. Phys. Rev. **79**, 314.
LEE, C. A., FABRICAND, B. P., CARLSON, R. O., and RABI, I. I. 1953. Phys. Rev. **91**, 1395.
PAULING, L. 1940. Nature of the chemical bond, 2nd ed. (Cornell University Press, Ithaca, N.Y.).
RITTNER, E. S. 1951. J. Chem. Phys. **19**, 1030.
STROKE, H. H., JACCARINO, V., EDMONDS, D. S., and WEISS, R. 1957. Phys. Rev. **105**, 590.
TOWNES, C. H. and SCHAWLOW, A. L. 1955. Microwave spectroscopy (McGraw-Hill Book Company, Inc., New York).
TRISCHKA, J. W. and BRAUNSTEIN, R. 1954. Phys. Rev. **96**, 968.

MASS SPECTROMETRIC ANALYSIS OF SOME HYDROGEN OXIDES. I[1]

LARKIN KERWIN AND MAURICE COTTIN[2]

ABSTRACT

Typical mass spectrograms for H_2O, D_2O, H_2O_2, and D_2O_2 are presented. Both positive and negative ions were observed. The variations of the abundances of the spectrogram components with pressure are given. Some features of the experimental data are discussed.

1. INTRODUCTION

The mass spectrometric investigation of the hydrogen oxides presents considerable experimental difficulty. Water has been studied by several workers, including Smyth and Mueller (1933), and Mann, Hustrulid, and Tate (1940) in which reference is made to other papers. Hydrogen peroxide has recently been studied by Robertson (1952). No systematic investigations of heavy water and deuterium peroxide have appeared in the literature, although Washburn, Berry, and Hall (1953) have made a careful study of the precautions to be taken when measuring the small quantities of D_2O present in natural water. Certain hydrogen–oxygen ions and free radicals have been the subject of close scrutiny, and papers by Foner and Hudson (1956) and the works cited therein are typical of results on such species as HO_2 and OH. Negative ions have received much less attention than positive ions.

We have begun a mass spectrometric study of water, heavy water, hydrogen peroxide, and deuterium peroxide. In this paper, we report the mass spectrograms obtained and the variation of the ion abundances as a function of pressure. The second part of the investigation dealing with appearance potentials and dissociation energies will be reported later.

2. EXPERIMENTAL

It is usual to improve the ion yield of a mass spectrometer source by causing the ionizing electrons to move in spiral paths, which effect is obtained by placing the source in a magnetic field. When the spectrometer fields are reversed for analyzing negative ions, the source field must be reversed as well, and even this does not usually eliminate the need for refocusing the ion beam. In addition, reversal of the source field inevitably affects the efficiency of the source, making comparisons difficult. In modifying our inflection spectrometer for studying negative ions the source magnets were removed. The inherent high intensity of the instrument (Kerwin 1950) resulted in the beam intensity still being sufficient to yield useful information. It was not necessary to reset the focusing controls, and positive and

[1]Manuscript received October 1, 1957.
Contribution from the Département de Physique, Université Laval, Québec, Que.
[2]On leave from L'Institut du Radium, Paris.

negative ions could be analyzed in rapid succession while source and sample characteristics remained constant.

The nature of the samples analyzed required meticulous avoidance of impurities in the pyrex sampling system. This was kept as short as possible. After repeated cleaning with fuming H_2SO_4, the glass was heated to the softening point. This last step was essential in preventing decomposition of the peroxides. The samples were introduced directly from the pyrex line into the ionizing electron beam. Two stopcocks in the line were greased with Dow Corning silicone grease. This, and the conditioning of the spectrometer source by flushing with deuterium oxide vapor before runs, minimized deuterium exchange with hydrogen from adsorbed water in the sample line during runs. These precautions are similar to those recommended by Washburn *et al.*

All of the samples were in liquid form. Vapor pressure was controlled in part by varying the sample line leak diameter, and in part by varying the temperature of the liquid samples. These were immersed in dry ice – acetone baths, melting ice, or mixtures of the two. Sometimes reproducible runs could be obtained at intermediate pressures by allowing the sample to warm slowly from one type of bath to another. The pressures reported were measured by several gauges, and represent the pressure in the ionizing region to within a probable factor of two.

The spectrometer was usually operated with a 100 ev. ionizing current of 10 μa. Positive and negative ions were detected with a vibrating reed electrometer. At 10^{-4} mm. Hg, the main spectrum components provided ion currents of about 10^{-10} amp., the smaller components currents of about 10^{-14} amp.

For a typical analysis, several runs were made on each of several successive days. Many such runs on the peroxides were rejected because slight decomposition from day to day altered the spectrogram significantly. The sample line would then be cleaned as described until the spectrogram could be repeated over a several-day period. The results presented here are composites of two series made at 3-month intervals, each series being composed of several runs considered acceptable as described. The spectra are considered typical of ordinary instrumental variations, all acceptable runs made over a period of months fitting them to within about 10%.

3. MASS SPECTROGRAMS

The first four figures show typical mass spectrograms of the species investigated. Their liquid purity was: water (distilled), heavy water (about 80% D), hydrogen peroxide (99.2% peroxide), deuterium peroxide (over 99% peroxide, and 99% D). These samples were graciously furnished by Professor Paul-A. Giguère.

The percentage abundance is referred to the total of all ion currents observed. The shaded portion of the abundance bars represents the variation in abundance with pressure from 10^{-4} mm. Hg to 10^{-6} mm. Hg. Therefore typical spectrograms obtained within this pressure range should fall within the shaded portion. The corresponding abundances for water reported by Mann, Hustrulid, and Tate are indicated. The expansion of the negative

ion abundance scale is to be noted. With each figure are listed the ions considered as corresponding to the various masses, in order of increasing mass. Except where noted, molecules containing O-18 were not considered as contributing significantly to peaks.

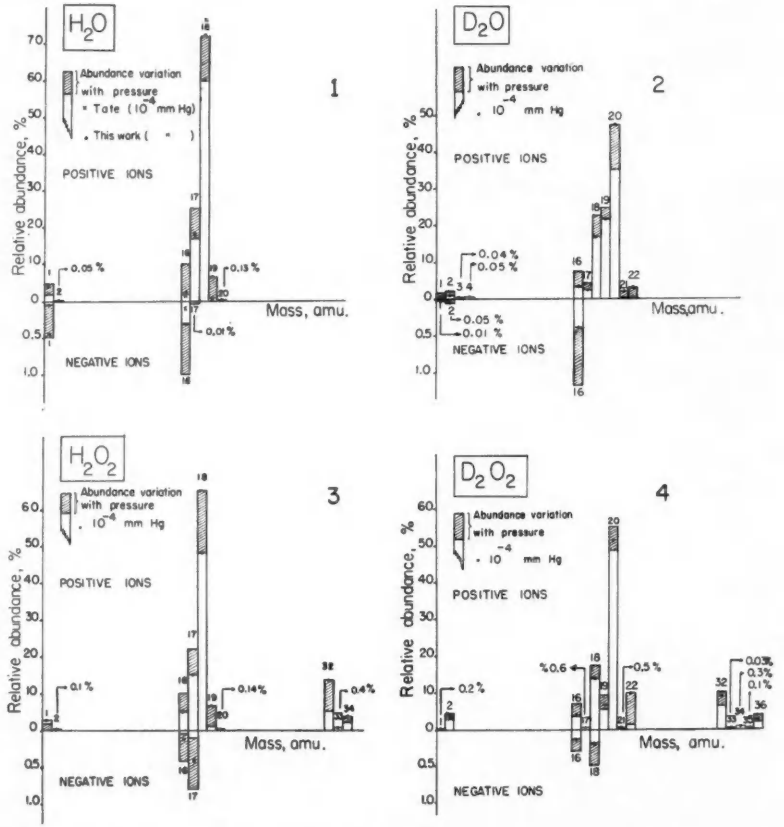

FIG. 1. Mass spectrogram of water. Ions considered observed: H^+, H_2^+, O^+, OH^+, H_2O^+, H_3O^+, and H_2O^+ (isotopic O-18); H^-, O^-, and OH^-.

FIG. 2. Mass spectrogram of heavy water. Ions considered observed: H^+, H_2^++D^+, DH^+, D_2^+, O^+, OH^+, H_2O^++DO^+, DHO^+, D_2O^+, D_2HO^+, and D_3O^+; H^-, D^-, and O^-.

FIG. 3. Mass spectrogram of hydrogen peroxide. Ions considered observed: H^+, H_2^+, O^+, OH^+, H_2O^+, H_3O^+, H_2O^+ (isotopic O-18), O_2^+, HO_2^+, and $H_2O_2^+$; O^-, and OH^-.

FIG. 4. Mass spectrogram of deuterium peroxide. Ions considered observed: H^+, H_2^++D^+, O^+, OH^+, H_2O^++OD^+, DHO^+, D_2O^+, D_2HO^+, D_3O^+, O_2^+, HO_2^+, DO_2^+, DHO_2^+, and $D_2O_2^+$; O^-, and DO^-.

4. ABUNDANCE VARIATIONS WITH PRESSURE

Figs. 5 and 6 show the variation of the major ion abundances as a function of pressure. In Fig. 5 are grouped the light and heavy waters, in Fig. 6, the

light and heavy peroxides. Thus in Fig. 5, the curve labelled H^+ also represents D^+, that labelled H_3O^+ also represents D_3O^+, D_2HO^+, and DH_2O^+, and so on for the other species.

The calculations involved for separating the effects of these species are simple but lengthy. As an example, from a spectrogram of heavy water such as is given in Fig. 2, peaks 21 and 22 may be ascribed to D_2HO^+ and D_3O^+, since no other hydrogen–oxygen ions may be considered at these masses. We let the deuterium abundance equal d, and the hydrogen abundance $(100-d)$. Now the D_2HO^+ ion may be present as DDHO, DHDO, or HDDO. Accordingly its abundance will be proportional to $3d^2(100-d)$. The abundance of the D_3O^+ ion will be proportional to d^3. We therefore have:

$$\frac{3d^2(100-d)}{d^3} = \frac{\text{abundance mass 21}}{\text{abundance mass 22}}.$$

From this equation d may be calculated to somewhat low precision, e.g. about 80%. However, the figures obtained serve to establish that peak 19 must be caused effectively by DHO^+, since H_3O^+ makes a negligible contribution, while peak 20 is caused by D_2O^+, the form DH_2O^+ being eliminated for the same reason. The value of d may then be established with more precision from these two peaks by the appropriate equation. For the 10^{-4} mm. Hg values illustrated in Fig. 2, $d = 79.9\%$. Finally, the contributions of the various ions to each mass peak may be calculated.

In this way it was shown that in general no isotopic effect was observed in the abundance–pressure relationships. Some particular effects that seem

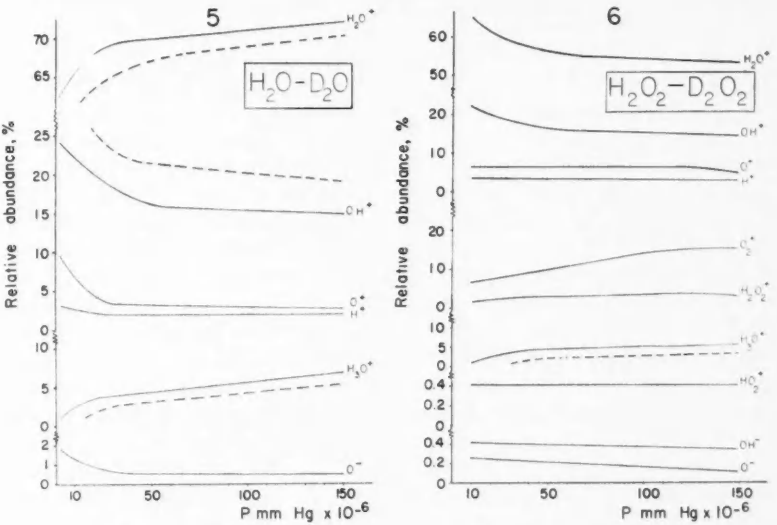

FIG. 5. Ion abundance as a function of pressure, water and heavy water.
FIG. 6. Ion abundance as a function of pressure, hydrogen peroxide and deuterium peroxide.

established will be mentioned later. Except for these, the curves of Figs. 5 and 6 represent the behavior of the isotopic variations of a given ion. The sum of the component abundances at a given pressure does not always equal exactly 100% because the curves are averages of many runs. The reproduction of the curves for the waters is somewhat better than that for the peroxides.

5. DISCUSSION

(*a*) *Water*

The type and abundance of the ions observed (Fig. 1) are essentially the same as those found by Mann *et al.*, with the exception of the low-abundance OH^- which they did not observe. Massey (1950) reported that Sloan and Love have observed OH^- in the residual gas background of their spectrometer. Smyth and Mueller also observed this ion. We found no HO_2^+, even when oxygen was mixed with water vapor in the source, although an abundance of 0.01% would have been detected.

At low pressures the decomposition of water into OH^+ and H^+ is relatively greater than at high pressures (Fig. 5) and it was verified that this was not a result of any variations in the ionizing current. The hydroxonium ion H_3O^+ increases in abundance as the square of the pressure (thus its percentage abundance increases linearly) as was observed by Smyth and Mueller, and Mann *et al.* In a few experiments at very high pressure (filament life was drastically curtailed) it was possible to obtain hydroxonium abundances as high as 100% of the parent H_2O^+ peak. This supports the view of Lefort (1954) that H_3O^+ would be one of the most abundant ions in radiolized liquid water. The variation of the ion abundance with the square of the pressure indicates formation by secondary reaction (Smyth and Mueller):

$$H_2O^+ + H_2O \rightarrow H_3O^+ + OH.$$

(*b*) *Heavy Water*

The D_2O spectrogram (Fig. 2) indicated essentially the same species of ions as were formed from water. When the various isotopic versions are separated out as described in Section 4, the calculated mass spectrogram of pure heavy water may be obtained, and is shown in Fig. 7.

This is seen to be similar to Fig. 1 for H_2O, with the exception of OD^- at mass 18, whose abundance was less than the limit of sensitivity of the apparatus, as may be calculated from the D content of the sample.

The variation in ion abundance with pressure was essentially the same as for water (Fig. 5) with the exception of the following small effects. The D_3O^+ concentration in the 'pure' heavy water spectrogram was about one-half that of the H_3O^+ concentration in the ordinary water spectrogram. This was true over the pressure range described. A second systematic effect indicated that the D_2O^+ ion abundance was about 5% lower than the corresponding H_2O^+ abundance, with the DO^+ abundance being correspondingly higher than the HO^+ abundance. These effects are indicated by dotted lines in Fig. 5.

(*c*) *Hydrogen Peroxide*

The higher-purity peroxide furnished by Professor Giguère gave about 96%

peroxide in the vapor phase. The relative abundance of the ions (Fig. 3) agrees roughly with those reported by Robertson, who did not give his complete spectrum in his paper, so that a peak-by-peak comparison is not possible.

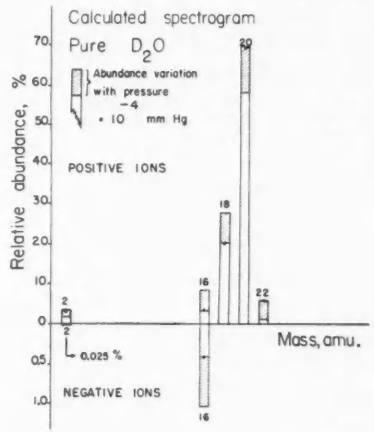

FIG. 7. Calculated mass spectrogram, pure D_2O.

Our spectrum for the O_2^+, HO_2^+, $H_2O_2^+$ group (32, 33, 34) corresponds to his but is about seven times more abundant compared with the H_2O^+ peak, indicating less spontaneous (non-electron-impact) dissociation in our instrument. Robertson states that he obtained much dissociation and oxidation of metal in his source.

The HO_2^+ ion appears in relatively high concentration—about 10% of the $H_2O_2^+$ ion. Foner and Hudson reported the ion as being 1% of the peroxide ion abundance when using a discharge source with water vapor mixed with the peroxide.

No negative hydrogen ions were found, doubtless because of lack of sensitivity. The OH^- ion was about twice as high as the O^- ion, while in the H_2O–D_2O analyses, OH^- was only about 1% of the O^- peak. This supports the generally-held view that the peroxide is most prone to division into 2(OH) as the primary step in its dissociation.

The pressure–abundance curves (Fig. 6) are essentially linear, except for the decrease in H_2O^+ and OH^+ abundance with pressure. The H_3O^+ ion increases with the square of the pressure as before.

(d) Deuterium Peroxide

The ions considered observed are listed under Fig. 4, from which the very low hydrogen content of the sample is apparent. Noteworthy are the peaks D_2HO^+ and D_3O^+ at 21 and 22, and the HO_2^+ and DO_2^+ peaks at 33 and 34. When the various ion species are separated out of Fig. 4 as indicated in Section 4, the calculated spectrogram for 'pure' deuterium peroxide may be obtained, and this is shown in Fig. 8.

Once again, no H^- ion was observed, because of lack of sensitivity. OD^- was as relatively abundant as the corresponding OH^- in the peroxide spectrum.

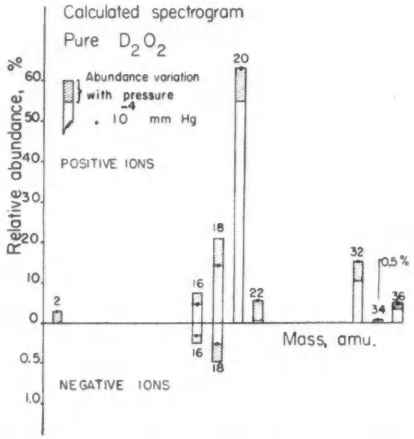

FIG. 8. Calculated mass spectrogram, pure D_2O_2.

The variation in ion abundance with pressure was essentially the same as for hydrogen peroxide. The isotope effect on hydroxonium formation was noted, but the effect on the D_2O^+ and DO^+ peaks was absent, to within the precision of the experiment.

6. CONCENTRATION OF O-18

The D_2O_2 used in these experiments is manufactured in an electrodeless discharge (Giguère, Secco, and Eaton 1953). The microwave spectrum of this heavy peroxide produced a great array of lines (Massey 1952; see also Massey 1954) and it has been suggested that these might have been caused by a concentration of the oxygen-18 isotope in the discharge. A careful examination of the mass spectrograms indicates that the concentration, if present, does not exceed a factor of three, i.e. the abundance of O-18 would be less than 0.7% of the O-16 isotope abundance.

ACKNOWLEDGMENTS

Grateful appreciation is extended to Dr. Don McElcheran for assistance with this research. Mr. David Chin of the Chemistry Department prepared several of the samples. Professor Paul A. Giguère was helpful throughout the work and during the preparation of the manuscript.

This program of research is supported by the Centre de Recherches of the Physics Department, the Defence Research Board (Grant 9510-13), and the National Research Council (Grant T-45). To all, our sincere thanks.

REFERENCES

FONER, S. N. and HUDSON, R. L. 1956. J. Chem. Phys. **25**, 601.
GIGUÈRE, PAUL A., SECCO, E. A., and EATON, R. S. 1953. Discussions Faraday Soc. **14**, 104.
KERWIN, L. 1950. Rev. Sci. Instr. **21**, 96.
LEFORT, M. 1954. J. chim. phys. **51**, 351.
MANN, M. M., HUSTRULID, A., and TATE, J. T. 1940. Phys. Rev. **58**, 340.
MASSEY, H. S. W. 1950. Negative ions (Cambridge University Press), p. 3.
MASSEY, J. T. 1952. Private communication to Professor Giguère.
——— 1954. J. Chem. Phys. **22**, 442.
ROBERTSON, A. J. B. 1952. Trans. Faraday Soc. **48**, 228.
SMYTH, H. D. and MUELLER, D. W. 1933. Phys. Rev. **43**, 116.
WASHBURN, H. W., BERRY, C. E., and HALL, L. G. 1953. Natl. Bur. Standards, Circular 522 (Washington, D.C.), p. 141.

ON VOLTERRA'S DISLOCATIONS IN A SEMI-INFINITE ELASTIC MEDIUM[1]

J. A. STEKETEE

ABSTRACT

In this paper a Green's function method is developed to deal with the problem of a Volterra dislocation in a semi-infinite elastic medium in such a way that the boundary surface of the medium remains free from stresses. (A Volterra dislocation is here defined as a surface across which the displacement components show a discontinuity of the type $\Delta\mathbf{u} = \mathbf{U} + \mathbf{\Omega} \times \mathbf{r}$, where $\mathbf{U}$ and $\mathbf{\Omega}$ are constant vectors.) It is found that the general problem requires the construction of six sets of Green's functions. The method for the construction is outlined and applied to one of the six sets, which is of the type of two double forces with moments in a plane parallel with the boundary. The displacement field thus generated is computed. Several of the results obtained are believed to be of geophysical interest, but a more detailed discussion of these applications is postponed to a further communication which is being prepared.

1. INTRODUCTION

In the orogenetic considerations of J. T. Wilson and A. E. Scheidegger an important part is played by island arcs and arcuate structures in mountain ranges. It is supposed that these arcuate structures are the surface representations of fracture zones in the orogenetic shell. These fracture zones, along which the foci of earthquakes are to be found, have been described on different occasions by the above authors (Wilson 1954; Scheidegger 1953) and others (compare Umbgrove 1954). It has been suggested by the author (Steketee 1955) that Volterra's theory of dislocations might be the proper tool for a more quantitative description of these fracture zones.[2] This suggestion was not made without reason. If the mechanism involved in earthquakes and the fracture zones is indeed one of fracture, there will exist discontinuities in the displacement components across the fractured surfaces. As dislocation theory may be described as that part of the theory of elasticity dealing with surfaces across which the displacement components are discontinuous, the suggestion seems reasonable.

Another argument is that in the last 20 years dislocation theory has become of major importance in solid state physics, and it should therefore not be excluded that also in geophysics it may be of some importance. Finally it was realized that the mathematical structure of dislocation theory is analogous to certain parts of potential theory in the sense that the first theory deals with the Navier equations and the second with the Laplace equation. In view of the many applications of potential theory in physics it was again felt that dislocation theory might be of some use in geophysics.

[1]Manuscript received October 21, 1957.

Contribution from the Department of Applied Mathematics, University of Toronto, Toronto 5, Ontario.

[2]Similar suggestions have been made at other places and similar times; the referee kindly informed me that G. W. Housner applied dislocations to earthquake faulting in 1953 (Housner 1955), while for example Dr. Kevlis-Borok in Moscow and Dr. Knopoff in California were probably working on similar problems at the time.

Rochester (1956) was the first one to obtain practical results with this theory when he worked out an example referring to the San Andreas fault in California. His results seemed to justify further work along these lines.

As usual in mathematical physics, it is necessary for simplicity's sake to omit certain features from reality and to retain only those which are expected to be of principal importance. We omit therefore the curvature of the earth, its gravity, temperature, magnetism, and non-homogeneity, and shall deal with a semi-infinite medium, homogeneous and isotropic, assuming further the laws of the classical linear elasticity theory.

The usual boundary conditions for dealing with the earth's problems require that the surface S of the elastic medium (the earth) shall be free from forces.

To solve this boundary-value problem for the case that a dislocation is present in the medium, Volterra (1907) has given the following method: First compute the stresses and displacements in an infinite elastic medium due to the dislocation, in particular compute the forces on S. Then consider the ordinary boundary-value problem for the elastic body with surface S, where the surface is subjected to forces equal and opposite to the ones obtained before. Superposition of the two solutions will give the required result with a dislocation in the elastic body and no normal or tangential forces on its surface.

It is clear that with this method for each new type of dislocation a new boundary-value problem has to be considered. Although the solution of this boundary-value problem does not offer fundamental difficulties in the case of the semi-infinite medium, the computations one has to face are complex so that for example in Rochester's work the ordinary boundary-value problem could only be solved approximately.

It will be the purpose of the following investigation to develop a Green's function method for the calculation of dislocations in a semi-infinite medium. The construction of these Green's functions is simple compared with the problems faced when following the method of Volterra. Once these functions are obtained, the problem of an arbitrary dislocation in the semi-infinite medium is reduced to the computation of certain surface integrals. If approximations have to be made, it can be done in these integrals in the final stage of the problem.

While the work contained in this paper was undertaken with the geophysical problem in mind, we shall be largely concerned here with the elasticity problem. It is expected to give some geophysical applications in a later communication.

In Sections 2 and 3 we deal with the theory of dislocations in an infinite elastic medium. In Section 4 the boundary-value problem is discussed and the method for the construction of the Green's functions is outlined. In Sections 5 and 6 some parts of the construction are dealt with in greater detail. Finally the method is applied in Section 7 to one of the six groups of Green's functions.

2. VOLTERRA'S THEORY OF DISLOCATIONS

Let O be the origin of a Cartesian frame of reference in an infinite elastic medium, x_i the Cartesian coordinates ($i = 1, 2, 3$), and $\mathbf{e}_i$ a unit vector in the positive x_i-direction. A force $\mathbf{F} = F\mathbf{e}_k$ at O, compensated by continuously dis-

tributed forces at infinity to establish equilibrium, generates a displacement field $u_i^k(P, O)$ which is determined by the well-known Somigliana tensor

$$u_i^k(P, O) = \frac{F}{8\pi\mu}(\delta_{ik} r_{,nn} - \alpha r_{,ik}). \tag{2.1}$$

In this relation δ_{ik} is the Kronecker delta, $\alpha = (\lambda+\mu)/(\lambda+2\mu)$, λ and μ are Lamé's constants, r is the distance from $P(x_j)$ to O. Further $r_{,i} = \partial r/\partial x_i$ and the summation convention applies. If the force is located in $Q(y_j)$ we have $r^2 = (x_j - y_j)^2$ and $\partial r/\partial x_i = -\partial r/\partial y_i$. It will be convenient to assume the constant $F/8\pi\mu$ equal to *one*. The dimension of this constant is $[L^2]$, so that the formula (2.1) gives indeed a displacement with the proper dimension.

The stresses due to the displacement field (2.1) are easily computed from the general relation

$$\tau_{ij} = \lambda\delta_{ij}u_{k,k} + \mu(u_{i,j} + u_{j,i}). \tag{2.2}$$

We find

$$\tau_{ij}^k(P, O) = 2\mu(1-\alpha)\left(\delta_{ij}\frac{x_k}{r^3} - \delta_{jk}\frac{x_i}{r^3} - \delta_{ik}\frac{x_j}{r^3}\right) - 6\alpha\mu\frac{x_i x_j x_k}{r^5}. \tag{2.3}$$

Further we denote the components of the force per unit area on a surface element, following Sokolnikoff and Specht (1946), as

$$\overset{\nu}{T}{}_i^k = \tau_{ij}^k \cdot \nu_j \tag{2.4}$$

where the ν_j's are the direction cosines of the normal to the surface element. A Volterra dislocation is defined as a surface Σ in the elastic medium across which there is a discontinuity Δu_i in the displacement components of the type

$$\begin{cases} \Delta u_i = u_i^+ - u_i^- = U_i + \Omega_{ij}x_j, \\ \Omega_{ij} = -\Omega_{ji}. \end{cases} \tag{2.5}$$

The formula (2.5) in which U_i and Ω_{ij} are constants is the well-known Weingarten relation which states that the discontinuity Δu_i should be of the type of a rigid body displacement, thereby maintaining continuity of the components of stress and strain across Σ. It is also clear that the edge of Σ will be a singularity as the displacement is essentially indeterminate.

The displacement field in an infinite elastic medium due to a dislocation of type (2.5) is then determined by the relation of Volterra (1907) (compare Bergman and Schiffer 1953, pp. 219–222):

$$u_k(y_l) = \frac{1}{8\pi\mu}\iint_\Sigma \Delta u_i \, \overset{\nu}{T}{}_i^k \, d\Sigma, \tag{2.6}$$

where $\overset{\nu}{T}{}_i^k$ is the i-component of the force per unit area on a surface element $d\Sigma$ containing the point $P(x_j)$ due to a force $8\pi\mu\mathbf{e}_k$ in $Q(y_l)$. The dimension of the constant in front of the integral is $[M\ L^{-1}\ T^{-2}]$ so that the formula gives the proper dimension for u_k.

Once the surface Σ is given, the dislocation is essentially determined by the six constants U_i and Ω_{ij}. We write therefore also:

$$(2.7)\quad u_k(y_l) = \frac{U_i}{8\pi\mu}\iint_{\Sigma}\tau_{ij}^{k}(P, Q)\,\nu_j\,d\Sigma + \frac{\Omega_{ij}}{8\pi\mu}\iint_{\Sigma}\{x_j\tau_{il}^{k}(P, Q)-x_i\tau_{jl}^{k}(P, Q)\}\nu_l\,d\Sigma,$$

where Ω_{ij} takes only the values Ω_{12}, Ω_{23}, Ω_{31}. Following Volterra (1907) and Love (1944) we call each of the six integrals in (2.7) an elementary dislocation ("Distorsion élémentaire").

It is clear from (2.6) and (2.7) that the computation of the displacement component $u_k(Q)$ is performed as follows: A force $8\pi\mu\mathbf{e}_k$ is put in Q, and the stresses $\tau_{ij}^{k}(P, Q)$ which this force generates are computed in the points $P(x_i)$ on Σ. In particular the components of the force on Σ are computed. After multiplication with prescribed weights of magnitude Δu_i these forces are integrated over Σ to give the displacement component in Q due to the dislocation on Σ. We shall later see that a different interpretation is possible which will turn out to be more practical.

3. FURTHER DEVELOPMENTS, SYMMETRY PROPERTIES

Once the displacement field $u_k(Q)$ has been obtained, the stresses can be found by differentiating to y_l according to (2.2). If the point $Q(y_l)$ is not on Σ, these differentiations can be performed in general under the integration sign where the variables x_l-y_l appear in τ_{ij}^{k}. We obtain then for points not on Σ

$$(3.1)\quad \tau_{kl}(Q) = \frac{U_i}{8\pi\mu}\iint_{\Sigma}G_{ij}^{kl}\nu_j d\Sigma + \frac{\Omega_{ij}}{8\pi\mu}\iint_{\Sigma}(x_jG_{in}^{kl}-x_iG_{jn}^{kl})\nu_n d\Sigma$$

where

$$(3.2)\quad G_{ij}^{kl}(P, Q) = \lambda\delta_{kl}\tau_{ij}^{n,n}+\mu(\tau_{ij}^{k,l}+\tau_{ij}^{l,k})$$

and

$$(3.3)\quad \tau_{ij}^{k,l} = \frac{\partial\tau_{ij}^{k}}{\partial y_l} = -\frac{\partial\tau_{ij}^{k}}{\partial x_l} = -\tau_{ij,l}^{k}.$$

Writing out the expression (3.2) for the case that Q is the origin, we obtain

$$(3.4)\quad -G_{ij}^{kl}(P, O) = 4\mu^2(2-3\alpha)\frac{\delta_{ij}\delta_{kl}}{r^3} - \frac{4\mu^2(1-\alpha)}{r^3}\{\delta_{ik}\delta_{jl}+\delta_{jk}\delta_{il}\}$$
$$-12\mu^2(1-\alpha)\left\{\delta_{kl}\frac{x_ix_j}{r^5}+\delta_{ij}\frac{x_kx_l}{r^5}\right\}+60\alpha\mu^2\frac{x_ix_jx_kx_l}{r^7}$$
$$+3\mu^2(1-2\alpha)\left\{\delta_{ik}\frac{x_jx_l}{r^5}+\delta_{il}\frac{x_jx_k}{r^5}+\delta_{jk}\frac{x_ix_l}{r^5}+\delta_{jl}\frac{x_ix_k}{r^5}\right\}.$$

It is immediately noticed that this expression does not change if:

(i) i and j are interchanged,
(ii) k and l are interchanged,
(iii) ij and kl are interchanged.

These symmetry properties reduce the number of different components of $G^{kl}_{ij}(P, Q)$ from 81 to 21. So far we have considered $\tau^k_{ij}(P, Q)$ as the stress tensor in P generated in an infinite elastic medium by a force $8\pi\mu\mathbf{e}_k$ in Q. For what follows it is necessary to consider $\tau^k_{ij}(P, Q)$ in a different way.

Inspection of (2.7) and (3.1) shows that the subscripts in τ^k_{ij} and G^{kl}_{ij} are determined by the given dislocation. In the simplest possible case, an elementary dislocation with only one of the U_i's different from zero, the three Ω_{ij}'s equal to zero, and Σ part of a plane perpendicular to a coordinate axis, there is only one set of subscripts ij. We also observe that the displacement and stress components in Q have subscripts which correspond with the superscripts in τ^k_{ij} and G^{kl}_{ij}. This suggests that τ^k_{ij} and G^{kl}_{ij} with fixed i and j should be considered respectively as displacement and stress components, giving altogether six different displacement and stress fields. To make this dimensionally correct we should consider $(U_i/\mu)\tau^k_{ij}$ as a displacement field, but for simplicity of argument we shall omit this refinement, and refer to τ^k_{ij} as displacement field.

That each of the displacement fields $\tau^k_{ij}(P, Q)$ considered either as function of $Q(y_i)$ with $P(x_i)$ fixed, or as function of $P(x_i)$ with $Q(y_i)$ fixed, satisfies the Navier equations

$$(\lambda+\mu)u_{j,ji}+\mu u_{i,jj} = 0 \tag{3.5}$$

everywhere, except when P and Q coincide, follows immediately from the symmetry in the suffixes of the Somigliana tensor, the linearity of (2.2), the homogeneity and linearity of (3.5), and the symmetry of the variables x_i-y_i.

To clear up further the nature of the displacement field $\tau^k_{ij}(P, Q)$, we turn back to the displacement field (2.1). This may be considered for fixed i and variable k as the displacement field in Q due to a force $8\pi\mu\mathbf{e}_i$ in P. This expression (2.1) and other displacement fields $u^{k,l}_i$ are usually referred to as nuclei of strain (Love 1944). For $i = l$ we have a double force without moment; for $i \neq l$ it is a double force with moment; if we have $i = l$ and sum over the range ($i = 1, 2, 3$) it is called a center of compression.

It follows that $\tau^k_{ij}(P, Q)$, which may be written

$$\tau^k_{ij}(P, Q) = -\lambda\delta_{ij}u^{k,l}_l-\mu(u^{k,j}_i+u^{k,i}_j), \tag{3.6}$$

may be considered as the displacement field due to some combinations of nuclei of strain; in the case $i = j$ this is a center of compression and an additional double force without moment; in the case $i \neq j$, it is a combination of two double forces with moment.

The displacement $u_k(Q)$ in (2.6) and (2.7) can therefore be considered as being generated by a distribution of these combinations of strain nuclei over the surface Σ of the dislocation.

4. THE BOUNDARY VALUE PROBLEM, THE GREEN'S FUNCTIONS

The relations and properties discussed so far all hold in an infinite elastic medium. We turn now to the case of the semi-infinite elastic medium. Let the surface S of the semi-infinite medium be the plane $x_3 = 0$ where the positive

x_3-axis penetrates into the medium. The boundary conditions we have to satisfy are that for each point $Q(y_1, y_2, 0)$,

$$\tau_{31}(Q) = \tau_{32}(Q) = \tau_{33}(Q) = 0, \tag{4.1}$$

while we shall in general require also that the stresses and displacements are continuous and differentiable everywhere, with the possible exception of Σ, and moreover vanish at infinity.

We have already seen that the expressions $\tau^k_{ij}(P, Q)$ and $G^{kl}_{ij}(P, Q)$ for fixed i and j can be interpreted as displacements and stresses while it is noticed that the conditions (4.1) affect the functions G^{31}_{ij}, G^{32}_{ij}, and G^{33}_{ij}. It is then clear that we have solved the problem of an arbitrary dislocation in a semi-infinite elastic medium if we can construct for each of the six combinations ij functions v^k_{ij}, w^k_{ij}, F^{kl}_{ij}, and H^{kl}_{ij} which satisfy the following conditions:

(i)
$$w^k_{ij}(x_n, y_n) = \tau^k_{ij}(x_n - y_n) + v^k_{ij}(x_n, y_n),$$

$$F^{kl}_{ij}(x_n, y_n) = G^{kl}_{ij}(x_n - y_n) + H^{kl}_{ij}(x_n, y_n). \tag{4.2}$$

(ii) v^k_{ij} and H^{kl}_{ij} considered as function of y_n and the superscripts form a displacement and stress field regular throughout the semi-infinite medium (including the surface Σ) so that

$$H^{kl}_{ij} = \lambda\delta_{kl} v^{n,n}_{ij} + \mu(v^{k,l}_{ij} + v^{l,k}_{ij}). \tag{4.3}$$

(iii) For points $Q(y_1, y_2, 0)$ we have

$$F^{3l}_{ij}(x_n, y_n) = G^{3l}_{ij}(x_n - y_n) + H^{3l}_{ij}(x_n, y_n) = 0 \qquad (l = 1, 2, 3). \tag{4.4}$$

The displacement and stress field in the semi-infinite elastic medium due to an arbitrary dislocation, while satisfying the boundary conditions (4.1), is then determined from the relations

$$\begin{aligned} u_k(y_n) &= \frac{U_i}{8\pi\mu} \iint_\Sigma w^k_{ij}\nu_j d\Sigma + \frac{\Omega_{ij}}{8\pi\mu} \iint_\Sigma (x_j w^k_{in} - x_i w^k_{jn})\nu_n d\Sigma, \\ \tau_{kl}(y_n) &= \frac{U_i}{8\pi\mu} \iint_\Sigma F^{kl}_{ij}\nu_j d\Sigma + \frac{\Omega_{ij}}{8\pi\mu} \iint_\Sigma (x_j F^{kl}_{in} - x_i F^{kl}_{jn})\nu_n d\Sigma. \end{aligned} \tag{4.5}$$

We shall now show that the functions v^k_{ij} and H^{kl}_{ij} are obtained by superposition of two solutions:

(i) an image solution such that the boundary conditions:

$$F^{31}_{ij} = F^{32}_{ij} = 0 \tag{4.6}$$

are satisfied for $(y_1, y_2, 0)$,

(ii) the solution of an ordinary boundary value problem where the surface of the semi-infinite medium is subjected to a normal load distribution and which takes care of the last boundary condition

$$F^{33}_{ij} = 0 \tag{4.7}$$

in the points $(y_1, y_2, 0)$.

We have already seen in Section 3 that $G_{ij}^{kl}(P, Q)$ can be considered as the stress in Q generated by certain combinations of double forces in P on Σ. It is also clear from (3.4) that in case G_{ij}^{31} and G_{ij}^{32} are odd (even) in x_3-y_3, the function G_{ij}^{33} is even (odd) in x_3-y_3. By putting the same (opposite) combinations of double forces in the image point $P'(x_1, x_2, -x_3)$ of P with respect to the plane $x_3 = 0$, we obtain by superposition of the original and image fields a stress field which satisfies the boundary conditions (4.5), while no singularities are added in the half-space where the dislocation is situated. It is clear that the normal stress is doubled for $x_3 = 0$. The solution of the boundary value problem where the plane $x_3 = 0$ is subjected to normal loads equal and opposite to the ones obtained from the double forces in P and P' has to be superposed to satisfy the condition (4.7).

While this finishes in outline the construction of the Green's functions, several details have to be added.

Inspection of some of the preceding expressions and papers dealing with problems similar to ours (Mindlin 1936; Westergaard 1952) shows that several expressions may become clumsy. Following these writers we shall make use of Galerkin vectors (Galerkin 1930; Papcovitch 1932). While these vectors do not assist a great deal in the actual solution of the problem, they enable one to state the results as compactly as possible. As we define the Galerkin vector in a slightly different way from some former authors and to make the treatment self-contained, we shall discuss these points in the next section.

The second part of the construction of the Green's functions is the solution of the semi-infinite elastic medium with a normal load, usually called after Boussinesq. This problem has received considerable attention in the past (see p. 169 of Love 1944). We shall use here a method of Fourier transforms due to Trefftz (1935) but modified for normal loads only and put in terms of Galerkin vectors by Westergaard (1952). This problem will be discussed in Section 6.

5. GALERKIN VECTORS

In analogy with a strain potential, where a displacement field is found by taking the gradient of a scalar function, the Galerkin vector Γ_i is defined as a vector which gives a displacement field by differentiating according to the Laplace operator and the grad div. We have the relation

$$u_i = \Gamma_{i,kk} - \alpha \Gamma_{k,ki}, \tag{5.1}$$

where α will be chosen in a convenient way. If the Galerkin vector is known for a problem, the problem is solved, as we have immediately for the strains e_{ij} and stresses τ_{ij},

$$\begin{aligned} e_{ij} &= \tfrac{1}{2}(\Gamma_{i,jkk}+\Gamma_{j,ikk}) - \alpha \Gamma_{k,kij}, \\ \tau_{ij} &= \lambda(1-\alpha)\delta_{ij}\Gamma_{k,kll} + \mu(\Gamma_{i,jkk}+\Gamma_{j,ikk}) - 2\mu\alpha\Gamma_{k,kij}. \end{aligned} \tag{5.2}$$

Substitution of (5.1) in the Navier equations (3.5) and selecting $\alpha = (\lambda+\mu)/(\lambda+2\mu)$ leaves us with the equation

$$\Gamma_{i,jjkk} = 0. \tag{5.3}$$

This shows that each component of the Galerkin vector is biharmonic.

With this definition it is clear from (2.1) that the solution of the infinite elastic medium with a force $8\pi\mu\mathbf{e}_k$ in O is given by the Galerkin vector $\mathbf{\Gamma} = r\mathbf{e}_k$, while the Somigliana tensor is obtained from the Galerkin tensor

$$\Gamma_i^k = \delta_i^k r = \delta_{ik} r. \tag{5.4}$$

It is also easily found that the Galerkin vector for the displacement f $\tau_{ij}^k(P, Q)$ with i and j fixed is given by

$$\Gamma_k = \Gamma_{ij}^k(P, Q) = \lambda\delta_{ij}r_{,k}+\mu(\delta_{ik}r_{,j}+\delta_{jk}r_{,i}). \tag{5.5}$$

If the differentiations to obtain the displacement field are performed to the coordinates y_l in Q, this expression has to be replaced by its opposite value as

$$r_{,k} = -r_{,k}.$$

6. THE BOUSSINESQ PROBLEM

Let the boundary of the semi-infinite medium be the plane $x_3 = 0$ where the positive x_3-axis points into the medium. According to Westergaard (1952) the solution of this problem is determined by a Galerkin vector

$$\Gamma = e_3\Gamma_3. \tag{6.1}$$

Let the double Fourier transform of Γ_3 be denoted as $\bar{\Gamma}_3$, then we have by definition

$$\begin{aligned}\Gamma_3(x_1, x_2, x_3) &= \frac{1}{2\pi}\int_{-\infty}^{+\infty}\bar{\Gamma}_3(\lambda_1, \lambda_2, x_3)\exp[i(\lambda_1x_1+\lambda_2x_2)]d\lambda_1d\lambda_2,\\ \bar{\Gamma}_3(\lambda_1, \lambda_2, x_3) &= \frac{1}{2\pi}\int_{-\infty}^{+\infty}\Gamma_3(x_1, x_2, x_3)\exp[-i(\lambda_1x_1+\lambda_2x_2)]dx_1dx_2.\end{aligned} \tag{6.2}$$

As Γ_3 is biharmonic, we find for $\bar{\Gamma}_3$, using the operational rules, the differential equation

$$(d^2/dx_3^2-\beta^2)^2\,\bar{\Gamma}_3 = 0 \tag{6.3}$$

with the general solution

$$\bar{\Gamma}_3 = (A+B\beta x_3)e^{-\beta x_3}+(C+D\beta x_3)e^{\beta x_3}, \tag{6.4}$$

where we have denoted $\beta = +\sqrt{(\lambda_1^2+\lambda_2^2)}$. Owing to the boundary conditions at infinity $C = D = 0$ and we are left with

$$\bar{\Gamma}_3(\lambda_1, \lambda_2, x_3) = (A+B\beta x_3)e^{-\beta x_3}. \tag{6.5}$$

From the general relation (5.1) and the operational rules we find easily the transforms of the displacement and stress components. In particular for $\bar{\tau}_{31}$ and $\bar{\tau}_{32}$ we have

$$\begin{aligned}\bar{\tau}_{31} &= i\mu\lambda_1\beta^2\{2B(2\alpha-1)e^{-\beta x_3}-2\alpha\bar{\Gamma}_3\},\\ \bar{\tau}_{32} &= i\mu\lambda_2\beta^2\{2B(2\alpha-1)e^{-\beta x_3}-2\alpha\bar{\Gamma}_3\}.\end{aligned} \tag{6.6}$$

As we have only a normal stress at $x_3 = 0$, the shearing stresses and their transforms have to vanish at $x_3 = 0$. This gives us:

$$A = (2-1/\alpha)B. \tag{6.7}$$

The remaining problem is to find B. Substitution of (6.7) in (6.5) and working out the displacement and stress components gives us:

$$\begin{aligned}
\bar{\Gamma}_3 &= B(2-1/\alpha+\beta x_3)e^{-\beta x_3},\\
\bar{u}_1 &= i\alpha\lambda_1\beta B(1-1/\alpha+\beta x_3)e^{-\beta x_3},\\
\bar{u}_2 &= i\alpha\lambda_2\beta B(1-1/\alpha+\beta x_3)e^{-\beta x_3},\\
\bar{u}_3 &= -\alpha\beta^2 B(1/\alpha+\beta x_3)e^{-\beta x_3},\\
\bar{\tau}_{11} &= 2\beta B\{\mu\alpha\lambda_1{}^2+\lambda(1-\alpha)\lambda_2{}^2-\mu\alpha\lambda_1{}^2\beta x_3\}e^{-\beta x_3},\\
\bar{\tau}_{22} &= 2\beta B\{\mu\alpha\lambda_2{}^2+\lambda(1-\alpha)\lambda_1{}^2-\mu\alpha\lambda_2{}^2\beta x_3\}e^{-\beta x_3},\\
\bar{\tau}_{33} &= 2\mu\alpha\beta^3 B(1+\beta x_3)e^{-\beta x_3},\\
\bar{\tau}_{23} &= -2i\mu\alpha\lambda_2\beta^3 x_3 Be^{-\beta x_3},\\
\bar{\tau}_{31} &= -2i\mu\alpha\lambda_1\beta^3 x_3 Be^{-\beta x_3},\\
\bar{\tau}_{12} &= -2\mu\alpha\lambda_1\lambda_2\beta B(1-1/\alpha+\beta x_3)e^{-\beta x_3}.
\end{aligned} \tag{6.8}$$

The boundary condition which determines B is the normal load distribution on $x_3 = 0$, that is

$$\tau_{33}(x_1, x_2, 0) = p(x_1, x_2). \tag{6.9}$$

If the Fourier transform of p is denoted as $\bar{p}$, we find B from the transform of equation (6.9) at $x_3 = 0$. We find easily

$$B(\lambda_1, \lambda_2) = \frac{1}{2\mu\alpha}\frac{\bar{p}(\lambda_1, \lambda_2)}{\beta^3}. \tag{6.10}$$

The remaining problem is the inversion. In this problem the use of the Galerkin vector may be advantageous as the inversion of the Galerkin vector may be easier than the inversion of the individual expressions (6.8). The displacements and stresses can then be found by differentiations once the Galerkin vector is known.

This finishes the general theory. In the following section we illustrate the method by computation of the displacement field $\tau_{12}^k(P, Q)$. To prevent confusion we shall adhere strictly to the notation developed in the preceding sections, although this is not necessary.

7. THE DISPLACEMENT FIELD $\tau_{12}^k(P, Q)$

As we have seen in the preceding sections $\tau_{12}^k(P, Q)$ is essentially the displacement field in Q generated by two double forces with moments in P. We choose for P the coordinates $(0, 0, c)$ while Q has the general coordinates $y_l (l = 1, 2, 3)$. It follows from (5.5) that the Galerkin vector $\Gamma_{12}^k(P, Q)$ for this case is given by

$$\Gamma_{12}^k(P, Q) = -\mu\delta_{1k}R^{,2}-\mu\delta_{2k}R^{,1} \tag{7.1}$$

where $R = \{y_1{}^2+y_2{}^2+(y_3-c)^2\}^{\frac{1}{2}}$. Writing out the displacements and stresses

in Q generated by these double forces in P we find, either by straight differentiations of (7.1) or from the general relations (2.3) and (3.4),

$$\tau_{12}^1 = 2\mu(1-\alpha)\frac{y_2}{R^3}+6\alpha\mu\frac{y_1^2y_2}{R^5},$$

$$\tau_{12}^2 = 2\mu(1-\alpha)\frac{y_1}{R^3}+6\alpha\mu\frac{y_1y_2^2}{R^5},$$

$$\tau_{12}^3 = 6\alpha\mu\frac{y_1y_2(y_3-c)}{R^5},$$

$$G_{12}^{11} = 12\mu^2\alpha^2\frac{y_1y_2}{R^5}-60\alpha\mu^2\frac{y_1^3y_2}{R^7},$$

$$G_{12}^{22} = 12\mu^2\alpha^2\frac{y_1y_2}{R^5}-60\alpha\mu^2\frac{y_1y_2^3}{R^7}, \tag{7.2}$$

$$G_{12}^{33} = 12\mu^2(1-\alpha)^2\frac{y_1y_2}{R^5}-60\alpha\mu^2\frac{y_1y_2(y_3-c)^2}{R^7},$$

$$G_{12}^{23} = 6\mu^2(2\alpha-1)\frac{y_1(y_3-c)}{R^5}-60\alpha\mu^2\frac{y_1y_2^2(y_3-c)}{R^7},$$

$$G_{12}^{31} = 6\mu^2(2\alpha-1)\frac{y_2(y_3-c)}{R^5}-60\alpha\mu^2\frac{y_1^2y_2(y_3-c)}{R^7},$$

$$G_{12}^{12} = 4\mu^2(1-\alpha)\frac{1}{R^3}+6\mu^2(2\alpha-1)\frac{y_1^2+y_2^2}{R^5}-60\alpha\mu^2\frac{y_1^2y_2^2}{R^7}.$$

We notice from these relations that the shearing stresses G_{12}^{23} and G_{12}^{31} are odd in y_3-c. Superposition of the stress field generated by the same double forces in $P'(0, 0, -c)$ cancels the shearing stresses at the boundary $y_3 = 0$ while doubling the normal stresses G_{12}^{33}.

The Galerkin vector for the original double forces in P and the image in $P'(0, 0, -c)$ is therefore given by

$$\Gamma_{12}^k = -\mu\delta_{1k}\left(\frac{y_2}{R}+\frac{y_2}{S}\right)-\mu\delta_{2k}\left(\frac{y_1}{R}+\frac{y_1}{S}\right), \tag{7.3}$$

where $S = \{y_1^2+y_2^2+(y_3+c)^2\}^{\frac{1}{2}}$.

It follows also that the normal surface load for the remaining Boussinesq problem is

$$p(y_1, y_2) = -24\mu^2(1-\alpha)^2\frac{y_1y_2}{\rho^5}+120\alpha\mu^2\frac{y_1y_2c^2}{\rho^7}, \tag{7.4}$$

where $\rho^2 = y_1^2+y_2^2+c^2$.

It is interesting to notice that the expression (7.4) is odd in both y_1 and y_2 so that we have immediately

$$\iint_{-\infty}^{+\infty} p(y_1, y_2)dy_1dy_2 = 0. \tag{7.5}$$

This property also makes it possible to reduce the exponential Fourier transforms to sine transforms. It is then easily found that

$$\bar{p}(\lambda_1, \lambda_2) = \frac{48\mu^2}{\pi}\{(1-\alpha)T_1 - 5\alpha c^2 T_2\}, \tag{7.6}$$

where T_1 and T_2 denote the integrals

$$\begin{aligned} T_1 &= \int_0^\infty\int_0^\infty \frac{y_1 y_2}{\rho^5}\sin(\lambda_1 y_1)\sin(\lambda_2 y_2)dy_1 dy_2, \\ T_2 &= \int_0^\infty\int_0^\infty \frac{y_1 y_2}{\rho^7}\sin(\lambda_1 y_1)\sin(\lambda_2 y_2)dy_1 dy_2. \end{aligned} \tag{7.7}$$

To evaluate these integrals we make use of Basset's integral for the modified Bessel functions of the second kind (Watson 1944, p. 172) and some recurrence relations for those functions and the cosine transforms (Magnus, Oberhettinger, and Tricomi 1954):

$$\begin{aligned} &\int_0^\infty K_0[\lambda_1\sqrt{(y_2^2+c^2)}]\cos(\lambda_2 y_2)dy_2 = \frac{\pi}{2}\frac{1}{\sqrt{(\lambda_1^2+\lambda_2^2)}}\exp[-c\sqrt{(\lambda_1^2+\lambda_2^2)}], \\ &\int_0^\infty \frac{K_1[\lambda_1\sqrt{(y_2^2+c^2)}]}{\sqrt{(y_2^2+c^2)}}\cos(\lambda_2 y_2)dy_2 = \frac{\pi}{2}\frac{1}{\lambda_1 c}\exp[-c\sqrt{(\lambda_1^2+\lambda_2^2)}]. \end{aligned} \tag{7.8}$$

In this way we finally obtain

$$\bar{p}(\lambda_1, \lambda_2) = 8\mu^2\lambda_1\lambda_2\left\{\frac{1-\alpha}{\beta} - \alpha c\right\}e^{-c\beta}, \tag{7.9}$$

where we have denoted $\beta = +\sqrt{(\lambda_1^2+\lambda_2^2)}$.

Substitution of (7.9) in (6.10) gives

$$B(\lambda_1, \lambda_2) = \frac{4\mu}{\alpha}\frac{\lambda_1\lambda_2}{\beta^3}\left(\frac{1-\alpha}{\beta} - \alpha c\right)e^{-c\beta}, \tag{7.10}$$

while the transform of the Galerkin vector is obtained from (6.8) as follows:

$$\bar{\Gamma}_3 = \frac{4\mu}{\alpha}\frac{\lambda_1\lambda_2}{\beta^3}\left\{\frac{(1-\alpha)(2\alpha-1)}{\alpha}\frac{1}{\beta} + [(1-\alpha)(y_3+c) - \alpha c] - \alpha c y_3\beta\right\}e^{-\beta(y_3+c)}. \tag{7.11}$$

It is again noticed that $\bar{\Gamma}_3$ is odd in λ_1 and λ_2 so that the exponential inversion integral can be reduced to sine transforms. Working this out we obtain for the Galerkin vector of the Boussinesq problem

$$\Gamma_3 = +\frac{2\mu}{\alpha\pi}\left\{\frac{(1-\alpha)(2\alpha-1)}{\alpha}I_1 + [(1-\alpha)(y_3+c) - \alpha c]I_2 - \alpha c y_3 I_3\right\}. \tag{7.12}$$

In this expression I_1, I_2, and I_3 denote the integrals

$$I_1 = -4\int_0^\infty\int_0^\infty d\lambda_1 d\lambda_2 \frac{\lambda_1\lambda_2}{\beta^4}\exp[-\beta(y_3+c)]\sin(\lambda_1 y_1)\sin(\lambda_2 y_2),$$

$$I_2 = -4\int_0^\infty\int_0^\infty d\lambda_1 d\lambda_2 \frac{\lambda_1\lambda_2}{\beta^3}\exp[-\beta(y_3+c)]\sin(\lambda_1 y_1)\sin(\lambda_2 y_2), \tag{7.13}$$

$$I_3 = -4\int_0^\infty\int_0^\infty d\lambda_1 d\lambda_2 \frac{\lambda_1\lambda_2}{\beta^2}\exp[-\beta(y_3+c)]\sin(\lambda_1 y_1)\sin(\lambda_2 y_2).$$

To check the results of these integrations we note that

$$\frac{\partial}{\partial y_3}(I_1) = -I_2, \qquad \frac{\partial}{\partial y_3}(I_2) = -I_3, \qquad \left(\frac{\partial^2}{\partial {y_1}^2}+\frac{\partial^2}{\partial {y_2}^2}\right)I_1 = -I_3. \tag{7.14}$$

It follows that I_1, I_2, and I_3 are harmonic functions of y_i so that (7.12) is biharmonic.

To evaluate the integrals (7.13) we substitute new variables $\lambda_1 = \beta\cos\phi$, $\lambda_2 = \beta\sin\phi$, $y_1 = r\cos\theta$, $y_2 = r\sin\theta$. The integrations to β are then easily performed as they are essentially Laplace transforms, while the integrations to ϕ are elementary but lengthy. Slipping over the details we obtain finally:

$$I_1 = +2\pi\frac{y_1y_2}{r^4}\left\{\frac{r^2}{2}-S^2+pS\right\},$$

$$I_2 = +2\pi\frac{y_1y_2}{r^4}\left\{2p-S-\frac{p^2}{S}\right\}, \tag{7.15}$$

$$I_3 = +2\pi\frac{y_1y_2}{r^4}\left\{-2+\frac{3p}{S}-\frac{p^3}{S^3}\right\},$$

where we have denoted $p = y_3+c$, while as before $S = \{{y_1}^2+{y_2}^2+(y_3+c)^2\}^{\frac{1}{2}}$.

Substitution of (7.15) into (7.12) gives us finally the Galerkin vector

$$\Gamma_3 = \frac{4\mu}{\alpha}\frac{y_1y_2}{r^4}\left\{\frac{1-\alpha}{\alpha}p^2-\frac{(1-\alpha)(2\alpha-1)}{2\alpha}r^2-\frac{(1-\alpha)^2}{\alpha}pS+\alpha cS\right. \tag{7.16}$$
$$\left.-2\alpha c^2+3\alpha\frac{c^2p}{S}-2\alpha\frac{cp^2}{S}-(1-\alpha)\frac{p^3}{S}-\alpha\frac{c^2p^3}{S^3}+\alpha\frac{cp^4}{S^3}\right\}.$$

To simplify our further work we make the assumption $\lambda = \mu$, which is not unusual in applications of elasticity to geophysics. It follows that $\alpha = \frac{2}{3}$. To obtain the displacement components τ_{12}^k we have to differentiate the Galerkin vector Γ_{12}^k, which we have now found to be

$$\Gamma_{12}^1 = -\mu\left(\frac{y_2}{R}+\frac{y_2}{S}\right),$$

$$\Gamma_{12}^2 = -\mu\left(\frac{y_1}{R}+\frac{y_1}{S}\right), \tag{7.17}$$

$$\Gamma_{12}^3 = \mu\frac{y_1y_2}{r^4}\left\{3p^2-\tfrac{1}{2}r^2-pS+4cS-8c^2+12\frac{pc^2}{S}\right.$$
$$\left.-8\frac{p^2c}{S}-2\frac{p^3}{S}-4\frac{p^3c^2}{S^3}+4\frac{p^4c}{S^3}\right\}.$$

Differentiation of (7.17) according to the formula (5.1) gives us the displacement components:

$$\tau_{12}^1 = \mu \frac{y_2}{r^4}\left\{A+\frac{y_1^2}{r^2}B\right\},$$

$$\tau_{12}^2 = \mu \frac{y_1}{r^4}\left\{A+\frac{y_2^2}{r^2}B\right\}, \tag{7.18}$$

$$\tau_{12}^3 = \mu \frac{y_1y_2}{r^4}\left\{4\frac{[R^2-(p-2c)^2]^2(p-2c)}{R^5}+4+2\frac{p}{S}\right.$$
$$-16\frac{c}{S}-14\frac{p^3}{S^3}-8\frac{p^2c}{S^3}+40\frac{pc^2}{S^3}+8\frac{p^5}{S^5}$$
$$\left.+64\frac{p^4c}{S^5}-80\frac{p^3c^2}{S^5}-40\frac{p^6c}{S^7}+40\frac{p^5c^2}{S^7}\right\},$$

while

$$A = \frac{2}{3}R-\frac{4}{3}\frac{(p-2c)^2}{R}+\frac{2}{3}\frac{(p-2c)^4}{R^3}-4p+\frac{4}{3}S+\frac{10}{3}\frac{p^2}{S}$$
$$+8\frac{pc}{S}-8\frac{c^2}{S}-\frac{2}{3}\frac{p^4}{S^3}-16\frac{p^3c}{S^3}+16\frac{p^2c^2}{S^3}+8\frac{p^5c}{S^5}-8\frac{p^4c^2}{S^5},$$

$$B = 4R-12\frac{(p-2c)^2}{R}+12\frac{(p-2c)^4}{R^3}-4\frac{(p-2c)^6}{R^5}+16p+2S \tag{7.19}$$
$$-36\frac{p^2}{S}-40\frac{pc}{S}+40\frac{c^2}{S}+26\frac{p^4}{S^3}+120\frac{p^3c}{S^3}$$
$$-120\frac{p^2c^2}{S^3}-8\frac{p^6}{S^5}-120\frac{p^5c}{S^5}+120\frac{p^4c^2}{S^5}+40\frac{p^7c}{S^7}-40\frac{p^6c^2}{S^7}.$$

One more differentiation will give the stresses. So far it has only been checked that $G_{12}^{33} = 0$ for $y_3 = 0$. The formulae (7.18) and (7.19) simplify a great deal if we restrict ourselves to the displacement components at $y_3 = 0$. We find:

$$\tau_{12}^1 = \mu\frac{y_2}{r^4}\left\{A+\frac{y_1^2}{r^2}B\right\},$$

$$\tau_{12}^2 = \mu\frac{y_1}{r^4}\left\{A+\frac{y_2^2}{r^2}B\right\}, \tag{7.20}$$

$$\tau_{12}^3 = \mu\frac{y_1y_2}{r^4}\left\{4-18\frac{c}{\rho}+26\frac{c^3}{\rho^3}-12\frac{c^5}{\rho^5}\right\},$$

$$A = -4c+2\rho+2\frac{c^2}{\rho},$$

$$B = 16c+6\rho-48\frac{c^2}{\rho}+38\frac{c^4}{\rho^3}-12\frac{c^6}{\rho^5},$$

where as before $\rho^2 = y_1^2+y_2^2+c^2$.

The discussion of the results obtained here with geophysical applications will be taken up in another communication which is being prepared.

ACKNOWLEDGMENTS

The author wishes to thank Professor J. T. Wilson of the University of Toronto for his invitation to work during the summer of 1955 on geophysical problems. His enthusiasm is a great source of encouragement. The author is grateful for financial assistance received during the summer of 1955 from the California Standard Oil Company and in the summer of 1957 from the National Research Council of Canada.

REFERENCES

BERGMAN, S. and SCHIFFER, M. 1953. Kernel functions and elliptic differential equations in mathematical physics (Academic Press Inc., New York, N.Y.).
GALERKIN, B. 1930*a*. Comp. rend. **190**, 1047.
——— 1930*b*. Compt. rend. acad. sci. U.R.S.S. p. 353.
HOUSNER, G. W. 1955. Bull. Seismol. Soc. Am. **45**, 197.
LOVE, A. E. H. 1944. The mathematical theory of elasticity (Dover Publications, New York).
MAGNUS, W., OBERHETTINGER, F., and TRICOMI, F. G. 1954. Tables of internal transforms, Vol. I (McGraw-Hill Book Co., Inc., New York).
MINDLIN, R. D. 1936. Physics, **7**, 195.
PAPCOVITCH, P. F. 1932. Compt. rend. **195**, 513, 754.
ROCHESTER, M. G. 1956. M.A. Thesis, University of Toronto, Toronto, Ontario.
SCHEIDEGGER, A. E. 1953. Bull. Geol. Soc. Am. **64**, 127.
SOKOLNIKOFF, I. S. and SPECHT, R. D. 1946. Mathematical theory of elasticity (McGraw-Hill Book Co., Inc., New York).
STEKETEE, J. A. 1955. Unpublished report, Department of Applied Mathematics, University of Toronto, Toronto, Ontario.
TREFFTZ, E. 1935. *In* P. FRANK and R. VON MISES. Die Differential und Integralgleichungen der Mechanik und Physik, Vol. II (Vieweg Verlag, Braunschweig).
UMBGROVE, J. F. H. 1954. The pulse of the earth (Martinus Nyhoff, The Hague).
VOLTERRA, V. 1907. Ann. sci. école norm. supérieure, Ser. 3, **24**, 401.
WATSON, G. N. 1944. Theory of Bessel functions (Cambridge University Press).
WESTERGAARD, H. M. 1952. Theory of elasticity and plasticity (Harvard University Press, Cambridge, Mass., and John Wiley & Sons, Inc., New York).
WILSON, J. T. 1954. *In* The earth as a planet *by* G. P. Kuiper (University of Chicago Press), Chap. IV.

RADIATION AND SURFACE CURRENTS FROM A SLOT ON AN INFINITE CONDUCTING CYLINDER[1]

F. H. NORTHOVER

ABSTRACT

The far field produced by an aperture in the surface of an infinite cylindrical antenna, whose interior is being electromagnetically excited in some way, has been calculated by Papas and others using a "saddle-point" method of approximation to the infinite integrals which express the external field. This method will not, however, serve to approximate to the far field *near the antenna surface.* Also, there seems to have been no attempt so far to estimate the order of magnitude of the error involved in using formulae derived by such methods. The object of the present paper is to remedy these deficiencies and to provide a basis for the calculation of the far field in wider regions than has so far been possible. In particular, the surface current distribution at large distances from the aperture has been worked out. Finally, a justification is given for the Papas procedure of integrating his approximation to the Poynting energy flux vector over the whole of the portion of the large sphere surrounding the aperture which is outside the cylinder itself.

1. INTRODUCTION

In recent years the slotted cylindrical antennae have become increasingly used in V.H.F. techniques and it is often a matter of some importance to know the characteristic behavior of the field many wavelengths from the aperture of the antenna. This far field has been calculated by Papas (1949) and others, but methods so far used fail for those far points that are close to the surface of the antenna.* Also, there seems to have been no attempt so far to estimate the degree of accuracy achieved by such methods; nor has a justification been given for the Papas procedure of integrating his approximation to the Poynting energy flux vector over the entire surface of that portion of a large sphere surrounding the aperture lying in the space outside the cylinder.

We assume that the antenna wall is a perfect conductor.

2. GENERAL EXPRESSIONS FOR THE FIELD OUTSIDE THE APERTURE

We shall follow closely the treatment given by Silver and Saunders (1950). Taking axes relative to aperture and antenna as in their paper (see also their figure) and using their notation we have the shape of the slot defined by curves $\phi_1(z)$ and $\phi_2(z)$ and bounded in the axial direction by planes $z = z_1$ and $z = z_2$.

The tangential electric field in the slot will in general have both ϕ and z components which we consider to be prescribed functions $f_1(\phi, z)$ and $f_2(\phi, z)$ respectively. In view of the infinite conductivity of the antenna wall, this

[1]Manuscript received November 7, 1957.
Contribution from the Department of Mathematics, Carleton University, Ottawa, Canada.
*Hallen's integral equation approach (1948) seems difficult to apply here.

represents a complete knowledge of the tangential electric field over the entire surface of the cylinder, namely

$$(1)\qquad \begin{cases} E_\phi = f_1(\phi, z) \qquad \phi_1 \leqslant \phi \leqslant \phi_2,\ z_1 \leqslant z \leqslant z_2 \\ \quad = 0 \text{ outside the slot,} \\ E_z = f_2(\phi, z) \qquad \phi_1 \leqslant \phi \leqslant \phi_2 \\ \quad = 0 \text{ outside the slot.} \end{cases}$$

Any field component is given by expressions of the form

$$E_\alpha(\rho, \phi, z) = \int_{-\infty}^{\infty} \tilde{\mathscr{E}}_\alpha(\rho, \phi, h)\, dh,$$

where

$$(2A)\qquad \begin{cases} \tilde{\mathscr{E}}_\rho = \left\{ \sum_{-\infty}^{\infty} \left[ihA_n \dfrac{\partial H_n^{(1)}(\Lambda\rho)}{\partial\rho} - \dfrac{n\omega\mu}{\rho} B_n H_n^{(1)}(\Lambda\rho) \right] e^{in\phi} \right\} e^{ihz}, \\ \tilde{\mathscr{E}}_\phi = \left\{ \sum_{-\infty}^{\infty} \left[-\dfrac{nh}{\rho} A_n H_n^{(1)}(\Lambda\rho) - i\omega\mu B_n \dfrac{\partial H_n^{(1)}(\Lambda\rho)}{\partial\rho} \right] e^{in\phi} \right\} e^{ihz}, \\ \tilde{\mathscr{E}}_z = \left\{ \sum_{-\infty}^{\infty} \left[(k^2 - h^2) A_n H_n^{(1)}(\Lambda\rho) \right] e^{in\phi + ihz} \right\}, \end{cases}$$

where

$$(2B)\qquad \Lambda = (k^2 - h^2)^{\frac{1}{2}}, \qquad k = (\omega^2\mu\epsilon + i\mu\sigma\omega)^{\frac{1}{2}},$$

and A_n and B_n are given by

$$(2C)\qquad \begin{cases} A_n = \dfrac{1}{4\pi^2(k^2 - h^2)H_n^{(1)}(\Lambda a)} \displaystyle\int_{z_1}^{z_2} d\xi \int_{\phi_1(\xi)}^{\phi_2(\xi)} f_2(\beta, \xi)\, e^{-in\beta - ih\xi} d\beta, \\ B_n = \dfrac{inh}{4\pi^2\omega\mu a(k^2 - h^2)(\partial H_n^{(1)}(\Lambda a)/\partial a)} \displaystyle\int_{z_1}^{z_2} d\xi \int_{\phi_1(\xi)}^{\phi_2(\xi)} f_2(\beta, \xi)\, e^{-in\beta - ih\xi} d\beta \\ \qquad + \dfrac{i}{4\pi^2\omega\mu\{\partial H_n^{(1)}(\Lambda a)/\partial a\}} \displaystyle\int_{z_1}^{z_2} d\xi \int_{\phi_1(\xi)}^{\phi_2(\xi)} f_1(\beta, \xi)\, e^{-in\beta - ih\xi} d\beta. \end{cases}$$

This is equivalent to

$$(3)\qquad \begin{cases} E_\rho = \displaystyle\int_{z_1}^{z_2} \int_{\phi_1(t)}^{\phi_2(t)} \mathscr{E}_\rho\, dt\, d\beta, \\ E_\phi = \displaystyle\int_{z_1}^{z_2} \int_{\phi_1(t)}^{\phi_2(t)} \mathscr{E}_\phi\, dt\, d\beta, \\ E_z = \displaystyle\int_{z_1}^{z_2} \int_{\phi_1(t)}^{\phi_2(t)} \mathscr{E}_z\, dt\, d\beta, \end{cases}$$

in which $adtd\beta$ is an element of area of the surface of the aperture, dt being

parallel to the z direction, and $d\beta$ being azimuthal, and the integration is over the slot surface, where

$$\text{(3A)}\quad \begin{cases} \mathscr{E}_\rho = \sum_{-\infty}^{\infty} \int_{-\infty}^{\infty} \left\{ i\zeta a_n \dfrac{\partial H_n^{(1)}(\Lambda\rho)}{\partial\rho} - \dfrac{n\omega\mu}{\rho} b_n H_n^{(1)}(\Lambda\rho) \right\} e^{in\phi + i\zeta z} d\zeta, \\ \mathscr{E}_\phi = \sum_{-\infty}^{\infty} \int_{-\infty}^{\infty} \left\{ -\dfrac{n\zeta}{\rho} a_n H_n^{(1)}(\Lambda\rho) - i\omega\mu b_n \dfrac{\partial H_n^{(1)}(\Lambda\rho)}{\partial\rho} \right\} e^{in\phi + i\zeta z} d\zeta, \\ \mathscr{E}_z = \sum_{-\infty}^{\infty} \int_{-\infty}^{\infty} (k^2 - \zeta^2)\, a_n H_n^{(1)}(\Lambda\rho)\, e^{in\phi + i\zeta z} d\zeta, \end{cases}$$

where

$$\text{(3B)}\quad \begin{cases} a_n = \dfrac{f_2(\beta, t)\, e^{-in\beta - i\zeta t}}{4\pi^2 (k^2 - \zeta^2) H_n^{(1)}(\Lambda a)}, \\ b_n = \dfrac{ie^{-in\beta - i\zeta t}}{4\pi^2 \omega\mu \{\partial H_n^{(1)}(\Lambda a)/\partial a\}} \left\{ \dfrac{n\zeta}{a(k^2 - \zeta^2)} f_2(\beta, t) + f_1(\beta, t) \right\}. \end{cases}$$

In the above f_1 and f_2 are as defined in Silver and Saunders' paper but here we take the time factor as $e^{-i\omega t}$ in order to obtain (after Papas) results in terms of Hankel functions of the first kind. The path of integration is along the real axis of the cut plane defined by the cuts

$$-3\pi/2 < \arg(\zeta - k) < \pi/2,$$
$$-\pi/2 < \arg\{\zeta - (-k)\} < 3\pi/2.$$

It is not necessary to write down the corresponding expressions for **H** as these can be obtained from the above via the fundamental relation

$$\text{(4)}\qquad -ik\,\mathbf{H} = \operatorname{curl}\mathbf{E}.$$

Inspection of the above shows that the field intensity **E** can be expressed in terms of fundamental integrals

$$\text{(5)}\quad \begin{cases} E = \displaystyle\int_{-\infty}^{\infty} \frac{H_n^{(1)}\{(k^2 - \zeta^2)^{\frac{1}{2}}\rho\}}{H_n^{(1)}\{(k^2 - \zeta^2)^{\frac{1}{2}}a\}} e^{i\zeta(z-t)} d\zeta, \\ F = \displaystyle\int_{-\infty}^{\infty} \frac{H_n^{(1)}\{(k^2 - \zeta^2)^{\frac{1}{2}}\rho\}}{[\partial H_n^{(1)}\{(k^2 - \zeta^2)^{\frac{1}{2}}a\}/\partial a]} e^{i\zeta(z-t)} d\zeta, \\ G = \displaystyle\int_{-\infty}^{\infty} \frac{1}{k^2 - \zeta^2} \frac{H_n^{(1)}\{(k^2 - \zeta^2)^{\frac{1}{2}}\rho\}}{H_n^{(1)}\{(k^2 - \zeta^2)^{\frac{1}{2}}a\}} e^{i\zeta(z-t)} d\zeta, \\ H = \displaystyle\int_{-\infty}^{\infty} \frac{1}{k^2 - \zeta^2} \frac{H_n^{(1)}\{(k^2 - \zeta^2)^{\frac{1}{2}}\rho\}}{[\partial H_n^{(1)}\{(k^2 - \zeta^2)^{\frac{1}{2}}a\}/\partial a]} e^{i\zeta(z-t)} d\zeta \end{cases}$$

as follows*

*No confusion should result from our different uses for the symbol E.

$$(6)\quad \begin{cases} E_\rho = \dfrac{1}{4\pi^2}\displaystyle\sum_{-\infty}^{\infty} e^{in\phi}\iint\Big[\Big\{\frac{\partial^2 G_n}{\partial\rho\partial z} - \frac{n^2}{\rho a}\frac{\partial H_n}{\partial z}\Big\}f_2(\beta,t) \\ \qquad\qquad - \dfrac{ni}{\rho}F_n f_1(\beta,t)\Big]e^{-in\beta}dtd\beta, \\ E_\phi = \dfrac{1}{4\pi^2}\displaystyle\sum_{-\infty}^{\infty} e^{in\phi}\iint\Big[ni\Big(\frac{1}{\rho}\frac{\partial G_n}{\partial z} - \frac{1}{a}\frac{\partial^2 H_n}{\partial\rho\partial z}\Big)f_2(\beta,t) \\ \qquad\qquad + \dfrac{\partial F_n}{\partial\rho}f_1(\beta,t)\Big]e^{-in\beta}dtd\beta, \\ E_z = \dfrac{1}{4\pi^2}\displaystyle\sum_{-\infty}^{\infty} e^{in\phi}\iint E_n f_2(\beta,t)e^{-in\beta}dtd\beta. \end{cases}$$

These fundamental integrals are connected by the equations

$$(7)\quad \begin{cases} \partial^2 G/\partial z^2 + k^2 G = E, \\ \partial^2 H/\partial z^2 + k^2 H = F. \end{cases}$$

3. THE FAR ZONE FIELD

It is convenient to describe the far-zone field in terms of spherical polar coordinates r, θ, ϕ and, accordingly, we shall later make the substitutions

$$(8)\qquad \rho = r\sin\theta\,, \qquad z = r\cos\theta.$$

In the work of approximation to the far field the case when the field point is near the antenna surface has to be treated separately from the case when this is not so. The reason for this will appear later.

3.1. The Field at Points not too near the Antenna Surface

This case is dealt with by Papas (1949) and Silver and Saunders (1950) by applying the saddle-point method of asymptotic approximation to the infinite integrals concerned. The expressions for the field given in the Silver and Saunders paper are first approximations only: the analysis necessary to estimate the order of the error involved in the use of these expressions is too lengthy to include here. It appears in a contemporary D.R.B. report by the writer (Northover 1958). The results are:

(1) when $ka\theta$ is not small the Silver and Saunders expressions must be multiplied by a factor of

$$1 + O(a^2/r\lambda)$$

to obtain the true result,

(2) when $ka\theta \ll 1$ but not so small as to make this type of approximation invalid,* their expressions have to be multiplied by a factor

$$1 + O\{1/[(kr)^2\theta^4]\}$$

in order to reach the accurate result.

For small values of $ka\theta$ the Silver and Saunders expressions are thus correct to order $1/(kr\theta^2)$ (i.e., the error involved is at most $O\{(kr)^{-2}\theta^{-4}\}$.

*I.e., we must have $\theta^2(kr) > 1$ as is shown in the report.

3.2. Approximation to the Field for z Large and ρ Moderate

3.2.1. The integrals to be approximated to are E, F, G, and H. We begin by considering the integral E.

Integral E

This integral is taken along the real axis with an upward indentation at $\zeta = -k$ and a downward one at $\zeta = k$, in the cut plane defined by

$$\begin{aligned} -\frac{3}{2}\pi < \arg(\zeta-k) < \frac{1}{2}\pi, \\ -\frac{1}{2}\pi < \arg(\zeta+k) < \frac{3}{2}\pi. \end{aligned} \tag{9}$$

We write for brevity z instead of $(z-t)$ (as the *form* of the integral is thereby unchanged) and assume first that $z > 0$;* then, owing to the convergence to zero of the integral over the arcs of the circle $|\zeta-k| = R$ defined by $-\pi > \arg(\zeta-k) > -\frac{3}{2}\pi$ and $0 < \arg(\zeta-k) < \frac{1}{2}\pi$, as $R \to \infty$, we may deform the path of integration away from the real axis into a path passing round $\zeta = k$ and going to infinity on opposite sides of the cut which starts from this branch point. In fact we deform the path of integration to the path shown in the figure:

As regards the contribution to the integral from the small circular part surrounding the branch point k, it is easy to see that this is at most of order ϵ, where ϵ is the radius of the indentation. Hence, writing

$$\zeta = k + i\eta/z$$

and noting that $k-\zeta = e^{i\pi}(\zeta-k)$, the integral becomes (after using well-known properties of Hankel functions and reducing)

$$-\frac{2}{z}e^{ikz}\int_0^\infty \frac{J_n(\rho_1)Y_n(a_1) - Y_n(\rho_1)J_n(a_1)}{J_n^2(a_1)+Y_n^2(a_1)}\, e^{-\eta}\, d\eta, \tag{10}$$

where

$$\begin{cases} \rho_1 = \rho\left(\dfrac{2k\eta}{z}\right)^{\frac{1}{2}} e^{-i\pi/4}\left(1+\dfrac{\eta i}{2kz}\right)^{\frac{1}{2}}, \\ a_1 = a\left(\dfrac{2k\eta}{z}\right)^{\frac{1}{2}} e^{-i\pi/4}\left(1+\dfrac{\eta i}{2kz}\right)^{\frac{1}{2}}. \end{cases} \tag{10A}$$

We now require the asymptotic forms of this integral for z large and ρ

*The case $z < 0$ would be dealt with by a corresponding deformation around the branch point $\zeta = -k$.

moderate. The analysis falls into two separate cases, namely, $n \neq 0$ and $n = 0$. We consider these in turn.

Case 1.—$n \neq 0$. For ξ small and $n > 0$

$$Y_n(\xi) \doteq -\frac{2^n}{\pi}\frac{(n-1)!}{z^n}. \tag{11}$$

Note that

$$\frac{H_{-\nu}^{(1)}(\xi)}{H_{-\nu}^{(1)}(\xi)} = \frac{H_{\nu}^{(1)}(\xi)}{H_{\nu}^{(1)}(\xi)}$$

so that it is only necessary to consider positive values of n. Therefore the above integral approximates to

$$-\frac{2e^{ikz}}{z}\int_0^\infty \frac{1}{n\pi}\left\{\left(\frac{\rho}{a}\right)^n - \left(\frac{a}{\rho}\right)^n\right\}\frac{\pi^2}{2^{2n}}\frac{a_1^{2n}e^{-\eta}}{\{(n-1)!\}^2}\,d\eta\,,$$

$$\sim -\frac{2\pi}{z}e^{ikz}\,i^{-n}(\tfrac{1}{2}ka\theta)^n\frac{1}{(n-1)!}\left\{1-\left(\frac{a}{\rho}\right)^{2n}\right\} \tag{12}$$

as a first approximation, on taking

$$a_1 \doteq a(2k\eta/z)^{\frac{1}{2}}\,e^{-i\pi/4}. \tag{13}$$

Case 2.—$n = 0$. Integral is

$$-\frac{2}{z}e^{ikz}\int_0^\infty \frac{J_0(\rho_1)Y_0(a_1) - Y_0(\rho_1)J_0(a_1)}{J_0^2(a_1)+Y_0^2(a_1)}\,e^{-\eta}\,d\eta.$$

For ξ small

$$Y_0(\xi) \doteq (2/\pi)\log\xi. \tag{14}$$

Hence the integral approximates* to

$$-\frac{4\pi}{z}e^{ikz}\log\left(\frac{a}{\rho}\right)\Big/\left\{\log\left(\frac{1}{a^2}\frac{z}{2k}\right)\right\}^2. \tag{15}$$

Integral F

Deforming the path of integration into the same contour as that used above, the integral becomes equal to

$$-\frac{2}{z}e^{ikz}\int_0^\infty \frac{J_n(\rho_1)Y_n'(a_1) - Y_n(\rho_1)J_n'(a_1)}{\{J_n'(a_1)\}^2+\{Y_n^2(a_1)\}^2}\,\frac{e^{-\eta}\,d\eta}{(2k\eta/z)^{\frac{1}{2}}\,e^{-i\pi/4}(1+\eta i/2kz)^{\frac{1}{2}}}$$

$$\sim -\frac{2\pi a}{z}e^{ikz}\,i^{-n}\frac{1}{n!}(\tfrac{1}{2}ka\theta)^n\left\{1+\left(\frac{a}{\rho}\right)^{2n}\right\} \qquad (n>0), \tag{16}$$

$$\sim \frac{\pi}{z}ae^{ikz} \qquad (n=0). \tag{17}$$

on carrying out an analysis similar to the preceding analysis.

The Integrals of G and H

It can be seen by inspection that deformation of the path of integration into the contour used above is not now permissible since these integrals would

*Cf. D.R.B. report or Appendix 1.

not converge along such a contour owing to the presence of the factor $1/(k^2-\zeta^2)$ in the integrand. We therefore proceed indirectly, using the relations (7). We illustrate the method of dealing with these two integrals by giving the analysis in full for the case of G.

Case $n \neq 0$.—We have

$$\frac{\partial^2 G}{\partial z^2} + k^2 G \sim -\frac{2\pi}{z^{n+1}} e^{ikz} i^{-n} (\tfrac{1}{2}ka\rho)^n \frac{1}{(n-1)!} \left\{1-\left(\frac{a}{\rho}\right)^{2n}\right\}. \tag{18}$$

Put

$$G = e^{ikz}\chi, \tag{19}$$

then

$$\chi'' + 2ik\chi' \sim -\frac{2\pi}{z^{n+1}} i^{-n} (\tfrac{1}{2}ka\rho)^n \frac{1}{(n-1)!} \left\{1-\left(\frac{a}{\rho}\right)^{2n}\right\} \tag{20}$$

and therefore

$$\chi \sim \frac{\pi}{ikz^n} i^{-n} \frac{1}{n!} (\tfrac{1}{2}ka\rho)^n \left\{1-\left(\frac{a}{\rho}\right)^{2n}\right\}, \tag{21}$$

so that

$$G \sim \frac{\pi}{ikz^n} e^{ikz-\frac{1}{2}n\pi i} \frac{1}{n!} (\tfrac{1}{2}ka\rho)^n \left\{1-\left(\frac{a}{\rho}\right)^{2n}\right\}. \tag{22}$$

This makes

$$|\chi''/k\chi'| = O(1/kz) \ll 1, \tag{23}$$

thus justifying the neglect of χ'' on the left of (20), which led to (22).

Case $n = 0$.—Here

$$\frac{\partial^2 G}{\partial z^2} + k^2 G \sim -\frac{4\pi}{z} e^{ikz} \log\left(\frac{a}{\rho}\right) \Big/ \left\{\log\left(\frac{1}{a^2}\frac{z}{2k}\right)\right\}^2. \tag{24}$$

Similar reasoning to the above gives

$$G \sim \frac{2\pi e^{ikz}}{ik} \log\left(\frac{a}{\rho}\right) \Big/ \left\{\log\left(\frac{1}{a^2}\frac{z}{2k}\right)\right\}. \tag{25}$$

Proceeding similarly for H, we have

$$H \sim \frac{\pi}{ikz^n} e^{ikz-\frac{1}{2}n\pi i} \frac{1}{n(n!)} (\tfrac{1}{2}ka\rho)^n \left\{1+\left(\frac{a}{\rho}\right)^{2n}\right\} \qquad (n > 0), \tag{26}$$

$$\sim \frac{\pi a}{2ik} e^{ikz} \log z \qquad (n = 0). \tag{27}$$

3.2.2. *Approximate Evaluation of the Far Field*

Using the above approximate expression, we have

$$\frac{\partial^2 G}{\partial z \partial \rho} \sim \frac{a\pi}{2iz^n} e^{ikz-\frac{1}{2}n\pi i} \frac{1}{(n-1)!} (\tfrac{1}{2}ka\rho)^{n-1} \left\{1-\left(\frac{a}{\rho}\right)^{2n}\right\} \qquad (n > 0), \tag{28}$$

$$\sim -\frac{2\pi}{\rho} \left\{1 \Big/ \log\left(\frac{1}{a^2}\frac{z}{2k}\right)\right\} \qquad (n = 0), \tag{29}$$

$$\frac{\partial H}{\partial z} \sim \frac{\pi}{z^n} e^{ikz-\frac{1}{2}n\pi i} \frac{1}{n(n!)} (\tfrac{1}{2}ka\rho)^n \left\{1+\left(\frac{a}{\rho}\right)^{2n}\right\}, \tag{30}$$

$$\frac{\partial G}{\partial z} \sim \frac{\pi}{z^n} e^{ikz-\frac{1}{2}n\pi i} \frac{1}{n!} (\tfrac{1}{2}ka\rho)^n \left\{1-\left(\frac{a}{\rho}\right)^{2n}\right\}, \tag{31}$$

$$\frac{\partial^2 H}{\partial\rho\partial z} \sim \frac{\pi ka}{2z^n} e^{ikz-\frac{1}{2}n\pi i} \frac{1}{n!} (\tfrac{1}{2}ka\rho)^{n-1} \left\{1+\left(\frac{a}{\rho}\right)^{2n}\right\}, \tag{32}$$

$$\frac{\partial F}{\partial\rho} \sim -\frac{\pi ka}{z^{n+1}} (\tfrac{1}{2}ka\rho)^{n-1} \frac{1}{(n-1)!} \left\{1+\left(\frac{a}{\rho}\right)^{2n}\right\} \qquad (n > 0), \tag{33}$$

$$\sim O(1/z^2) \qquad (n = 0). \tag{34}$$

Writing

$$\gamma = \iint f_2(\beta, t)\, dtd\beta, \tag{35}$$

the double integral being taken over the aperture, the first approximation to the field for z large and moderate is as follows:

$$\begin{cases} E_\rho \sim \dfrac{\gamma}{2\pi\rho} \dfrac{e^{ikz}}{\log Z}, \\ E_\phi \sim O\left(\dfrac{1}{z^2}\right), \\ E_z \sim -\dfrac{\gamma}{\pi z} \dfrac{e^{ikz}}{(\log Z)^2} \log\left(\dfrac{a}{\rho}\right), \end{cases} \tag{36}$$

where

$$Z = \frac{1}{a^2} \frac{z}{2k}. \tag{36A}$$

This gives

$$E_\theta \sim -\frac{\gamma}{2\pi\rho} \frac{e^{ikz}}{\log Z}. \tag{37}$$

It will be noticed that the field is dominated by the mode $n = 0$: the corresponding expressions for **H** (as obtained from (4)) are

$$\begin{cases} H_\rho = O\left(\dfrac{1}{z^2}\right), \\ H_\phi \sim -\dfrac{\gamma}{2\pi\rho} \dfrac{e^{ikz}}{\log Z}, \\ H_z \sim O\left(\dfrac{1}{z^2}\right). \end{cases} \tag{38}$$

4. CONCLUSION

The main interest in the elucidation of the field near the metal surface of the antenna is that this allows the surface currents at long distances from

the slot to be investigated. For if $\mathbf{H}_t$ is the surface component of $\mathbf{H}$ and $\mathbf{j}$ is the conduction current vector on the surface, $\mathbf{j}$ is perpendicular to $\mathbf{H}_t$ and $4\pi|\mathbf{j}| = |\mathbf{H}_t|$.

At the ends of a finite antenna the component of the surface conduction current perpendicular to the bounding edge is zero. By superposing suitable extra terms on the surface current terms appropriate to the infinite antenna it may be possible to realize this condition and thus to treat the case of a finite antenna. It is hoped to follow up this idea in a later investigation.

The appendices deal mainly with the question of the range of validity of the two types of approximation and with that of the validity of the Papas procedure of using the saddle-point type of approximations for $\mathbf{E}$ and $\mathbf{H}$ for the Poynting energy flux vector in an integration of the normal component of this vector over an outside surface completely enclosing the radiating aperture.

ACKNOWLEDGMENTS

It is a pleasure to acknowledge here the valuable advice and encouragement received from Dr. J. Wait of the U.S. National Bureau of Standards Laboratories at Boulder, Colorado. I am also deeply indebted to Dr. R. Langille and the staff of the Radio Physics Laboratory, Defence Research Board of Canada, for many useful consultations.

REFERENCES

HALLÉN, E. 1948. J. Appl. Phys. **19**, 1140.
NORTHOVER, F. H. 1958. R. P. L. Report No. 19-0-16 (1958 revision).
PAPAS, C. H. 1949. J. Appl. Phys. **20**, 437.
SILVER, S. and SAUNDERS, W. K. 1950. J. Appl. Phys. **27**, 153.

APPENDIX 1

Conditions under Which This Type of Approximation Is Valid

It is sufficient to consider a typical integral, viz.,

$$\int_{-\infty}^{\infty} \frac{H_0^{(1)}\{(k^2-\zeta^2)^{\frac{1}{2}}\rho\}}{H_0^{(1)}\{(k^2-\zeta^2)^{\frac{1}{2}}a\}}\, e^{i\zeta z}\, d\zeta.$$

This is expressible as

$$-\frac{2}{z}\, e^{ikz} \int_0^{\infty} \frac{J_0(\rho_1)\, Y_0(a_1) - Y_0(\rho_1)\, J_0(a_1)}{J_0^{\,2}(a_1) + Y_0^{\,2}(a_1)}\, e^{-\eta}\, d\eta.$$

We split up the range of integration into $0 \leqslant \eta \leqslant K$, $\eta > K$, where K is taken large enough to ensure that

$$\left| \int_K^{\infty} \right| \ll \left| \int_0^K \right|$$

but small enough to make the approximation

$$\frac{J_0(\rho_1)\, Y_0(a_1) - Y_0(\rho_1)\, J_0(a_1)}{J_0^{\,2}(a_1) + Y_0^{\,2}(a_1)} \doteq \frac{2}{\pi}\, \frac{\log(a/\rho)}{1 + (4/\pi^2)\{\log(a_1\sqrt{\alpha})\}^2},$$

(where $\alpha = \frac{1}{4}e^{-2\gamma}$, γ being Euler's constant) good throughout the range $0 \leqslant \eta \leqslant K$. This requires* that

$$z > 2k\rho^2 K,$$

while K has to be taken large enough to make

$$\left| \int_K^\infty \right| \ll \left| \int_0^K \right| .$$

We then wish to know under what circumstances the following holds:

$$\int_0^K \frac{e^{-\eta}\, d\eta}{1+(1/\pi^2)\{\log(\eta/z)-\frac{1}{2}i\pi\}^2} \doteq \frac{1}{1+(1/\pi^2)(\log Z+\frac{1}{2}i\pi)^2}$$

wherein we have used the formula (13) for a_1 and written

$$Z = 2e^{2\gamma}(z/ka^2).$$

We further split the range 0 to K of the integral $\int_0^K$ into the ranges 0 to $Z^{-\frac{1}{3}}$ and $Z^{-\frac{1}{3}}$ to K; the first integral here is obviously at most of order $Z^{-\frac{1}{3}}(\ln Z)^{-2}$ and the second approximates to

$$(e^{-Z^{-1/3}} - e^{-K}) \frac{1}{1+(1/\pi^2)(\ln Z+\frac{1}{2}i\pi)^2}$$

since the integrand in this range approximates to

$$\frac{e^{-\eta}}{1+(1/\pi^2)(\ln Z+\frac{1}{2}i\pi)^2}$$

(with $K < Z^{\frac{1}{3}}$, say, Z large). Since K is not small, $\int_K^\infty$ is evidently $O(e^{-K})$ and safe criteria for the desired approximations are

(i) $Z > 27$,
(ii) K such that $e^{-K} \ll \pi^2/(\ln Z)^2$,
(iii) $z > 2k\rho^2 K$.

(i) and (iii) are satisfied for sufficiently large Z and (ii) is satisfied if, for example,

$$K > 2\ln(\ln Z).$$

If we take

$$Z > 4e^{2\gamma}K,$$

i.e., say

$$Z > 8e^{2\gamma} \ln(\ln Z),$$

then this requires $Z >$ at least 30 (and K at least about 2.6).

Hence a sufficient condition for this approximation to be valid is that $Z >$ about 30.

*$|\rho_1| < 1$ through $0 \leqslant \eta \leqslant K$ requires that $z > 2k\rho^2 K$.

If, further, $Z >$ about $e^{3\pi}$, then

$$\frac{1}{1+(1/\pi^2)(\ln Z+\frac{1}{2}i\pi)^2} \sim \frac{\pi^2}{(\ln Z)^2}$$

and the simple type approximations we have used in the text are then valid.

APPENDIX 2

On the Validity of the Papas Procedure of Integrating the Poynting Energy Flux Vector

Papas uses his expressions for $\mathbf{E}$ and $\mathbf{H}$ to evaluate

$$\iint (\mathbf{E} \wedge \mathbf{H}) . d\mathbf{S}$$

over the *whole* of that part of an infinite sphere outside the cylinder and containing the radiating aperture, whereas his approximate expressions are only valid* for $\theta > (kr)^{-\frac{1}{2}}$. However, by the radiation conditions, $r|\mathbf{E}|$ and $r|\mathbf{H}|$ are finite as $r \to \infty$, so the error involved is at most of order

$$\int_{a/r}^{\sqrt{K}/\sqrt{r}} B\theta \, d\theta$$

where B is a constant, and this integral approaches 0 as $r \to \infty$. ($|\mathbf{E} \wedge \mathbf{H} . d\mathbf{S}|$ will be at most $O(r^{-2} 2\pi r^2 \sin\theta \, d\theta)$.)

APPENDIX 3

On the Surface Value of $\mathbf{H}_t$ *for Large z*

It has been conjectured that the saddle-point type approximations give the correct value for the surface component of $\mathbf{H}$ (tangential component of $\mathbf{H}$ at the surface of the cylinder).† However, this is not the case.

At the surface, $\mathbf{E}_t = 0$ and we consider $\mathbf{H}_t$. We have

$$ikH_\phi = \frac{\partial E_\rho}{\partial z} - \frac{\partial E_z}{\partial \rho},$$

$$ikH_z = \frac{1}{\rho}\frac{\partial}{\partial \rho}(\rho H_\phi).$$

Therefore

$$ikH_\phi \sim -\frac{ik\gamma}{2\pi\rho}\frac{e^{ikz}}{\ln Z} - \frac{\gamma}{\pi z\rho}\frac{e^{ikz}}{(\ln Z)^2},$$

$$\sim -\frac{ik\gamma}{2\pi\rho}\frac{e^{ikz}}{\ln Z},$$

where

$$\gamma = \iint f_2(\beta, t) \, dt \, d\beta.$$

*Cf. the D.R.B. report (References).

†This surface component is of importance in calculating the surface current.

This gives

$$ikH_z \sim O(1/z^2).$$

Also

$$ikH_\rho = -\partial E_\rho/\partial z = O(1/z^2).$$

However, the saddle-point type expressions give

$$E_\rho \sim \frac{1}{4\pi^2}\iint f_2(\beta, t)\,\frac{2i\cot\theta}{r}e^{ikr}\,\{H_0^{(1)}(ka\theta)\}^{-1}d\beta\,dt$$

$$\sim \frac{\gamma}{4\pi\rho}\frac{e^{ikz}}{\ln(ka\rho/z)},$$

$$E_\phi \sim \frac{1}{2\pi^2}\frac{e^{ikr}}{r}\left(\frac{2}{\pi}\frac{i}{ka\theta}\right)^{-1}\iint f_1(\beta, t)\,d\beta\,dt$$

$$= O\left(\frac{1}{r^2}\right),$$

$$E_z \sim \frac{1}{4\pi^2}\iint f_2(\beta, t)\,d\beta\,dt \times \left(-\frac{2i}{r}\right)\frac{e^{ikr}}{H_0^{(1)}(ka\theta)}$$

$$\sim \frac{\gamma}{4\pi}\frac{e^{ikr}}{\ln(ka\rho/z)},$$

and these give, for the surface value of **H**,

$$H_z \sim O(1/r^2),$$
$$H_\rho \sim O(1/r^2),$$
$$ikH_\phi \sim \frac{ik\gamma}{4\pi\rho}\frac{e^{ikz}}{\ln(ka\rho/z)} = -\frac{ik\gamma}{4\pi a}\frac{e^{ikz}}{\ln(z/ka^2)} \sim -\frac{ik\gamma}{4\pi a}\frac{e^{ikz}}{\ln Z}.$$

The Papas approximations therefore give half the correct result. Wait has suggested the following physical explanation: "the Papas result when extrapolated to the cylinder surface should be multiplied by two to account for the imaging of the conductor".

APPENDIX 4

Gap in the Range of Applicability of the Approximations

The theory of this paper shows that neither of the two types of approximation to the field developed can be used in the intermediate range

$$0.435(kr)^{-\frac{1}{3}} < \theta < (kr)^{-\frac{1}{3}}$$

(taking K about 2.6 in Appendix 1).

Unfortunately considerable difficulty is encountered when attempts are made to close this gap. Fortunately, it is relatively narrow: however, if the field was required therein, there would probably be no alternative to heavy numerical computation.

HIGH RESOLUTION RAMAN SPECTROSCOPY OF GASES

XI. SPECTRA OF CS_2 AND CO_2[1]

B. P. STOICHEFF

ABSTRACT

The vibrational Raman spectra of CS_2, $C^{12}O_2$, and $C^{13}O_2$, consisting of the strong Fermi diad ν_1, $2\nu_2$, have been photographed with a 21 ft. grating. In the spectrum of CS_2, 12 additional sharp Q branches were observed in the region of the diad; three are due to isotopic molecules and the remainder are "hot" bands. The rotational structure of the strong ν_1 band was also obtained. These measurements together with infrared data are used to determine the vibrational constants ω_i^0 and x_{ik} of CS_2. The pure rotational spectrum of CS_2, with rotational lines up to $J = 94$, yields the constants $B_{000} = 0.10910 \pm 0.00005$ cm^{-1}, $D_{000} = 1.0 \times 10^{-8}$ cm^{-1}, and $r_0(C{=}S) = 1.5545 \pm 0.0003$ Å. For $C^{12}O_2$, the rotational structure of the diad was analyzed and the results are in agreement with recent infrared data.

A. INTRODUCTION

One of the vibrational Raman spectra most frequently studied in the past is that of the CS_2 molecule. Interest in this spectrum was stimulated primarily by its unexpected complexities, for example: the Fermi resonance between ν_1 and $2\nu_2$ (Placzek 1934), the appearance of the forbidden bands ν_2 and ν_3 (Wood and Collins 1932; Venkateswaran 1932; Evans and Bernstein 1956), and the appearance of "hot" bands (Langseth, Sorensen, and Nielsen 1934) and of vibrational bands due to isotopic molecules (Giulotto and Caldirola 1941). All of these investigations were carried out with liquid CS_2. The Raman spectrum of solid CS_2 has been studied by Sirkar (1936), and that of the vapor by Imanishi (1935), who observed the ν_1 and $2\nu_2$ Q branches.

In order to unravel the complex vibrational spectrum, Langseth, Sorensen, and Nielsen (1934) and Giulotto and Caldirola (1941) used spectrographs of relatively large dispersion (7 Å/mm.) and were successful in interpreting most of the observed details. However, as will be evident from the present results, much more information can be obtained from the Raman spectrum of the *vapor* particularly when the spectrum can be photographed at high resolution.

The infrared absorption spectrum of CS_2 vapor was studied by Bailey and Cassie (1933) and the rotational structure of one of the infrared bands was first resolved by Sanderson (1935). The ultraviolet electronic spectrum was photographed under high resolution by Liebermann (1941) and yielded accurate values of the rotational constants and of the vibrational interval $2\nu_2$. More recently, several of the overtone and combination bands have been observed at high resolution by Gailar and Plyler (1952) and Allen, Plyler, and Blaine (1956). These investigations provide further information about the rotational and vibrational constants.

[1]Manuscript received October 30, 1957.
Contribution from the Division of Pure Physics, National Research Council, Ottawa, Ontario.
Issued as N.R.C. No. 4607.

The vibrational Raman spectrum of CO_2 has also been studied frequently, and as in CS_2, the Fermi diad ν_1, $2\nu_2$ has been the most interesting feature in the spectrum. But in contrast to CS_2, the infrared spectrum of CO_2 has also been the subject of a large number of investigations. One of the most extensive of these is the recent study by Courtoy (1957). During his research, further data on the diad ν_1, $2\nu_2$ were desirable and one of the possible means of obtaining this information was by photographing the Raman spectrum at high resolution.

Up to the present time, this series of papers has dealt with the pure rotational spectra of molecules and not with the less intense rotation–vibration spectra. In contrast, the primary purpose of the present investigation was to attempt to photograph the vibrational spectra of CS_2 and CO_2 with a 21 ft. grating and if possible to observe the rotational structure of the most intense bands. Fortunately, the vibrational spectra of these molecules are relatively intense and several plates of the rotational structure of the vibrational bands were obtained in reasonable exposure times. These have yielded useful information, particularly about the role of Fermi resonance. Also in the CS_2 spectrum, sufficient data were obtained from the "hot" bands to permit the calculation of vibrational frequencies and anharmonic constants. In addition, the pure rotational spectrum of CS_2 was photographed and has given precise values of the rotational constant and internuclear distance for the ground state.

B. EXPERIMENTAL PROCEDURE

The apparatus, including the mirror-type Raman tube, mercury lamps, and 21 ft. grating spectrograph, has been described in the first paper of this series (Stoicheff 1954). For the pure rotational spectrum of CS_2, the cell was filled to a pressure of 10 cm. Hg. Exposure times of 4 hours were used with a slit width of 0.02 mm. For the vibrational spectrum of CS_2, pressures up to 1 atmosphere were used and the cell was kept at a temperature of 60° C. A filter of $NaNO_2$ solution was circulated around the cell. Since the vibrational spectra are much weaker than pure rotational spectra in the Raman effect, a cylindrical lens was placed in the spectrograph, in front of the photographic plate as described in paper VIII (Callomon and Stoicheff 1957). This reduced the exposure times by a factor of about 15. Several plates of the vibrational spectrum were obtained with exposure times of 4 to 20 hours, using slit widths of 0.02 and 0.05 mm.

The spectra of CO_2 and (of a 60% enriched sample) of $C^{13}O_2$, consisting of the sharp Q branches ν_1, $2\nu_2$, were photographed with gas pressures of 1 atmosphere, using the cylindrical lens, in exposure times of 4 to 8 hours. Exposures lasting 30 hours were necessary to photograph the rotational structure of the ν_1 and $2\nu_2$ bands of $C^{12}O_2$.

All of the spectra were photographed in the second order of the N.R.C. 21 ft. grating spectrograph (dispersion of 1.25 Å/mm.). Second- and third-order iron lines were used as standards. The plates were measured with a photoelectric scanning comparator built in this laboratory, after the design of Tomkins and Fred (1951).

C. ROTATIONAL SPECTRUM OF CS_2

A photograph of the pure rotational spectrum of CS_2 is shown in Fig. 1(*a*). The Stokes and anti-Stokes branches extend to 40 cm^{-1} from the exciting line and include lines from $J = 10$ to $J = 94$. The line spacing is 0.87 cm^{-1}. Two plates were evaluated and the average values of the wavenumber shifts, accurate to ± 0.02 cm^{-1} or better, are listed in Table I.

TABLE I

WAVENUMBER SHIFTS (UNITS CM^{-1}) IN THE ROTATIONAL RAMAN SPECTRUM OF CS_2

J	$\Delta\nu$[a]	J	$\Delta\nu$[a]
10	4.958	50	22.469
12	5.868	52	23.343
14	6.761	54	24.217
16	7.637	56	25.091
18	8.497	58	25.959
20	———*	60	26.826
22	10.247*	62	27.695
24	11.125	64	28.560
26	12.002	66	29.423
28	12.871	68	30.299
30	13.745	70	31.176
32	14.615	72	32.037
34	15.483	74	32.909
36	16.355	76	33.790
38	17.230	78	34.657
40	18.109	80	35.529
42	19.003*	82	36.401
44	19.839	84	37.271
46	20.723	86	38.151
48	21.589	88	38.997
		90	39.862
		92	40.742
		94	41.594

[a]All values are averages of the Stokes and anti-Stokes lines measured on two plates.
*Lines blended with grating ghosts.

Since the CS_2 molecule has a center of symmetry (point group $D_{\infty h}$) and the most abundant isotope, S^{32}, has a nuclear spin of zero (Bose statistics), alternate rotational levels are missing. Since the ground electronic state is $^1\Sigma_g^+$, it is the odd rotational levels which are absent. The selection rule for rotational transitions is $\Delta J = 2$ and leads to the expression

$$|\Delta\nu| = 4B_{000}(J+\tfrac{3}{2}) - 8D_{000}(J+\tfrac{3}{2})^3, \qquad J = 0, 2, 4, \ldots,$$

for the displacements of the rotational lines from the unshifted Rayleigh line ($\Delta J = 0$). The rotational and centrifugal distortion constants were evaluated in the usual way by plotting a graph of $|\Delta\nu|/(J+\frac{3}{2})$ against $(J+\frac{3}{2})^2$ as shown in Fig. 2. The values* obtained are

*At the Symposium on Molecular Structure and Spectroscopy, Ohio, 1957, A. H. Guenther, T. A. Wiggins, and D. H. Rank reported the results of their investigations of the $3\nu_2$ and $\nu_2+3\nu_3-\nu_2$ infrared bands. They obtained $B_0 = 0.10910 \pm 0.00002$ and $D_0 = (1.1 \pm 0.3) \times 10^{-8}$ cm^{-1}, in good agreement with the present values determined from the Raman spectrum, which were also reported at this symposium.

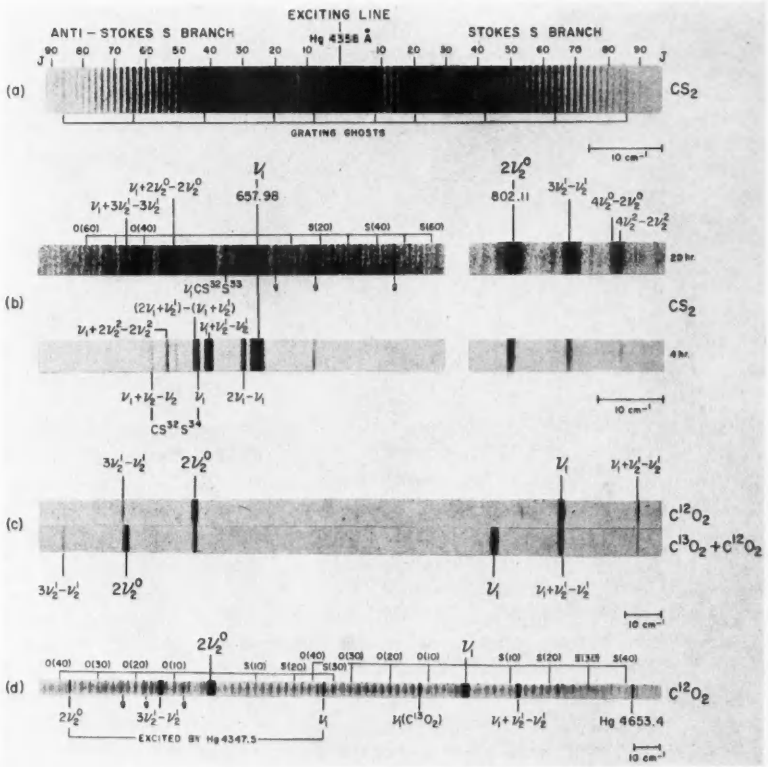

FIG. 1. Raman spectra of CS_2 and CO_2 photographed with a 21 ft. grating. (*a*) Pure rotational spectrum of CS_2. (*b*) Fermi diad ν_1, $2\nu_2$ of CS_2 photographed in exposure times of 4 hours and 20 hours. (*c*) *Q* branch lines of the Fermi diad ν_1, $2\nu_2$ of $C^{12}O_2$ and $C^{13}O_2$. (*d*) Rotational structure in the diad ν_1, $2\nu_2$ of $C^{12}O_2$.

$$B_{000} = 0.10910 \pm 0.00005 \text{ cm}^{-1} \quad \text{and} \quad D_{000} = 1.0 \times 10^{-8} \text{ cm}^{-1}.$$

The effective moment of inertia is therefore

$$I_0 = \frac{27.9890}{B_{000}} \times 10^{-40} = (256.54 \pm 0.12) \times 10^{-40} \text{ g. cm.}^2$$

and gives

$$r_0(\text{C}{=}\text{S}) = 1.5545 \pm 0.0003 \text{ Å}.$$

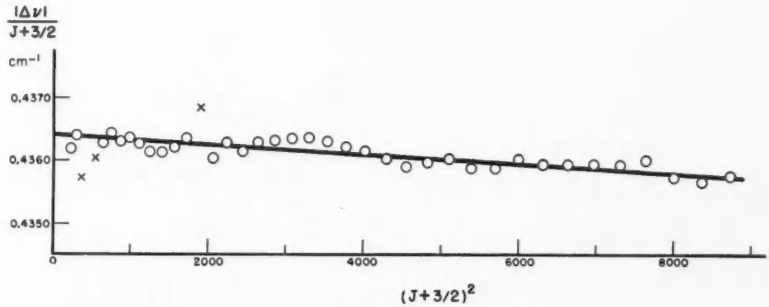

FIG. 2. $|\Delta\nu|/(J+3/2)$ graph for the ground state of CS_2 (X represents rotational lines blended with grating ghosts).

The present values of the constants are considered to be an improvement over the recent infrared values given by Allen, Plyler, and Blaine (1956). Their value of $D_0 = 4.34 \times 10^{-8}$ is high and is reflected in their high value of $B_0 = 0.10927$ cm^{-1}. The relation $D_0 = 4B_0^3/\omega_1^2$ should give a reliable value of D_0. With $B_0 = 0.109$ and $\omega_1 = 659$ cm^{-1}, one obtains $D_0 = 1.2 \times 10^{-8}$ cm^{-1}, which is almost the same as the value obtained in the present research.

In order to determine B_e and hence the equilibrium internuclear distance in CS_2, the quantity $\frac{1}{2}(\alpha_1+2\alpha_2+\alpha_3)$ must be known. Its value can be obtained experimentally from the convergence of rotational lines in the band $\nu_1+2\nu_2+\nu_3$, or in three bands which include the vibrations ν_1, ν_2, ν_3. For CS_2, the infrared band $\nu_1+2\nu_2+\nu_3$ at 2961.7 cm^{-1} has been investigated by Allen, Plyler, and Blaine (1956), who report a value of $\alpha_1+2\alpha_2+\alpha_3 = 0.000460$ cm^{-1}. Unfortunately, there appears to be an error in the measurement of this band since it gives high values of B_0 and D_0; there is therefore some uncertainty (about 10%) in their value. Consequently larger errors than those found for B_0 and r_0 are assigned to the values of B_e and r_e:

$$B_e = 0.10933 \pm 0.00008 \text{ cm}^{-1}, \qquad r_e = 1.5529 \pm 0.0005 \text{ Å}.$$

D. VIBRATIONAL SPECTRUM OF CS_2

Photographs of the vibrational spectrum of CS_2 are shown in Fig. 1(*b*). The lower strip shows the strong vibrational lines photographed in 4 hours, and the upper strip shows the rotational structure of the ν_1 band as well as other

weaker vibrational Q branches photographed in 20 hours. The vibrational spectrum is indeed a complex one consisting of the prominent Fermi diad ν_1, $2\nu_2$ and including three Q branches of isotopic molecules as well as nine "hot" bands.

(1) The ν_1 Band

The most intense line in the spectrum is the Q branch of the ν_1 band. The weak rotational structure on either side of this line forms the S and O branches of this band. The wavenumber shifts are listed in Table II.

TABLE II

WAVENUMBER SHIFTS[a] (UNITS cm^{-1}) OF THE LINES IN THE ν_1 BAND OF CS_2

J	$S(J)$	$O(J)$	J	$S(J)$	$O(J)$
8	———	654.90	42	676.67	639.62
10	662.92	653.77	44	677.68	638.77
12	663.79	652.99	46	678.42	637.76
14	664.72	652.13	48	679.13	636.94
16	665.57	651.29	50	679.99	636.04
18	666.25	———	52	680.83	635.04
20	667.22	———	54	681.65	634.21
22	668.16	649.11	56	682.56	633.41
24	668.99	———	58	683.33	632.49
26	669.86	646.80	60	684.17	631.74
28	670.68	645.79	62	684.96	630.58
30	671.52	645.02	64		629.62
32	672.39	644.11	66		628.49
34	673.26	643.21	68		627.86
36	674.13	642.33	70		626.87
38	675.00	641.29	72		626.00
40	676.67	640.62	74		625.22

[a]Average values of measurements of two plates.

The formulae of the rotation–vibration lines are given by the well-known equations

$$S(J) = \nu_0+6B'+(5B'-B'')J+(B'-B'')J^2, \qquad J = 0, 2, 4, 6 \ldots,$$
$$O(J) = \nu_0+2B'-(3B'+B'')J-(B'-B'')J^2, \qquad J = 2, 4, 6 \ldots.$$

These can be written as a single equation:

$$\nu = \nu_0-2B''+(B'+3B'')m+(B'-B'')m^2,$$

where $m = J+2$ for the S branch, and $m = -J+1$ for the O branch. A graph of ν versus m gave the relative numbering of the lines in the O and S branches, and the absolute numbering was then determined from the known value of B'' and the assumption $B' = B''$. The band origin ν_0 and $(B'-B'')$ were determined from a graph (Fig. 3) of the combination sum

$$\tfrac{1}{2}[S(J)+O(J)] = \nu_0+4B'+(B'-B'')J(J+1).$$

The values are $\nu_0 = 657.98$ cm^{-1} and $(B'-B'') = -0.000155$ cm^{-1}. This value of $B'-B''$ gives $-\alpha_1$ to a very good approximation (see part (2) of this section), since the Fermi resonance of the (10^00) and (02^00) levels is weak.

This fact also explains the value $D'-D''=0$ observed for this band, while in CO_2, where the resonance is very strong, values of $D' \neq D''$ have been observed for many of the interacting levels (Courtoy and Herzberg 1955).

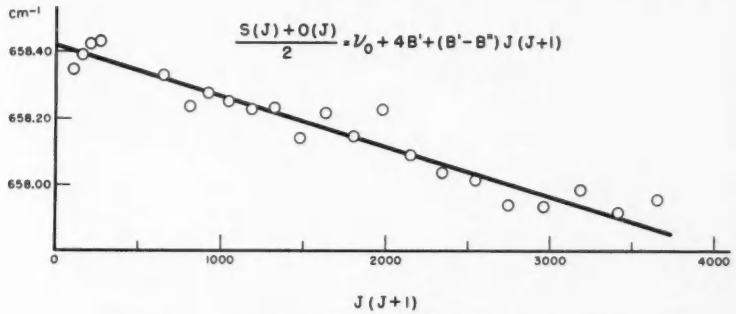

FIG. 3. A graph of $\frac{1}{2}[S(J)+O(J)]$ for the ν_1 band of CS_2.

(2) The Vibrational Spectrum and Vibrational Constants

The wavenumber shifts and assignments of the vibrational lines are given in Table III. The assignment of the isotopic bands was carried out with the aid of known isotopic abundances (CS_2^{32} = 90%, $CS^{32}S^{33}$ = 1.4%, $CS^{32}S^{34}$ = 8%, $C^{13}S_2^{32}$ = 1%) and with the aid of the expected isotopic shifts $\Delta\nu_1(CS^{32}S^{33} = -5\ cm^{-1}$, $CS^{32}S^{34} = -9.7\ cm^{-1}$, and $C^{13}S_2^{32} = -2.5\ cm^{-1}$). For the assignment of the "hot" bands, the Boltzmann factor $e^{-h\nu/kT}$ and the known degeneracy of the initial levels must be taken into account. All of the assignments given here obey these requirements except for the band assigned as $(2\nu_1+\nu_2)-(\nu_1+\nu_2)$, which appears to have almost double the expected intensity. At the bottom of Table III are listed the known infrared fundamentals and overtone bands. In Fig. 4, all of the observed transitions are represented in an energy level diagram.

The vibrational levels of a linear triatomic molecule (with respect to the lowest vibrational state) can be represented by

$$(1)\qquad G_0(v_1, v_2, v_3) = \omega_1{}^0 v_1+\omega_2{}^0 v_2+\omega_3{}^0 v_3+x_{11}v_1{}^2+x_{22}v_2{}^2+x_{33}v_3{}^2+x_{12}v_1v_2 +x_{13}v_1v_3+x_{23}v_2v_3+g_{22}l_2{}^2$$

if no resonance occurs. In Eq. (1), l_2 is the quantum number of the vibrational angular momentum about the symmetry axis ($l_2 = v_2, v_2-2, \ldots, 1$, or 0). Since Eq. (1) has 10 unknown constants, ω_i, x_{ik}, and g_{22}, 10 of the Raman and infrared bands, marked with an asterisk (*) in Table III, were chosen for calculating these constants. The values obtained are

$$(2)\qquad \begin{array}{lll} \omega_1{}^0 = 659.23, & x_{11} = -1.25, & x_{12} = -7.74, \\ \omega_2{}^0 = 396.55, & x_{22} = 2.25, & x_{23} = -6.67\dagger, \\ \omega_3{}^0 = 1537.63\dagger, & x_{33} = -5.13\dagger, & x_{13} = -4.96, \\ & & g_{22} = -2.00. \end{array}$$

Only the values marked with a dagger (†) are not affected by Fermi resonance.

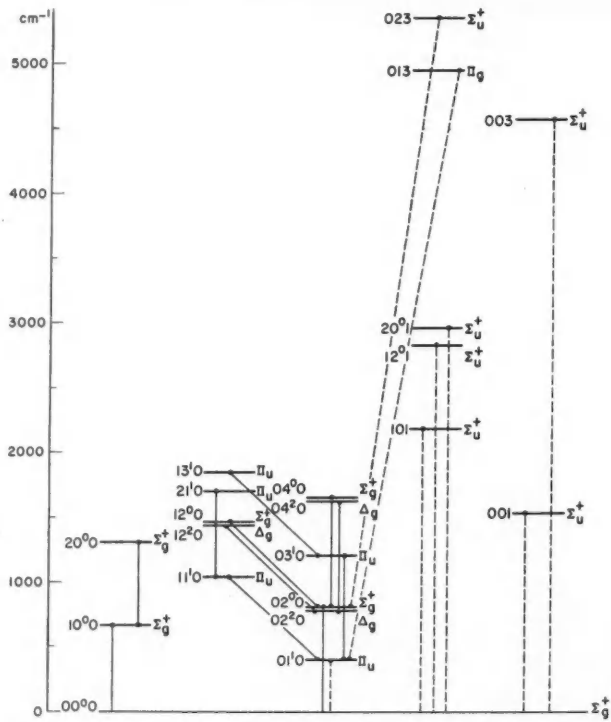

FIG. 4. Vibrational levels of the ground electronic state of CS_2. The vertical solid lines connecting various vibrational levels (horizontal lines) represent observed Raman transitions: the broken lines represent observed infrared transitions.

The constants were then used to calculate the remaining nine bands. Fair agreement is obtained as shown in column three of Table III. The deviations are due in part to the use of Q branch measurements instead of band origins and to the limited accuracy with which some of the vibrational frequencies are known. But the greatest part of the deviations are presumably due to the neglect of Fermi resonance amongst many of the vibrational levels.

The occurrence of Fermi resonance between the vibrational levels (10°0) and (02°0) in CS_2 is most clearly shown by the appearance of a relatively strong Raman line at almost twice the frequency of the fundamental ν_2 band. To be sure, even without Fermi resonance, a weak line is expected at this frequency in the Raman spectrum; however, its intensity would most likely be much less than 1% of the ν_1 band and would only be observed with long exposure times. In contrast to this expectation, the observed intensity of the $2\nu_2$ band is between 5 and 10% of the intensity of the ν_1 band. For this reason, and since a satisfactory analysis of the vibrational spectrum is then possible,

TABLE III

VIBRATIONAL BANDS OBSERVED IN THE RAMAN AND INFRARED SPECTRA OF CS_2 VAPOR

ν (cm^{-1})	Assignment	O—C (cm^{-1})
Raman bands		
637.76	$(\nu_1+3\nu_2^1)-3\nu_2^1$	3.0
641.29	$(\nu_1+\nu_2^1)-\nu_2^1$ $CS^{32}S^{34}$	
643.64	$(\nu_1+2\nu_2^2)-2\nu_2^2$	1.14
645.02	$(\nu_1+2\nu_2^0)-2\nu_2^0$	2.52
648.01	$(2\nu_1+\nu_2^1)-(\nu_1+\nu_2^1)$	0.26
648.37	ν_1 $CS^{32}S^{34}$	0.07
650.24	$(\nu_1+\nu_2^1)-\nu_2^1$	0 *
652.99	ν_1 $CS^{32}S^{33}$	0
655.49	$2\nu_1-\nu_1$	0 *
657.98[a]	ν_1	0 *
802.11	$2\nu_2^0$	0 *
811.12	$3\nu_1^1-\nu_2^1$	0 *
818.15	$4\nu_2^0-2\nu_2^0$	−1.95
819.18	$4\nu_2^2-2\nu_2^2$	−0.92
Infrared bands		
396.8[a,b]	ν_2^1	0 *
1532.5[a,c]	ν_3	0 *
2185.52[a,d]	$\nu_1+\nu_3$	0 *
2833.14[a,d]	$2\nu_1+\nu_3$	−2.90
2961.73[a,d]	$\nu_1+2\nu_2+\nu_3$	−1.49
4566.69[a,c]	$3\nu_3$	0 *
4546.7[a,c]	$(\nu_2^1+3\nu_3)-\nu_2^1$	0 *
4527.2[a,c]	$(2\nu_2+3\nu_3)-2\nu_2$	0.5

*Bands used to calculate vibrational and anharmonic constants listed in (2).

[a]Band origins; other values of ν represent measurements of sharp Q branches.

[b]Measurements by Bailey and Cassie (1933).

[c]Measurements by Gailar and Plyler (1952).

[d]Measurements by Allen, Plyler, and Blaine (1956).

the band at 802.11 cm^{-1} is considered to arise from the transition (02°0)← (00°0), which gains intensity through the interaction of the upper level (02°0) with the nearby level (10°0).

The Fermi resonance in CS_2 is, however, not strong, as is evident from the large difference in intensity of the ν_1 and $2\nu_2$ bands. A good estimate of the positions of the unperturbed levels and of the interaction energy can be readily obtained from the positions of the four Raman bands ν_1, $2\nu_2$ and $(\nu_2+\nu_2-\nu_2)$, $3\nu_2-\nu_2$. The spacing $2\nu_2-\nu_1$ gives $(\delta^2+4W^2)^{\frac{1}{2}}$, and $(3\nu_2-\nu_2)-(\nu_1+\nu_2-\nu_2)$ gives $(\delta^2+8W^2)^{\frac{1}{2}}$, if anharmonicity is neglected. In these expressions, δ is the separation of the unperturbed levels and W is the matrix element of the cubic term α_{122} in the potential energy which gives rise to the perturbation. One obtains $\delta = 126.0$ cm^{-1} and $|W| = 35.4$ cm^{-1}.

If anharmonicity is taken into account, one finds

$$
\begin{aligned}
&[2\nu_2^0-\nu_1^0]^2 = 4W^2+\delta^2,\\
&[3\nu_2^1-(\nu_1+\nu_2^1)]^2 = 8W^2+(\delta+4x_{22}-x_{12})^2,\\
&[4\nu_2^2-(\nu_1+2\nu_2^2)]^2 = 12W^2+(\delta+8x_{22}-2x_{12})^2,
\end{aligned}
\tag{3}
$$

where $\delta = 2\omega_2^0 + 4x_{22} - \omega_1^0 - x_{11}$, as before. On substituting the observed frequency differences, 144.13, 160.88, and 175.54 cm^{-1}, respectively, one obtains

$$\delta = 124.80 \text{ cm}^{-1} \qquad \text{and } |W| = 36.05 \text{ cm}^{-1},$$

very close to the values obtained when anharmonicity is neglected. The smallness of the effect of anharmonicity on δ and $|W|$ is due to the smallness of the value of $4x_{22} - x_{12} = -0.355$ cm^{-1}. The shift in the vibrational levels due to Fermi resonance is 9.67 cm^{-1} up for (02°0) and 9.67 cm^{-1} down for (10°0).

According to the above definition, δ is a positive quantity, but only the magnitude of W can be determined from Eq. (3) and not its absolute value. The latter can be found in the following way: The rotation vibrational coupling constant α_2 is given by the formula (Dennison 1940)

$$\alpha_2 = \frac{B_e^2}{\omega_2} + \frac{4B_e^2\omega_2}{(\omega_3^2 - \omega_2^2)} - \frac{8B_e^3 I_e'^{3/2}}{\omega_1^2\omega_2}\frac{\alpha_{122}}{hc}.$$

On the right-hand side, the last term (containing α_{122}) is the predominant one, and can be given in terms of W (see Herzberg 1945, p. 218). From these equations and the experimental value of $\alpha_2 = -0.00023$ (Allen, Plyler, and Blaine 1956), it follows that $W = -31.8$ cm^{-1} in good agreement with the value determined from the Raman data alone, and with a negative sign.

The separation of the unperturbed levels, given by δ, is almost 90% of the observed separation ($\Delta\nu$) and shows that the perturbation of the two levels is not strong. The mixing of the two levels affects their eigenfunctions and, of course, affects the rotational constants of the interacting levels. For example, the observed rotational constant B_{100} for the 1,0,0 level in terms of the unperturbed constants B_{100}^0 and B_{020}^0 is given by the equation

$$B_{100} = a^2 B_{100}^0 + b^2 B_{020}^0,$$

where the coefficient $a^2 = (\Delta\nu + \delta)/2\Delta\nu$ and $b^2 = (\Delta\nu - \delta)/2\Delta\nu$. In the present case $a^2 = 0.93$ and $b^2 = 0.07$. Therefore if one uses the experimental value of B_{100} reported in Section D(1), one obtains $B_{100}^0 = 0.10892$ cm^{-1} (or $\alpha_1 = 0.00018$ cm^{-1}) for the unperturbed value of the rotational constant of the 1,0,0 level.

The vibrational constants and anharmonic coefficients (except for x_{13}) can now be determined without neglecting the effect of Fermi resonance. The sums of the wavenumbers of a resonance multiplet (diad, triad . . .) are given by the same formula as without Fermi resonance. For example, $\nu_1 + 2\nu_2^0 = \omega_1^0 + x_{11} + 2\omega_2^0 + 4x_{22} = 1460.09$ cm^{-1}. Similarly, $(\nu_1 + \nu_2^1) + 3\nu_2^1 = 2254.96$ cm^{-1}, $2\nu_1^0 + (\nu_1 + 2\nu_2^0) + 4\nu_2^0 = 4380.86 cm^{-1}$, $(\nu_1 + 2\nu_2^2 - 2\nu_2^2) + (4\nu_2^2 - 2\nu_2^2) = 1462.82 cm^{-1}$. Other information used was $\delta = 124.80$ cm^{-1} and $4x_{22} - x_{12} = -0.355$ cm^{-1} evaluated from Eq. (3), and $\nu_2 = 396.8$ cm^{-1}. The constants ω_3^0, x_{33}, and x_{23} remain as in (2) since they were calculated from the bands ν_2, ν_3, $3\nu_3$, and $\nu_2 + 3\nu_3 - \nu_2$, which are not affected by Fermi resonance. Also since the available data are not sufficient to determine x_{13}, the assumption is made that the diad $(\nu_1 + \nu_3, 2\nu_2 + \nu_3)$, of which only $\nu_1 + \nu_3$ is observed, can be described by the same values of δ and W found for the diad $(\nu_1, 2\nu_2)$. This assumption leads to a

shift of 9.67 cm^{-1} to lower frequency for the $\nu_1+\nu_3$ band from its unperturbed position. The constants (in cm^{-1}) obtained from the preceding analysis are as follows:

$$
\begin{array}{llll}
\omega_1^0 = 668.69, & x_{11} = -1.05_4, & x_{12} = 0.86_1, \\
\omega_2^0 = 395.97, & x_{22} = 0.12_6, & x_{23} = -6.6_7, \\
\omega_3^0 = 1537.64, & x_{33} = -5.13_5, & x_{13} = -4.9_5, \\
\delta = 124.80, & g_{22} = 0.67_1, & \\
W = -36.05. & &
\end{array} \tag{4}
$$

The frequencies (in cm^{-1}) for infinitesimal amplitudes, ω_i, obtained from the above ω_i^0 and x_{ik} (Herzberg 1945, p. 206) are

$$\omega_1 = 671.36, \quad \omega_2 = 398.62, \quad \omega_3 = 1551.92.$$

Apart from errors in measurement or assignment, any uncertainty in the constants given here derives largely from the unknown accuracy of the value $4x_{22}-x_{12} = -0.355$ cm^{-1}. This quantity was determined from the difference of two large numbers (see Eq. (3)) and hence may contain a considerable error.

Unfortunately, all of the available infrared and Raman vibrational data have been used in the determination of the constants (4) so that a check of their accuracy is not possible at present. For this purpose and for the improvement of the present set of constants, it would be desirable to investigate the ν_2 fundamental and other overtone and combination infrared bands at high resolution.

E. VIBRATIONAL SPECTRA OF $C^{12}O_2$ AND $C^{13}O_2$

The vibrational Raman spectrum of CO_2 is characterized by two intense and sharp Q branches, of almost equal intensity, which form the diad ν_1, $2\nu_2$. Adjacent to each of these lines are the much weaker Q branches of the related diad $\nu_1+\nu_2-\nu_2$, $3\nu_2-\nu_2$, in which the lower level is $0,1^1,0$. The Q branches of these diads have been photographed for both $C^{12}O_2$ and $C^{13}O_2$, and are shown in Fig. 1(*c*). The ν_1 Q branch of $C^{12}O_2$ is sharp and symmetrical; in fact this Raman line clearly shows the hyperfine components of the Hg 4358 exciting line. On the other hand, the $2\nu_2$ Q branch is slightly broader and is degraded towards the ν_1 band. For $C^{13}O_2$, the ν_1 and $2\nu_2$ Q branches are degraded towards each other. Also the ν_1 band of $C^{13}O_2$ is about three times the intensity of the $2\nu_2$ band, while in $C^{12}O_2$ the corresponding intensity ratio is approximately 2:1. The wavenumber shifts of these lines are given in Table IV. For $C^{12}O_2$ the average measurements of six plates are shown, the deviation from the average being at most ± 0.06 cm^{-1}. For $C^{13}O_2$, the average measurement of three plates is shown, except for the line $\nu_1+\nu_2-\nu_2$, which was only measured on one plate.

TABLE IV

WAVENUMBER SHIFTS (UNITS cm^{-1}) OF THE Q BRANCHES OBSERVED IN THE VIBRATIONAL SPECTRA OF $C^{12}O_2$ AND $C^{13}O_2$

	$3\nu_2^1-\nu_2^1$	$2\nu_2^0$	ν_1^0	$\nu_1^0+\nu_2^1-\nu_2^1$
$C^{12}O_2$	1265.17	1285.51	1388.15	1409.44
$C^{13}O_2$	1248.23	1266.03	1369.90	1388.47

The separation of the Q branches in each of the two diads was used to determine δ and W, by the method described in Section D(2). The values (in cm^{-1}) obtained are:

$$\text{for } C^{12}O_2\text{: } \delta = 15.8, \qquad W = -50.7;$$
$$\text{for } C^{13}O_2\text{: } \delta = 46.4, \qquad W = -47.1.$$

These lead to shifts of 43.4 cm^{-1} up for ν_1 and down for $2\nu_2{}^0$ in $C^{12}O_2$, and to shifts of 28.7 cm^{-1} in $C^{13}O_2$. The values of δ and W given here are necessarily approximate since they are based on Q branch measurements only and since higher order terms discussed by Taylor, Benedict, and Strong (1952) and Courtoy (1957) have been omitted. Nevertheless these values show that W for both isotopic molecules is nearly equal, as expected. Also, the resonance is not as strong in $C^{13}O_2$ as it is in $C^{12}O_2$, as shown by the fact that the separation of the unperturbed levels in $C^{12}O_2$ is three times the separation in $C^{12}O_2$. This, of course, explains the much larger intensity ratio of $\nu_1/2\nu_2$ in $C^{13}O_2$ evident in the spectrum shown in Fig. 1(*c*).

Several plates showing the weak rotational O and S branches of the $C^{12}O_2$ diad ν_1, $2\nu_2$ were obtained and a photograph is shown in Fig. 1(*d*). The average wavenumber shifts measured on two plates are given in Table V. Unfortunately even an exposure of 30 hours (with a cylindrical lens in front of the photographic plate) produced only a weak spectrum; only rotational lines up to $J = 40$ were observed, and these were difficult to measure. The analysis of the bands was carried out as outlined in Section D(1).

TABLE V

WAVENUMBER SHIFTS[a] (UNITS cm^{-1}) OF THE LINES IN THE ν_1 AND $2\nu_2$ BANDS OF $C^{12}O_2$

	ν_1 Band		$2\nu_2$ Band	
J	$S(J)$	$O(J)$	$S(J)$	$O(J)$
0				
2	1393.58			
4	1396.56		1294.02	
6	1399.85	1379.28	1297.16	1276.65
8	1403.00	1376.42	1300.25	1272.94
10	1406.10	1373.30	1303.42	1270.55
12	1409.42	1369.88	1306.50	1267.46
14	1412.32	1366.24	1309.63	1264.43
16	1415.46	1363.96	1312.84	1261.27
18	1418.55	1360.77	1315.83	1258.16
20	1421.69	1357.72	1319.04	1254.99
22	1424.78	1354.60	1322.20	1251.72
24	1427.91	1351.71	1325.30	1248.83
26	1431.10	1348.26	1328.48	1245.72
28	1434.19	1345.28	1331.16	1242.67
30	1437.16	1342.14	1334.91	1239.57
32	1440.31	1339.04	1337.93	1236.45
34	1443.33	1335.92	1341.10	1233.14
36	1446.60	1332.83	1344.23	1230.12
38	1449.71	1329.78	1348.26	1227.01
40		1326.49	1350.82	
42			1353.77	
44		1320.392		

[a]Average values of measurements of two plates.

The constants (in cm^{-1}) obtained are:

$$\nu_{100} = 1388.15, \qquad B_{100} - B_{000} = -0.00003,$$
$$\nu_{02^00} = 1285.40, \qquad B_{02^00} - B_{000} = 0.00019.$$

All of the values are in good agreement with those reported by Rossman, France, Rao, and Nielsen (1956) and by Courtoy (1957). However, the smaller, yet significant effects, such as $D' \neq D''$, observed by these authors were not evident in the present analysis.

The smallness of the values of $B' - B''$ immediately explains the sharpness of the Q branches of the ν_1 and $2\nu_2$ bands; the larger value for the $2\nu_2$ band is in agreement with the observed broader line, and its + sign agrees with the observed degradation towards longer wavelengths. Furthermore, the small values of $B' - B''$ confirm the identical values of the Q branch measurement and band origin of the ν_1 band and the very close agreement of the corresponding values for the $2\nu_2$ band. Since the resonance in $C^{12}O_2$ is strong, the values of $B' - B''$ given here do not even represent approximately the coupling constants α_1 and α_2; for a discussion of the effect of resonance on the rotational constants of CO_2 the reader is referred to the detailed account by Courtoy (1957).

F. CONCLUSIONS

Although the rotational structure of some vibrational bands in CS_2 and CO_2 has been photographed with a 21 ft. grating, the spectra are rather weak. It is an unfortunate fact that the low intrinsic intensity of rotation–vibrational Raman spectra still presents formidable difficulties and one must resort to the use of high gas pressures and long exposure times. Yet in spite of these difficulties, the investigation of vibrational Raman spectra at high resolution should be pursued, since much useful information can be obtained in this way. Two examples of the type of information obtainable are shown by the present study. When rotational structure is resolved, the band origins and rotational constants can be determined; when no rotational structure is observed, but only sharp Q branches, the vibrational constants can be evaluated with relatively good accuracy.

One of the most interesting features of the present investigation has been the appearance of many "hot" bands in the Raman spectrum of CS_2. As shown in Section D(2), these have led to the determination of the effect of Fermi resonance on the ν_1 and $2\nu_2$ bands, and to the evaluation of a set of vibrational frequencies and anharmonic constants. Clearly, this situation is not peculiar to the spectrum of CS_2. "Hot" bands may occur in the spectrum of any molecule having a low-lying vibrational frequency ($<400\ cm^{-1}$), and similar studies of their Raman spectra at high resolution may prove useful in determining vibrational and anharmonic constants.

It is well known that Fermi resonance is of frequent occurrence in the spectra of polyatomic molecules, and the present results on CS_2 once again demonstrate the importance of determining the effects of the resonance, even when the interaction is weak. For example, in CS_2 the unperturbed vibrational levels

are separated by 125 cm^{-1}. Yet each level is shifted by 9.7 cm^{-1} through their mutual interaction. As a consequence of this shift, there is a significant effect on the vibrational frequencies and anharmonic constants obtained from an analysis of the vibrational spectrum which includes resonance as compared with the values obtained neglecting resonance. Thus some care is necessary in evaluating the accuracy or usefulness of vibrational constants (and in some cases, of rotational constants) of molecules in which Fermi resonance is known or suspected to occur but has not been adequately treated.

REFERENCES

ALLEN, H. C., PLYLER, E. K., and BLAINE, L. R. 1956. J. Am. Chem. Soc. **78**, 4843.
BAILEY, C. R. and CASSIE, A. B. D. 1933. Proc. Roy. Soc. **140**, 605.
CALLOMON, J. H. and STOICHEFF, B. P. 1957. Can. J. Phys. **35**, 373.
COURTOY, C-P. 1957. Can. J. Phys. **35**, 608.
COURTOY, C-P. and HERZBERG, G. 1955. J. Chem. Phys. **23**, 975.
DENNISON, D. M. 1940. Revs. Modern Phys. **12**, 175.
EVANS, J. C. and BERNSTEIN, H. J. 1956. Can. J. Chem. **34**, 1127.
GAILAR, N. M. and PLYLER, E. K. 1952. J. Research Natl. Bur. Standards, **48**, 392.
GIULOTTA, L. and CALDIROLA, P. 1941. Z. physik. Chem. B, **49**, 34.
HERZBERG, G. 1945. Infrared and Raman spectra of polyatomic molecules (D. Van Nostrand Company, Inc., Princeton, N.J.).
IMANISHI, S. 1935. Nature, **135**, 396.
LANGSETH, A., SORENSEN, J. O., and NIELSEN, J. R. 1934. J. Chem. Phys. **2**, 402.
LIEBERMANN, L. N. 1941. Phys. Rev. **60**, 496.
PLACZEK, G. 1934. Marx, Handbuch der Radiologie, **6**, 2 (Akademische Verlagsgesellshaft m.b.H., Leipzig), p. 205.
ROSSMAN, K., FRANCE, W. L., RAO, K. N., and NIELSEN, H. H. 1956. J. Chem. Phys. **24**, 1007.
SANDERSON, J. A. 1935. Phys. Rev. **50**, 209.
SIRKAR, S. C. 1936. Indian J. Phys. **10**, 189.
STOICHEFF, B. P. 1954. Can. J. Phys. **32**, 330.
TAYLOR, J. H., BENEDICT, W. S., and STRONG, J. 1952. J. Chem. Phys. **20**, 1884.
TOMKINS, F. S. and FRED, M. 1951. J. Opt. Soc. Am. **41**, 641.
VENKATESWARAN, S. 1932. Phil. Mag. **14**, 258; **15**, 263.
WOOD, R. W. and COLLINS, G. 1932. Phys. Rev. **42**, 386.

A SEARCH FOR α-PARTICLES FROM THE DECAY OF Bi^{209} [1]

E. P. HINCKS AND C. H. MILLAR

With an appendix by G. C. HANNA

ABSTRACT

A search for α-particles from Bi^{209} has been carried out in Ilford C-2 bismuth-loaded nuclear emulsions maintained at 5° C. for 3 years before development. Contrary to the findings of Faraggi and Berthelot (1951), Riezler and Porschen (1952), and Porschen and Riezler (1956), no evidence was obtained of α-particles in the 3 Mev. region which could be unambiguously attributed to bismuth, the experimental lower limit for the half-life thus determined being $T_{1/2} > 2\times10^{18}$ years. A detailed study of the energy available for the α-disintegration of Bi^{209} by the method of reaction cycles gives a value of 2.93±0.11 Mev. For this disintegration energy the half-life of Bi^{209} predicted on the basis of α-decay theory and systematics is between 5×10^{19} and 5×10^{22} years.

INTRODUCTION

Bi^{209}, which occurs in nature, has long been known to be unstable against α-particle emission by about 3 Mev., and several attempts have been made to observe this activity. Jenkner and Broda (1949), using bismuth-impregnated emulsions, found no evidence for the α-activity of bismuth and concluded that the half-life is greater than 3×10^{15} years. Faraggi and Berthelot (1951), using bismuth-loaded emulsions, observed some α-particle tracks which they attributed to bismuth and concluded that Bi^{209} emits 3.15 Mev. α-particles with a half-life of 2.7×10^{17} years. The present authors carried out a similar experiment the following year and reported (Hincks and Millar 1952) that they found no α-particle tracks that could be unambiguously attributed to bismuth. Shortly thereafter Riezler and Porschen (1952) published the results of a study of bismuth-impregnated emulsions in which they attributed seven α-particle tracks to Bi^{209} and deduced an α-particle energy of 2.9 Mev. and a half-life of 2×10^{17} years, in rough agreement with the work of Faraggi and Berthelot. In a later comprehensive paper Porschen and Riezler (1956) reported five additional α-particle tracks presumed due to Bi^{209} and revised their estimate of the α-particle energy to 3.0±0.2 Mev.

The present authors delayed formal publication of their results pending a proposed confirmatory experiment with counters; however, since this experiment has not been done and since no more conclusive results have appeared in the literature, the authors feel that the publication of their original data, re-evaluated in the light of the latest available information, will constitute a useful contribution to the question of the natural radioactivity of bismuth.

EXPERIMENTAL PROCEDURE

Type C-2 bismuth-loaded nuclear emulsions which were manufactured by

[1]Manuscript received November 12, 1957.
Contribution from Physics Division, Atomic Energy of Canada Limited, Chalk River, Ontario.
Issued as A.E.C.L. No. 539.

Ilford, Ltd. on February 10, 1949, were kept in a refrigerator at 5° C. until March, 1952, at which time they were examined and it was found that the emulsion had become detached from the glass backing. It was possible, however, to develop and fix the loose emulsion and, by means of a final wash in a weak gelatin solution, to reattach the developed emulsion to a glass backing with less than 1% distortion in the lateral dimensions. For comparison purposes, an unloaded Ilford C-2 emulsion, 50 microns thick, manufactured in November, 1949, and stored with the bismuth-loaded emulsion, was developed in the normal manner. An area of 92 mm.^{2} of the bismuth-loaded emulsion was searched for single α-particle tracks; this corresponds to a volume of 0.014 cm.^{3}, since the emulsion was actually 150 microns in thickness instead of the nominal 100 microns. The emulsion was studied with a Cooke, Troughton, and Simms nuclear research microscope, the initial scan being carried out at a nominal magnification of 405 ($45\times6\times1.5$) and the track measurements at a magnification of 1425 ($95\times10\times1.5$). In the background plate an area of 68 mm.^{2} ($\sim$0.0034 cm.^{3}) was searched for single α-particle tracks.

AUXILIARY EXPERIMENTS

It was realized that there were several factors that could lead to the misinterpretation of any tracks observed, so a series of test experiments and checks was carried out to eliminate such errors as far as possible. These auxiliary experiments will be discussed first, since the interpretation of the observations in the main experiment is dependent on them.

The fact that bismuth-loaded emulsion differs significantly in composition from normal emulsion gives rise to the possibility that the usual range–energy relationship for α-particles may not be valid. The emulsion compositions as supplied by Ilford Limited are shown in Table I.

TABLE I

ATOMIC COMPOSITION OF ILFORD C–2 EMULSION

Emulsion type	Atomic composition (g./cm.^{3})										
	Ag	Br	I	C	H	O	N	S	Na	Bi	Total
Normal	1.85	1.34	0.052	0.27	0.056	0.27	0.067	0.01	—	—	3.915
Bi-loaded	1.39	1.01	0.039	0.33	0.047	0.43	0.062	0.002	0.06	0.27	3.640

Yagoda (1949, p. 83) suggests a method of range correction based on the Bragg and Kleeman (1905) observation that for α-particles atomic stopping power varies directly as the square root of the atomic weight. The application of Yagoda's formula would lead to a correction factor of 1.0165 to convert ranges in bismuth-loaded emulsion to ranges in standard emulsion. It seems doubtful, however, that this empirical "law" is valid to a sufficient degree to justify using it to determine a correction factor to better than a few per cent. In addition Rotblat (1950) notes that in the low-energy region α-particle ranges in emulsion under "atmospheric" conditions are about 3% greater than in "vacuum-dry" emulsion. Since the standard range–energy relationships are

given for "vacuum-dry" emulsions (Lattes, Fowler, and Cüer 1947; Rotblat 1951) some adjustment must be made to take into account the fact that our "refrigerator-desiccated" emulsion presumably had a moisture content somewhere between "vacuum-dry" and "atmospheric" during its sensitive lifetime.

Since there would appear to be some uncertainty in making each of these corrections, we have chosen to calibrate the emulsion using α-particles of known energy, and obtain an experimental total correction factor in this way.

In the first calibration experiment both faces of a stripped, bismuth-loaded emulsion were exposed to α-particles from a thin U^{233} source. The emulsion was then developed, reaffixed to a glass backing, and the lengths of a group of surface tracks measured. The mean range of 44 of these tracks was 19.7 ± 0.3 microns, which agrees with the value given by the standard range–energy relationship for U^{233} α-particles (mean energy 4.808 Mev.) and indicates that ranges in the bismuth-loaded emulsion are within $\pm 1.5\%$ of those in standard dry emulsion.

The second check experiment gave information on several aspects of the main experiment and thus merits detailed consideration. A general survey of the bismuth-loaded plate showed that the great majority of radioactive "stars" from successive α-disintegrations of naturally radioactive contamination in the emulsion originated from Ra^{226}. These four-pronged stars were easily distinguishable from the rare five-pronged stars from thorium, and a considerable number of them showed the characteristic separation by a few microns of the Ra^{226} α-particle track from the remaining three prongs of the star—a well-known phenomenon caused by the diffusion of Em^{222} during its 3.8-day half-life. These separated Ra^{226} tracks provided an unambiguous set of monoenergetic α-particle tracks deposited throughout the emulsion which were presumably typical of the tracks from any long-lived α-particle-emitting isotope contained in the emulsion. Careful measurements of these Ra^{226} α-particle tracks were carried out, and in addition the tracks were divided into three categories—"dense", "medium", and "faint"—depending on their observed grain density. The results of this survey are shown graphically in the histograms of Fig. 1 and numerically in Table II.

First it may be noted that the mean range of the dense tracks is $19.6_8 \pm 0.2$ microns, which is $1.3 \pm 1.0\%$ greater than the 19.4_3 micron range predicted for the 4.766 Mev. (mean energy) α-particles of Ra^{226} from the standard range–energy relationship for dry emulsion. This is in good agreement with the result obtained with U^{233} α-particles. We are thus confident that when the ranges of low-energy α-particle tracks in our bismuth-loaded emulsion are multiplied by 0.99 to correct for atomic composition and moisture content, α-particle energies may be reliably determined from the relationships of Lattes, Fowler, and Cüer (1947) or of Rotblat (1951).

The range straggling of the tracks may be conveniently measured by computing the r.m.s. deviations about the mean of the observed values. These r.m.s. deviations are shown in Table II, and it will be noted that the values increase by a factor of two from the dense tracks of small dip angle to the faint tracks of all angles. The increase in the r.m.s. deviation caused by adding

the steep dense tracks—arbitrarily defined as those with an observed dip of more than 3 microns—to the flat dense tracks is indicative of the large effect of the dip measurement inaccuracy in these special plates, whose shrinkage factor is as high as 4.6. The increase of r.m.s. deviation with decreasing track density is indicative of the increasing probability that some of the tracks will be shortened by fading of the end grains.

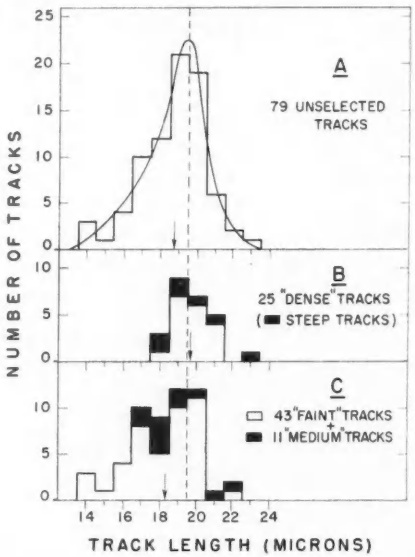

FIG. 1. Histograms of various classes of Ra^{226} α-particles measured in the bismuth-loaded emulsion in which the search for α-particles from Bi^{209} was carried out. Predicted mean range for standard dry emulsion is shown dotted. Solid curve in (A) is smoothed distribution fitted to histogram.

TABLE II

MEAN RANGES AND R.M.S. DEVIATIONS OBSERVED FOR VARIOUS CATEGORIES OF Ra^{226} α-PARTICLE TRACKS IN BISMUTH-LOADED C-2 EMULSION

Type of track	No. observed	Mean range (microns)	r.m.s. deviation (%)
Dense (excluding steep tracks)	18	$19.6_6 \pm 0.2$	4.9
Dense (all tracks)	25	$19.6_8 \pm 0.2$	6.1
Medium (all tracks)	11	$18.6_8 \pm 0.5$	8.2
Faint (all tracks)	43	$18.1_1 \pm 0.3$	9.9
All tracks observed	79	18.7 ± 0.2	9.3

These r.m.s. deviations are considerably greater than the value 2.9% which Rotblat (1950) obtains for α-particles of this energy in normal emulsion; however, our value of 4.9% for dense "flat" tracks is comparable to the value

of 4.7% (our calculation) obtained by Faraggi and Berthelot (1951) for the tracks from Th^{232} in a bismuth-loaded emulsion similar to ours. This greater apparent range straggling in bismuth-loaded emulsion is presumably due to the loading, which causes the silver bromide grains to be less closely packed, as well as to the large shrinkage factor.

It will be noted from Fig. 1 that the addition of the "medium" and "faint" tracks to the "dense" ones not only lowers the value of the mean track length and increases the r.m.s. deviation, but also produces a skew distribution with a tail on the low-energy side. This is seen clearly in Fig. 1A, where a smooth curve is fitted to the experimental points and thus represents the empirical distribution function for α-particles of a single energy emitted at a constant rate throughout the sensitive lifetime of the emulsion.

Table II shows also that the mean range for the dense tracks does not change with the addition of the steep track measurements to those of the flatter tracks, indicating that our shrinkage corrections are accurate despite the very large value of shrinkage factor.

A third experiment was carried out to check on the fading of tracks produced uniformly throughout the emulsion during its sensitive lifetime. This consisted of searching a large area (2.05 $cm.^2$) of the emulsion for the tracks of μ-mesons which came to rest therein and comparing the number found with the number predicted. Identification of these tracks was of necessity based on a visual estimate that the scattering near the end of the track was characteristic of μ-mesons, it being impossible because of fading to make use of the grain density. This made it difficult to distinguish short or steep meson tracks from proton tracks; however, each track that entered and stopped in the emulsion was classified visually as either a meson or a proton, and the "mesons" thus selected were further classified as either "certain" or "probable".

From the emulsion composition, the meson intensity, and the time of exposure it was calculated that between 50 and 100 μ-mesons should have stopped in the area scanned. A more precise estimate of this number was not possible because of the lack of accurate knowledge of atomic stopping powers at low velocities corresponding to μ-mesons of ranges $\sim$100 microns and less, and also because the absorbing material surrounding the emulsion during its storage period was neither controlled nor recorded.

We observed 16 "certain" and 37 "probable" meson tracks terminating in this area and, by assuming that roughly as many protons were counted as "probable" mesons as mesons were misidentified as protons, we estimate that a total of about 50 true meson tracks were observed. Thus the product of the "fading factor" and our scanning efficiency for this type of track is in the range 0.5 to 1 and on this basis we feel sure that for the more densely ionizing α-particles the value of this over-all efficiency factor is at least 0.5.

Another qualitative observation on the fading of tracks in the emulsion was provided by the radium stars for which a search was conducted in connection with the range–energy calibration. Because of their characteristic appearance the efficiency for observing faded stars should be greater than for similarly faded single α-particle tracks. However, no stars were observed in which the

individual α-particle tracks were faded to a degree such that if the tracks had been separate they would have been missed by the observer. This result adds confirmation to our previous conclusion that in our experiment fading of the latent image did not cause a serious loss in observing efficiency.

Finally, to check that the emulsion really contained bismuth, samples were ashed, and the residue, when analyzed qualitatively, was found to contain a large percentage of bismuth. We were thus satisfied that there had been no mix-up of emulsions nor large loss of the bismuth component during either manufacture or storage.

On the basis of these check experiments, we feel confident that for α-particle tracks in bismuth-loaded emulsions we know the range–energy relationship with considerable accuracy, as well as the range distribution caused by straggling, fading, and measuring error. We also know that the over-all loss of tracks due to both fading of the latent image and observer inefficiency was less than 50%.

MAIN EXPERIMENT RESULTS

The histogram in Fig. 2A shows the corrected ranges of the 212 single α-particle tracks (excluding Ra^{226} tracks) found in the bismuth-loaded plate.

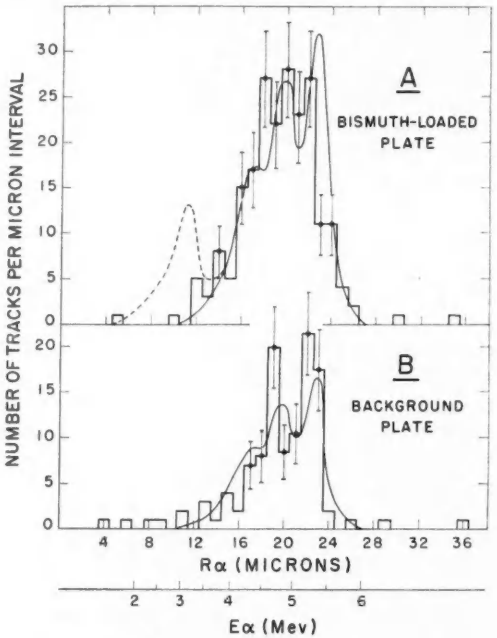

FIG. 2. Histograms of short single α-particle tracks found in (A) bismuth-loaded plate and (B) unloaded "background" plate. Solid curves show fitted "background" curve (see text). Dotted curve in (A) shows size and position predicted for peak due to Bi^{209} if its α-particle energy were 3 Mev. and its half-life 2×10^{17} years. Track lengths have been corrected for emulsion composition and moisture content. The α-particle energy scale is from Rotblat (1951).

Standard deviations are shown for the higher intensity points. The range–energy scale shown is from Rotblat (1951).

Fig. 2B shows the range distribution of the 114 single α-particle tracks found in the background plate. There would appear to be no *a priori* reason why two batches of different types of emulsion should have the same amount of radioactive contamination and this is borne out by the observation that in the background plate the number of single α-particle tracks (per unit volume per unit time of "exposure") was 2.6 times that in the bismuth-loaded plate. It would seem that some method other than the subtraction of a "background" distribution of normalized intensity must be sought in order to determine whether the loaded plate contains an extra group of tracks which might be attributable to the loading. Our method of analysis is based on the following considerations.

Single α-particle tracks in nuclear emulsion will most probably arise from contaminants from one of the three naturally occurring radioactive series; however, short tracks could also arise from the α-decay of Sm^{147} and the (n, p) reaction from the capture of thermal neutrons in the nitrogen of the emulsion. The characteristics of these "contamination tracks" are shown in Table III.

TABLE III

POSSIBLE NATURAL SOURCES OF SHORT, SINGLE "CONTAMINATION TRACKS" IN NUCLEAR EMULSION

Source	Isotope	Mean α-particle energy (Mev.)	Track length (microns)
$(4n+2)$ series	U^{238}	4.18	16.1
	U^{234}	4.75	19.3
	Th^{230}	4.67	18.9
	Po^{210}	5.30	22.6
$(4n+3)$ series	U^{235}	4.41	17.4
	Pa^{231}	4.95	20.5
$(4n)$ series	Th^{232}	4.00	15.2
Samarium	Sm^{147}	2.18	7.3
Neutron capture in nitrogen	$N^{14}(n, p)C^{14}$	—	6.6 (El Bedewi 1951)

We know from the abundance ratios and half-lives of U^{235} and U^{238} that in natural uranium contamination the activities of the members of the $(4n+3)$ series will be only 4.5% that of the members of the $(4n+2)$ series, assuming radioactive equilibrium exists within each series. We may also infer from the relative scarcity of five-pronged thorium stars as compared with the four-pronged radium stars that uranium contamination was a much stronger source of background tracks than thorium contamination in the emulsion studied. Thus, to a first approximation, we may attribute all single α-particles from contamination by elements of naturally occurring radioactive series to the four members of the $(4n+2)$ series listed in Table III. These α-particles have mean

ranges of from 16.1 to 22.6 microns and their tracks should thus be quite well separated from any bismuth α-particle tracks, which are expected to have a range of 10–11 microns, and from tracks due to either samarium α-particles or $N^{14}(n, p)C^{14}$ reactions, each of which has a range of about 7 microns.

Considering in detail the members of the $(4n+2)$ series that have long-lived daughter products so that their α-particles may appear singly in nuclear emulsion, it is evident that if radioactive equilibrium has been established, α-particles from U^{238}, U^{234}, and Th^{230} will appear in equal numbers unless there has been some chance separation of the few parts per hundred thousand of Th^{230} that exists in equilibrium with its uranium parents. Po^{210} α-particle tracks will not necessarily be equally abundant, since in this case the source is probably the Em^{222} normally present in the atmosphere rather than the uranium contained in the emulsion.

On these premises a semiempirical curve to compare with the observed distribution of α-particle tracks in our background plate was obtained in the following manner. Three smoothed distributions as obtained in Fig. 1A of equal amplitude and of mean ranges corresponding to the energies of α-particles from U^{238}, U^{234}, and Th^{230} were added to a fourth such distribution of mean range corresponding to Po^{210} α-particles. The relative amplitude of the Po^{210} distribution was adjusted so that the mean range of the combined distribution corresponded to the mean range for all tracks observed between 10 and 28 microns, the range limits of the semiempirical distribution. This combined distribution, normalized to the total number of tracks observed within its range limits, is shown as a solid curve in Fig. 2B, and it will be seen that it provides a statistically good fit to the observed points.

In applying this same technique to the tracks observed in the bismuth-loaded emulsion it was noted that the mean range of tracks between 10 and 28 microns was 19.3 microns as compared with 19.9 microns for the background plate. These differ by nearly twice the standard error of the difference of the two means (0.35 microns) indicating either a lower relative abundance of Po^{210} or, possibly, the presence of a new group of low-energy particles. A semiempirical distribution fitted on the basis of the first of these possibilities does, indeed, give a statistically good fit to the observed distribution. However, if a new group of short tracks is present, this fitting process is not justified. To check this second possibility we have shown in Fig. 2A the curve obtained by renormalizing the semiempirical distribution obtained for the background plate. It will be seen that on the lower side of the peak the curve provides a statistically adequate fit to the observed points and there is little indication of any excess of tracks which might be attributed to bismuth α-particles. On the other hand, the experimental points in the region of the Po^{210} peak fall below the curve, which is some evidence that the shorter mean range of tracks in the bismuth-loaded plate is due to a relatively lower abundance of Po^{210} rather than to a new group of short-range tracks.

In neither observed distribution is there definite evidence for the 4.00 Mev. α-particles from Th^{232} nor the 2.18 Mev. α-particles from Sm^{147}. Porschen and

Riezler (1956) have suggested that our technique was insensitive to low-energy α-particles and cite our non-observation of tracks in the 2–3.2 Mev. region as proof. In their own work they find tracks in this region in their background plates which they attribute to Sm^{147} and to protons from $N^{14}(n, p)C^{14}$ reactions.

From the known flux of cosmic-ray neutrons we estimate that of the order of 10 $N^{14}(n, p)C^{14}$ reactions would have occurred in the area searched in our bismuth-loaded emulsion during its sensitive life. However, for the proton tracks from this reaction, we expect a greater loss from fading than for the denser α-particle tracks, and the extreme shortness of these tracks (6.6 microns) presumably leads to a greater loss through non-observation than for the longer-α-particle tracks studied in the check experiments. Thus we might well have for the short *and* lightly-ionizing proton tracks an over-all observation efficiency less than 0.5, which means that we might have expected to observe less than five tracks from neutron capture in the nitrogen. The fact that only one track was observed in this range region in the bismuth-loaded emulsion (and two others in the background plate) is not incompatible with the above predictions, but it does not give firm proof that our technique was, indeed, sensitive to low-energy α-particles. However, on the basis of our efficiency for observing lightly-ionizing μ-meson tracks, of the consistency of our results in measuring α-particles of 4–5 Mev., and of our previous experience in studying extremely short α-particle tracks (e.g. Millar and Cameron 1953), we feel confident that our technique was not anomalously insensitive to α-particle tracks in the 3 Mev. region.

The dotted curve in Fig. 2A shows the predicted distribution for the 42 α-particles that we would expect to have observed if the half-life of Bi^{209} were 2×10^{17} years and the α-particle energy 3.0 Mev. as suggested by Porschen and Riezler (1956), and if our observation efficiency were only 0.5. Bearing in mind that the lower limit of our detection efficiency has been used, and that no cosmic-ray background has been subtracted, it would appear from our observations that the upper limit of the specific activity of Bi^{209} is about an order of magnitude lower than that represented by the dotted curve—that is the specific activity is less than 3×10^{-5} disintegrations per second per gram. The corresponding half-life limit is $T_{1/2}(Bi^{209}) \geqslant 2\times10^{18}$ years. The experimental limit of the half-life will vary, but not very rapidly, with the α-particle energy chosen. We estimate that it should be approximately a factor of two smaller at 3.5 Mev. and a factor of two greater at 2.5 Mev. As will be shown in the next section, reaction-cycle calculations indicate that the energy available for α-particle emission from Bi^{209} is probably < 3.0 Mev.

THEORETICAL CONSIDERATIONS

Disintegration Energy

Neither semiempirical mass formulae nor the methods of α-decay systematics (e.g. Perlman, Ghiorso, and Seaborg 1950) are adequate to predict accurately the α-disintegration energy of Bi^{209}, which has a magic number of neutrons (126) and one proton more than magic (83). Mass spectroscopic data are also

not accurate enough for our purpose, but a fairly good estimate of the available energy can be made on the basis of reaction cycles. Fig. 3 is a chart of the nuclides involved in pertinent closed cycles for which experimental data are available.

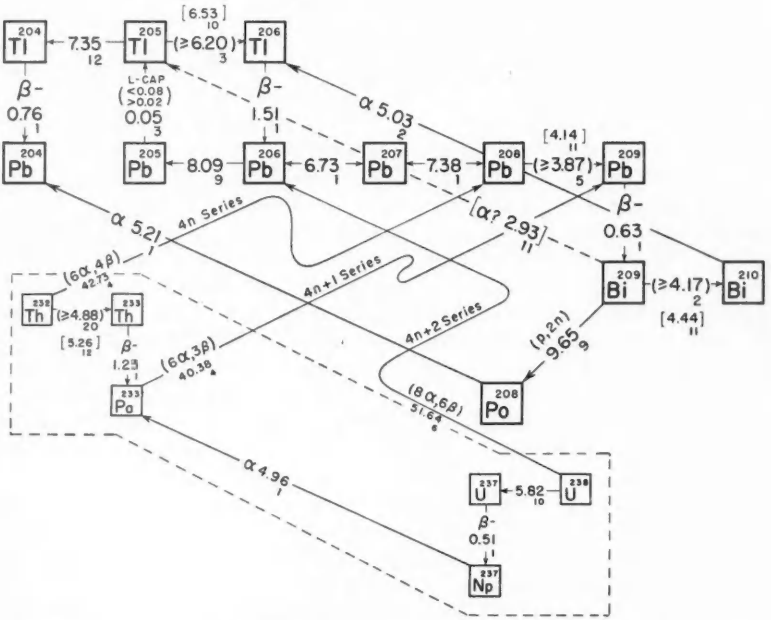

FIG. 3. Diagram showing pertinent decay and reaction energies used in the determination of the energy available for the α-disintegration of Bi^{209} by the method of reaction cycles. Arrows indicate direction of decay or of reaction on which values have been based. Numbers in parentheses are experimental limiting values. Numbers in square brackets are derived from reaction cycles. Error limits are shown beneath the appropriate figure.

On this diagram are shown the natural α- and β-decays and the artificially induced reactions (n, γ), (γ, n), $(p, 2n)$, etc., with the direction of the decay or reaction indicated. The experimental total energies—disintegration energies, neutron binding energies, or Q-values—are given, the lower figures showing the uncertainties in these values. Where experimental data give only a limiting value for the energy difference, this is shown in parentheses, while values derived indirectly from reaction cycles are shown in square brackets. The sources of these experimental energies and of their uncertainties are given in Appendix I.

The energy available for the α-decay of Bi^{209}, $E_\alpha(Bi^{209})$, may be obtained without reference to any derived energy values from the cycle

(1) $$Bi^{209} - Po^{208} - Pb^{204} - Tl^{204} - Tl^{205}.$$

The energies involved (see Appendix I) are:

$$\begin{aligned} Q(Bi^{209}(p, 2n)) &= -9.65\pm0.09 \text{ Mev.} \\ E_\alpha(Po^{208}) &= 5.21\pm0.01 \text{ Mev.} \\ -E_\beta(Tl^{204}) &= -0.76\pm0.01 \text{ Mev.} \\ E_n(Tl^{205}) &= 7.35\pm0.12 \text{ Mev.} \\ M_n - M_p &= 0.78\pm0.00 \text{ Mev.} \\ \text{therefore} \quad E_\alpha(Bi^{209}) &= 2.93\pm0.15 \text{ Mev.} \end{aligned}$$

There are two other possible cycles that are independent of (1). These are

(2) $Bi^{209} - Pb^{209} - Pb^{208} - Pb^{207} - Pb^{206} - Pb^{205} - Tl^{205}$

and

(3) $Bi^{209} - Bi^{210} - Tl^{206} - Pb^{206} - Pb^{205} - Tl^{205}$,

but both of these unfortunately involve a neutron binding energy for which only a lower limit is directly measured, that is $E_n(Pb^{209})$ in cycle (2) and $E_n(Bi^{210})$ in cycle (3).

In the case of cycle (2), it is possible to trace an alternative route from Pb^{209} to Pb^{206} via the $4n+1$ and $4n+2$ radioactive series for which all energy values are known from experiment, thus avoiding the uncertainty introduced by including $E_n(Pb^{209})$ in the calculation. Referring to Fig. 3 this alternative route is $Pb^{209} - Pa^{233} - Np^{237} - U^{237} - U^{238} - Pb^{206}$.

The energies involved in cycle (2) via this alternative route are:

$$\begin{aligned} -E_\beta(Bi^{209}) &= -0.63\pm0.01 \text{ Mev.} \\ -E_{6\alpha,3\beta}(Pa^{233}) &= -40.38\pm0.04 \text{ Mev.} \\ -E_\alpha(Np^{237}) &= -4.96\pm0.01 \text{ Mev.} \\ -E_\beta(U^{237}) &= -0.51\pm0.01 \text{ Mev.} \\ E_n(U^{238}) &= 5.82\pm0.10 \text{ Mev.} \\ E_{8\alpha,6\beta}(U^{238}) &= 51.64\pm0.06 \text{ Mev.} \\ -E_n(Pb^{206}) &= -8.09\pm0.09 \text{ Mev.} \\ E_{L-cap.}(Pb^{205}) &= 0.05\pm0.03 \text{ Mev.} \\ \text{therefore} \quad E_\alpha(Bi^{209}) &= 2.94\pm0.16 \text{ Mev.} \end{aligned}$$

It is not possible to derive a value for $E_n(Bi^{210})$ which is independent of cycles (1) and (2), so that cycle (3) cannot be used to provide an independent value of $E_\alpha(Bi^{209})$.

Combining the values from cycles (1) and (2) we obtain a best estimate for $E_\alpha(Bi^{209})$ of 2.93 ± 0.11 Mev.

It is of interest to note that the best derived value of $E_n(Bi^{210})$ is a few hundred kilovolts above the value obtained from (n, γ) and (d, p) reactions in agreement with arguments advanced by Pryce (1952) and Harvey (1953).

Similarly the best derived value of $E_n(Pb^{209})$ is greater than that obtained from a (d, p) reaction which is consistent with the argument that, since it is necessary to add a neutron with four or five units of angular momentum to Pb^{208} to produce Pb^{209} in the ground state, it is unlikely that the ground state transition would have been observed in a (d, p) reaction.

Lifetime

Assuming a value for the Bi^{209} α-disintegration energy enables its half-life to be estimated by analogy with the decay characteristics of neighboring bismuth isotopes. Such an estimate has been carried out by G. C. Hanna (see Appendix II) and his prediction of the half-life as a function of the α-disintegration energy is shown by the solid curve in Fig. 4. In particular, we note that the estimated half-life for $E_\alpha = 2.93$ Mev. is 1.5×10^{21} years, although the uncertainties in the theory would allow it to be as low as 3×10^{20} or as high as 6×10^{22} years.

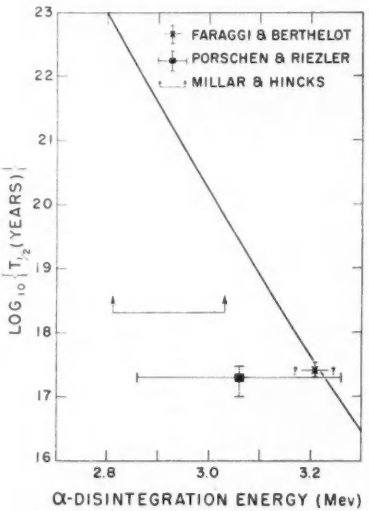

FIG. 4. Diagram showing results of various experiments on the α-decay of Bi^{209} together with the prediction from α-decay systematics of the half-life as a function of disintegration energy (see Appendix II).

CONCLUSION

In a search of 0.014 cm.^{3} of bismuth-loaded emulsion that had been "exposed" for 3.1 years we have found no evidence for a group of α-particle tracks that could be attributed to Bi^{209}. The disintegration energy obtained from reaction cycles using the best available experimental data is 2.93 ± 0.11 Mev., corresponding to an α-particle energy of 2.87 ± 0.11 Mev. We have used this result as a basis on which to obtain from our experimental data the best estimate of the lower limit set on the Bi^{209} half-life. This limit is 2×10^{18} years and is well below (see Fig. 4) the best estimate based on α-decay systematics of 5×10^{19} to 5×10^{22} years for the range of disintegration energy quoted above.

Our result is in disagreement with previous results of Faraggi and Berthelot (1951) and Porschen and Riezler (1956), who found an apparent α-activity due to bismuth with a half-life of $\sim2\times10^{17}$ years and an α-particle energy in

the region of 3 Mev. This half-life is inconsistent with the predictions of α-decay systematics unless the α-disintegration energy is at least 3.2 Mev., a value that is rather improbable on the basis of reaction-cycle analysis.

ACKNOWLEDGMENTS

The authors wish to express their thanks to G. C. Hanna and L. G. Elliott for criticism of this paper, to C. G. Scully for some searching of the plates, to Mrs. P. I. K. Lennox for computing assistance, and to L. Yaffe for making the chemical analysis for bismuth.

APPENDIX I. ENERGY VALUES FOR REACTION-CYCLE CALCULATIONS

All energy values and their uncertainties in this Appendix are quoted to the nearest 10 kev.

(*a*) *α-Disintegration Energies*

$E_\alpha(Po^{208})$	= **5.21±0.01 Mev.**	(Perlman and Rasmussen 1956)
$E_\alpha(Bi^{210})$	= **5.03±0.02 Mev.**	(Levy and Perlman 1954)
$E_\alpha(Np^{237})$	= **4.96±0.01 Mev.**	(Magnusson *et al.* 1955)

(*b*) *β-Disintegration Energies*

$E_\beta(Tl^{204})$	= **0.76±0.01 Mev.**	(King 1954)
$E_\beta(Tl^{206})$	= **1.51±0.01 Mev.**	(King 1954)
$E_\beta(Pb^{209})$	= **0.63±0.01 Mev.**	(King 1954)
$E_\beta(Th^{233})$	= **1.23±0.01 Mev.**	(King 1954)
$E_\beta(U^{237})$	= **0.51±0.01 Mev.**	(King 1954)
$E_{L-cap.}(Pb^{205})$	= **0.05±0.03 Mev.**	(see below)

The value for $E_{L-cap.}(Pb^{205})$ is based on the observation of Huizenga and Wing (1956) that Pb^{205} decays by *L*-capture with a half-life of 5×10^7 years and on the conclusion by Herber *et al.* (1956) that decay by *K*-capture must have a half-life $> 10^{10}$ years to account for the non-observation of Tl *K* X-rays. We have assumed that the decay energy lies between the *K*- and *L*-capture thresholds and have chosen an energy and uncertainty value to encompass this range.

(*c*) (*p*, *2n*) *Reaction Energy*

$Bi^{209}(p, 2n)Po^{208}$ **Q = 9.65±0.09 Mev.** (Andre *et al.* 1956)

Andre *et al.* give ±80 kev. as their cyclotron energy-calibration uncertainty. We have added ±50 kev. in quadrature to account for a possible departure from the linear theory upon which their extrapolation is based.

(*d*) *Neutron Binding Energies*

Several neutron binding energies are based on the threshold for the (γ, n) reaction, and many of these measurements make use of the $Cu^{63}(\gamma, n)Cu^{62}$ threshold energy for calibration purposes. The four most recent and nominally most precise measurements of this value are

$E_n(Cu^{63}) = 10.73\pm0.03$ Mev. (Robinson *et al.* 1956)
$= 10.78\pm0.05$ Mev. (Bendel *et al.* 1956)
$= 10.54\pm0.04$ Mev. (de Souza Santos *et al.* 1955)
$= 10.61\pm0.05$ Mev. (Birnbaum 1954).

Since it is evident that the differences between these four values are quite inconsistent with the errors indicated, we can only assume that each one is equally likely to be affected by a considerably larger systematic error and take the simple mean, 10.67 Mev., as the best value. We have arbitrarily assigned an uncertainty of 100 kev. to this value so that it is not in disagreement with any one of the four values quoted, that is

$$E_n(Cu^{63}) = 10.67\pm0.10 \text{ Mev.}$$

This 100 kev. uncertainty has been added in quadrature to the quoted uncertainty of any (γ, n) threshold energy referred to the $Cu^{63}(\gamma, n)$ threshold.

$E_n(Tl^{205}) = 7.35\pm0.12$ Mev.

This value is obtained from the three following determinations of the (γ, n) threshold:

(1) Parsons and Collie (1950) give an "absolute" value of 7.3 ± 0.25 Mev.

(2) Sher *et al.* (1951) give a value of 7.55 ± 0.20 Mev., but this is based on an energy calibration that gives the $Cu^{63}(\gamma, n)$ threshold as 10.85 Mev. Thus their value should be adjusted to 7.42 ± 0.22 Mev.

(3) Hanson *et al.* (1949) give a value of 7.48 ± 0.15 Mev. based on a Cu^{63} (γ, n) threshold of 10.9 Mev. The adjusted value is therefore 7.32 ± 0.18 Mev.

The weighted mean value of these three corrected determinations is $7.35\pm$ 0.12 Mev.

$E_n(Tl^{206}) \geqslant 6.20\pm0.03$ Mev.
$= [6.53\pm0.10$ Mev.]

The first value is based on the (n, γ) reaction studied by Bartholomew and Kinsey (1953) and the (d, p) reaction studied by Harvey (1951). However, neither study proves conclusively that this represents a ground-state reaction, and indeed the indication of a 6.54 Mev. neutron binding energy ascribed by both to Tl^{204} on an intensity basis could possibly be properly ascribed to Tl^{206}, or could mask a Tl^{206} binding energy in this region. Because of this uncertainty we believe that the best value is the one obtained from the reaction cycle $Tl^{206} - Pb^{206} - Pb^{205} - Tl^{205}$. The value of $E_n(Tl^{206})$ thus derived is 6.53 ± 0.10 Mev.

$E_n(Pb^{206}) = 8.09\pm0.09$ Mev. (Harvey 1953; Palevsky and Hanson 1950)

Harvey's value of 8.09 ± 0.10 Mev. has been determined from the (d, t) reaction, using the $Pb^{208}(d, t)Pb^{207}$ reaction for energy-calibration purposes. The latter is accurately known (see below). Palevsky and Hanson obtain a value of 8.25 ± 0.10 Mev. from the (γ, n) threshold, but this value is based on a value of 10.9 Mev. for the $Cu^{63}(\gamma, n)$ threshold. Adjusting to 10.67 Mev. for

this latter value, we obtain $E_n(Pb^{206}) = 8.08 \pm 0.14$ Mev. Combining these two values and their errors, we obtain the value 8.09 ± 0.09 Mev.

$E_n(Pb^{207}) = 6.73 \pm 0.01$ Mev. (Kinsey *et al.* 1951)

The accurate value of the highest-energy γ-ray of neutron capture is used here since confirmation that this is the transition to the ground state has been found in the (d, p) reaction (Harvey 1951), the (d, t) reaction (Harvey 1953), and the (γ, n) reaction (Parsons and Collie 1950; Sher *et al.* 1951; Palevsky and Hanson 1950). (The values in the last two references need to be adjusted to the proper $Cu^{63}(\gamma, n)$ threshold.)

$E_n(Pb^{208}) = 7.38 \pm 0.01$ Mev. (Kinsey *et al.* 1951)

The same arguments and references as for $E_n(Pb^{207})$ apply here.

$E_n(Pb^{209}) \geqslant (3.87 \pm 0.05$ Mev.) (Harvey 1951)
$= [4.14 \pm 0.11$ Mev.]

The value shown in parentheses is obtained from the highest-energy proton group observed in the (d, p) reaction and therefore can set only a lower limit on the neutron binding energy. This is confirmed by the decay cycle $Pb^{208} - Th^{232} - Th^{233} - Pa^{233} - Pb^{209}$, which gives a value of $\geqslant 3.76 \pm 0.21$ Mev., again only a lower limit since the only experimental value of $E_n(Th^{233})$ has been obtained from a (d, p) reaction.

Absolute values of $E_n(Pb^{209})$ may be obtained from two different cycles which are independent except for the $Pb^{206} - Pb^{207} - Pb^{208}$ chain whose energy separations are accurately known.

The cycle $Pb^{209} - Pa^{233} - Np^{237} - U^{237} - U^{238} - Pb^{206} - Pb^{207} - Pb^{208}$ gives a value $E_n(Pb^{209}) = 4.14 \pm 0.12$ Mev.

The cycle $Pb^{209} - Bi^{209} - Po^{208} - Pb^{204} - Tl^{204} - Tl^{205} - Pb^{205} - Pb^{206} - Pb^{207} - Pb^{208}$ gives a value $E_n(Pb^{209}) = 4.15 \pm 0.18$ Mev.

The weighted mean value of these two independent determinations is 4.14 ± 0.11 Mev.

$E_n(Bi^{210}) \geqslant 4.17 \pm 0.02$ Mev.
$= [4.44 \pm 0.11$ Mev.]

Here again both the (n, γ) reaction (Kinsey *et al.* 1950) and the (d, p) reaction (Harvey 1951; Wall 1953) give only a minimum value ($\geqslant 4.17 \pm 0.02$ Mev.) for the neutron binding energy, while theoretical considerations indicate that the true value is probably somewhat higher (Pryce 1952; Harvey 1953). Here again two independent estimates may be made of $E_n(Bi^{210})$ but these involve cycles similar to those used for estimating $E_n(Pb^{209})$. We therefore obtain a best value for $E_n(Bi^{210})$ by using the derived value for $E_n(Pb^{209})$ in the cycle $Bi^{209} - Pb^{209} - Pb^{208} - Pb^{207} - Pb^{206} - Tl^{206} - Bi^{210}$. The value thus obtained is $E_n(Bi^{210}) = 4.44 \pm 0.11$ Mev.

$E_n(Th^{233}) \geqslant 4.88 \pm 0.20$ Mev. (Harvey 1951)
$= [5.26 \pm 0.12$ Mev.]

Harvey's experimental value is based on a (d, p) reaction and therefore sets only a lower limit.

The derived value consistent with other experimentally measured values may be obtained from the cycle $Th^{232} - Pb^{208} - Pb^{209} - Pa^{233} - Np^{233}$ and is 5.26 ± 0.12 Mev.

$E_n(U^{238}) = 5.82 \pm 0.10$ Mev.

From the (γ, n) reaction Parsons and Collie (1950) obtained an absolute value of 5.8 ± 0.15 Mev. for $E_n(U^{238})$. From the same reaction Huizenga *et al.* (1951) obtained 5.97 ± 0.10 Mev., but this was based on a $Cu^{63}(\gamma, n)$ threshold value of 10.9 Mev. Correcting this latter value, we obtain 5.84 ± 0.14 Mev. The weighted mean of these two values is 5.82 ± 0.10 Mev.

(*e*) *Natural Radioactive Series Decay Energies*

(i) "$4n$" series **$Th^{232}(6\alpha, 4\beta)Pb^{208}$ $E = 42.73 \pm 0.04$ Mev.**

$E_\alpha(Th^{232})$	$= 4.08 \pm 0.01$ Mev.	(Harvey *et al.* 1957)
$E_\beta(Ra^{228})$	$= 0.03 \pm 0.02$ Mev.	(see below)
$E_\beta(Ac^{228})$	$= 2.24 \pm 0.02$ Mev.	(Kyles *et al.* 1953)
$E_\alpha(Th^{228})$	$= 5.52 \pm 0.00$ Mev.	(Asaro *et al.* 1953)
$E_\alpha(Ra^{224})$	$= 5.78 \pm 0.00$ Mev.	(Briggs 1954)
$E_\alpha(Em^{220})$	$= 6.40 \pm 0.00$ Mev.	(Briggs 1954)
$E_\alpha(Po^{216})$	$= 6.90 \pm 0.00$ Mev.	(Briggs 1954)
$E_\beta(Pb^{212})$	$= 0.58 \pm 0.01$ Mev.	(King 1954)
$E_\beta(Bi^{212})$	$= 2.25 \pm 0.02$ Mev.	(King 1954)
$E_\alpha(Po^{212})$	$= 8.95 \pm 0.00$ Mev.	(Briggs 1954)
Total	$= 42.73 \pm 0.04$ Mev.	

The decay scheme and energy of Ra^{228} are not well known; however, the value chosen has sufficient range to encompass most measured values (see King (1954) for references).

(ii) "$4n+1$" series **$Pa^{233}(6\alpha, 3\beta)Pb^{209}$ $E = 40.38 \pm 0.04$ Mev.**

$E_\beta(Pa^{233})$	$= 0.56 \pm 0.02$ Mev.	(King 1954)
$E_\alpha(U^{233})$	$= 4.90 \pm 0.00$ Mev.	(Gol'din *et al.* 1955)
$E_\alpha(Th^{229})$	$= 5.11 \pm 0.01$ Mev.	(Hagemann *et al.* 1950)
$E_\beta(Ra^{225})$	$= 0.36 \pm 0.03$ Mev.	(Perlman *et al.* 1955)
$E_\alpha(Ac^{225})$	$= 5.92 \pm 0.01$ Mev.	(Stephens 1955)
$E_\alpha(Fr^{221})$	$= 6.45 \pm 0.01$ Mev.	(Stephens 1955)
$E_\alpha(At^{217})$	$= 7.18 \pm 0.01$ Mev.	(Stephens 1955)
$E_\beta(Bi^{213})$	$= 1.39 \pm 0.01$ Mev.	(King 1954)
$E_\alpha(Po^{213})$	$= 8.51 \pm 0.01$ Mev.	(Stephens 1955)
Total	$= 40.38 \pm 0.04$ Mev.	

(iii) "$4n+2$" series $U^{238}(8a, 6\beta)Pb^{206}$ **$E = 51.64 \pm 0.06$ Mev.**

$E_\alpha(U^{238})$	$= 4.27 \pm 0.01$ Mev.	(Harvey *et al.* 1957)
$E_\beta(Th^{234}, UX_1)$	$= 0.19 \pm 0.01$ Mev.	(Stoker *et al.* 1953)[2]
$E_\beta(Pa^{234}, UX_2)$	$= 2.30 \pm 0.01$ Mev.	(Stoker *et al.* 1953)[2]
$E_\alpha(U^{234})$	$= 4.85 \pm 0.00$ Mev.	(Harvey *et al.* 1957)
$E_\alpha(Th^{230})$	$= 4.77 \pm 0.01$ Mev.	(Briggs 1954)
$E_\alpha(Ra^{226})$	$= 4.86 \pm 0.01$ Mev.	(Briggs 1954)
$E_\alpha(Em^{222})$	$= 5.59 \pm 0.00$ Mev.	(Briggs 1954)
$E_\alpha(Po^{218})$	$= 6.11 \pm 0.00$ Mev.	(Briggs 1954)
$E_\beta(Pb^{214})$	$= 0.99 \pm 0.04$ Mev.	(King 1954)
$E_\beta(Bi^{214})$	$= 3.26 \pm 0.03$ Mev.	(Daniel and Nierhaus 1956)
$E_\alpha(Po^{214})$	$= 7.83 \pm 0.00$ Mev.	(Briggs 1954)
$E_\beta(Pb^{210}, RaD)$	$= 0.06 \pm 0.00$ Mev.	(King 1954)
$E_\beta(Bi^{210}, RaE)$	$= 1.16 \pm 0.01$ Mev.	(Plassmann and Langer 1954)
$E_\alpha(Po^{210})$	$= 5.40 \pm 0.01$ Mev.	(Perlman and Rasmussen 1956)
Total	$= 51.64 \pm 0.06$ Mev.	

APPENDIX II. THE EXPECTED α-HALF-LIFE OF Bi^{209}

By G. C. Hanna

(*a*) *General*

In this appendix the α-half-life of Bi^{209} is estimated, for a range of values of energy release near 3 Mev., by using a relation between lifetime and energy that is derived from a study of the experimental data on different types of α-emitting nuclei.

The experimentally observed regularities in α-decay can be presented in several ways; we have chosen here the one originated by Winslow (1955). This approach recognizes that the dependence of lifetime on energy is controlled by the barrier penetration, an effect that is calculable if spherical symmetry can be assumed. Thus for a (spherical) α-emitter of known energy and lifetime, the amplitude of the α-particle wave can be evaluated at any radius, and with the further assumption of a sharp nuclear boundary of known radius, at the nuclear surface itself. In this way the experimental data are used to give information on the specifically nuclear features of α-decay, that is on the probability of forming an α-particle out of nuclear matter.

It is reasonable to expect that formation probabilities, or "surface wave amplitudes", will be similar for α-emitters of similar type. In particular it should be possible to predict, with some assurance, the lifetime of an unknown species if there exists a series of similar nuclei all having similar values of surface wave amplitude.

There are essentially two uncertainties. First, especially near a closed shell, the value of either the surface wave amplitude or the nuclear radius of the

[2]Error values quoted are our estimate based on the Fermi–Kurie plots shown in the reference quoted.

unknown species may differ from that of the rest of the series. Secondly, it is not possible to distinguish clearly between the inside and outside of the nucleus.[3] In the present context this difficulty reduces to that of choosing an appropriate "effective" value for the radius, R; fortunately the results are not very sensitive to R.

(*b*) *Calculation of the Surface Wave Amplitude*

The only α transitions of interest for the present purpose happen to be ones in which L, the angular momentum of the α-particle, is uniquely defined. This is fortunate, since only in such cases can the surface wave amplitudes be calculated without additional information on the relative importance of the different L waves.

The parameter to be calculated is the dimensionless product $R|\phi(R)|^2$, where $\phi(R)$ is R times the radial wave function; this product will henceforward be abbreviated to S. It can be shown (Winslow 1955) that

$$S \equiv R|\phi(R)|^2 = \frac{\lambda R}{v} G_L^{\,2}(R) \equiv \frac{\lambda R}{v} G^2(R) Q_L$$

where λ is the decay constant, v is the velocity of the α-particle relative to the recoil nucleus, and $G_L(R)$ is the irregular Coulomb function. $G(R)$ is that part of $G_L(R)$ not containing L, that is

$$G(R) = \left(\frac{1-x}{x}\right)^{-1/4} \exp\left\{\left(\frac{2BR}{\hbar v}\right)(\arccos x^{1/2} - x^{1/2}(1-x)^{1/2})\right\},$$

and

$$Q_L \doteq \exp\left\{\frac{2(L+\tfrac{1}{2})^2}{kR} x^{1/2}(1-x)^{1/2}\right\}.$$

A more complete expression for Q_L has been used by Winslow and the results given graphically. In these expressions

B, the barrier height $= 2Ze^2/R$, Z being the atomic number of the daughter nucleus,

$x = E/B$, E being the α-disintegration energy (particle plus recoil),

and $k = Mv/\hbar = (2ME)^{1/2}/\hbar$, M being the reduced mass of the α-particle $= (M_\alpha M_R)/(M_\alpha + M_R)$.

Numerically for $R = 9.3$ fermis these expressions reduce to

$$-\log S = 21.033 + \log T_{1/2}(\text{sec.}) + \tfrac{1}{2}\log[E(1+4/A)] - \log Q_L - 2\log G(R)$$

with

$$2\log G(R) = -\tfrac{1}{2}\log\left(\frac{1-x}{x}\right) + \frac{1.0946\,Z}{[E(1+4/A)]^{1/2}}[\arccos x^{1/2} - x^{1/2}(1-x)^{1/2}],$$

[3]Winslow formally avoids this difficulty by considering the wave amplitude *near* the nucleus, that is, at a radius large enough for the use of pure Coulomb wave functions. However, the whole procedure is useful only if it achieves a largely complete separation of the barrier penetration term. In fact Winslow uses a value of 9.3 fermis for the radius, which is certainly too small for the calculation to be accurate, but which is a reasonable estimate of the "effective" nuclear surface.

where A is the mass number of the daughter, E is in Mev., and all logarithms are to the base 10.

These expressions refer to a bare nucleus. The effect of electron screening is taken into account by using a value for E larger than the observed disintegration energy by an amount E_s. Perlman and Rasmussen (1956) give

$$E_s = 65.3Z_p^{7/5} - 80Z_p^{2/5} \text{ electron volts,}$$

where Z_p is the atomic number of the parent nucleus.

For bismuth α-decay $E_s = 31$ kev.

(c) Observed Regularities: Prediction for Bi^{209}

The even–even α-emitters with a neutron number $N \geqslant 128$ all have similar values of S, and lifetimes can therefore be predicted rather accurately. In other nuclei α-decay is generally less probable, especially for even–even α-emitters with $N \leqslant 126$ and the bismuth isotopes. Table AI lists the values of S for various relevant categories of α-emitters. Only ground-to-ground-state transitions are considered, since it seems probable that in Bi^{209} decay, transitions to excited states will be of minor importance (see below). Allowance has been made for the effect of spin-change, that is, the "centrifugal barrier" term Q_L; the values of L were obtained from shell theory, except for Bi^{212} and Bi^{210} decay, where the values adopted by Perlman and Rasmussen (1956) have been used.[4]

TABLE AI

α-DECAY SURFACE WAVE AMPLITUDES NEAR THE CLOSED SHELLS $Z = 82$, $N = 126$

α-Emitter		L	$-\log_{10}S$		Nucleon configuration (proton: neutron)
Category	Example		Individual	Average	
$Z = 84$, $N > 128$	Po^{218}	0	1.40		
	Po^{216}	0	1.43	1.46	$(6h)^2$, $(6g)^2$
	Po^{214}	0	1.42		
	Po^{212}	0	1.60		
$Z = 84$, $N < 126$	Po^{210}	0	2.85		
	Po^{208}	0	2.69	2.69	$(6h)^2$, $(4p)^2$
	Po^{206}	0	2.54		
$Z = 84$, $N = 127$	Po^{211}(AcC′)	5	3.17	(3.17)	$(6h)^2$, $6g\ 4p$
$Z = 83$, $N > 128$	Bi^{213}	5	3.07		
	Bi^{212}	5	3.49	3.27	$6h\ 3s$, $(6g)^2$
	Bi^{211}	5	3.24		
$Z = 83$, $N = 126$	Bi^{209}	5	?	?	$6h\ 3s$, $(4p)^2$
$Z = 83$, $N = 127$	Bi^{210}(RaE)	?2	5.55		$6h\ 3s$, $6g\ 4p$
	Bi^{210}(long)	?4	7.42		

The last column of Table AI gives the shell model assignments (see e.g. Klinkenberg 1952) of the protons and neutrons from which the α-particle has to be assembled. Following the ideas of Perlman and Rasmussen (1956), it will

[4]The measured spin of Bi^{209} is 9/2, and that of Tl^{205} is 1/2, so that, independent of shell model considerations, which fix the parity, it is known that $L = 4$ or 5.

be seen that there is a correlation between the value of S and the overlap of the nucleon wave-functions. For example, in the case of the polonium isotopes the considerable reduction in S with $N \leqslant 126$ is reasonably ascribed to the poorer overlap of the wave functions of the $6h$ protons and $4p$ neutrons, compared with the $6g$ neutrons above the shell. On the other hand the 126-neutron effect is not expected to be so large for the bismuth isotopes because of the broken proton configuration (one low and one high orbital), and it will be assumed here that the value of S for Bi^{209} decay is the same as for the decay of the heavier bismuth isotopes.

Regarding α-decay to the first excited state of Tl^{205} (at 205 kev., probably a $d_{3/2}$ state), the nucleon overlap might be somewhat larger ($6h\ 4d\ (4p)^2$) and the spin change smaller ($L = 3$), but these effects should be much less important than that of the lower energy release which corresponds to a factor of about 700 in barrier penetration. This mode of decay should therefore be quite unimportant.

A complication arises from the possibility of a significant difference in nuclear radius between Bi^{209} decay and the "comparison" decays. It will be noted that S is rather smaller for Po^{212} decay than for the heavier polonium isotopes (and these have somewhat lower values of S than the emanation and radium α-emitters). This behavior might possibly indicate a shrinkage in radius as the closed shell is approached. However, this effect appears to be less serious than the other uncertainties.

With the assumption that $\log_{10}S$ is -3.25, values of α-half-life have been calculated for a range of disintegration energies. The results are given in Table AII, and plotted graphically in Fig. 4.

TABLE AII

CALCULATED VALUES OF HALF-LIFE FOR Bi^{209} α-DECAY

α-Disintegration energy (Mev.)	Half-life (years)
2.72	1.0×10^{24}
2.82	3.5×10^{22}
2.92	1.5×10^{21}
3.02	7.5×10^{19}
3.12	4.3×10^{18}
3.22	2.8×10^{17}

Note: The disintegration energies are the "observed" values, i.e. before the 31 kev. electron screening correction is added.

It is difficult to give a reliable estimate of the uncertainty. The error due to poor choice of R is not expected to exceed a factor of 2 (corresponding to a change of 25% in R). The value assumed for S is probably less reliable. However, Bi^{209} decay would certainly be expected to be no more probable than Po^{210} decay, for which S is roughly 2.5 times greater; on the other hand a finite 126-neutron effect would increase the predicted lifetime, by a factor of 20 if it were as important as for the polonium isotopes.

Rather conservatively then, the half-life is expected to be not less than 0.2

times and not greater than 40 times as large as the value given, for any energy, in Table AII.

REFERENCES

ANDRE, C. G., HUIZENGA, J. R., MECH, J. F., RAMLER, W. J., RAUH, E. G., and ROCKLIN, S. R. 1956. Phys. Rev. **101**, 645.

ASARO, F., STEPHENS, F., and PERLMAN, I. 1953. Phys. Rev. **92**, 1495.

BARTHOLOMEW, G. A. and KINSEY, B. B. 1953. Can. J. Phys. **31**, 1025.

BENDEL, W. L., MCELHINNEY, J., and TOBIN, R. A. 1956. Bull. Am. Phys. Soc. **1**, 192.

BIRNBAUM, M. 1954. Phys. Rev. **93**, 146.

BRAGG, W. H. and KLEEMAN, R. 1905. Phil. Mag. (6), **10**, 318.

BRIGGS, G. H. 1954. Revs. Modern Phys. **26**, 1.

DANIEL, H. and NIERHAUS, R. 1956. Z. Naturforsch. **11A**, 212.

DE SOUZA SANTOS, M.D., GOLDEMBERG, J., PIERONI, R. R., SILVA, E., BORELLO, O. A., VILLACA, S. S., and LOPES, J. L. 1955. Geneva Conference on Peaceful Uses of Atomic Energy, Paper P/897.

EL-BEDEWI, F. A. 1951. Proc. Phys. Soc. (London), A, **64**, 584.

FARAGGI, H. and BERTHELOT, A. 1951. Compt. rend. **232**, 2093.

GOL'DIN, L. L., NOVIKOVA, G. I., and TRET'YAKOV, E. F. 1955. Proceedings of Conf. of Acad. of Sci. of U.S.S.R. on Peaceful Uses of Atomic Energy, July 1–5, 1955, Div. of Phys. and Math. Sciences, p. 226.

HAGEMANN, F., KATZIN, L. I., STUDIER, M. H., SEABORG, G. T., and GHIORSO, A. 1950. Phys. Rev. **79**, 435.

HANSON, A. O., DUFFIELD, R. B., KNIGHT, J. D., DIVEN, B. C., and PALEVSKY, H. 1949. Phys. Rev. **76**, 578.

HARVEY, B. G., JACKSON, H. G., EASTWOOD, T. A., and HANNA, G. C. 1957. Can. J. Phys. **35**, 258.

HARVEY, J. A. 1951. Phys. Rev. **81**, 353.

——— 1953. Can. J. Phys. **31**, 278.

HERBER, R. H., SUGIHARA, T. T., CORYELL, C. D., BENNETT, W. E., and HUIZENGA, J. R. 1956. Phys. Rev. **103**, 955.

HINCKS, E. P. and MILLAR, C. H. 1952. Proc. Roy. Soc. Can. **46**, 143.

HUIZENGA, J. R., MAGNUSSON, L. B., FIELDS, P. R., STUDIER, M. H., and DUFFIELD, R. B. 1951. Phys. Rev. **82**, 561.

HUIZENGA, J. R. and WING, J. 1956. Phys. Rev. **102**, 926.

JENKNER, K. and BRODA, E. 1949. Nature, **164**, 412.

KING, R. W. 1954. Revs. Modern Phys. **26**, 327.

KINSEY, B. B., BARTHOLOMEW, G. A., and WALKER, W. H. 1950. Phys. Rev. **78**, 77.

——— 1951. Phys. Rev. **82**, 380.

KLINKENBERG, P. F. A. 1952. Revs. Modern Phys. **24**, 63.

KYLES, J., CAMPBELL, C. G., and HENDERSON, W. J. 1953. Proc. Phys. Soc. (London), A, **66**, 519 (and private communication).

LATTES, C. M. G., FOWLER, P. H., and CÜER, P. 1947. Proc. Phys. Soc. (London), **59**, 883.

LEVY, H. B. and PERLMAN, I. 1954. Phys. Rev. **94**, 152.

MAGNUSSON, L. B., ENGELKEMEIR, D. W., FREEDMAN, M. S., PORTER, F. T., and WAGNER, F. 1955. Phys. Rev. **100**, 1237.

MILLAR, C. H. and CAMERON, A. G. W. 1953. Can. J. Phys. **31**, 723.

PALEVSKY, H. and HANSON, A. O. 1950. Phys. Rev. **79**, 242.

PARSONS, R. W. and COLLIE, C. H. 1950. Proc. Phys. Soc. (London), A, **63**, 839.

PERLMAN, I., GHIORSO, A., and SEABORG, G. T. 1950. Phys. Rev. **77**, 26.

PERLMAN, I. and RASMUSSEN, J. O. 1956. University of California Radiation Laboratory Report, UCRL-3424.

PERLMAN, I., STEPHENS, F., and ASARO, F. 1955. Phys. Rev. **98**, 262.

PLASSMANN, E. A. and LANGER, L. M. 1954. Phys. Rev. **96**, 1593.

PORSCHEN, W. and RIEZLER, W. 1956. Z. Naturforsch. **11A**, 143.

PRYCE, M. H. L. 1952. Proc. Phys. Soc. (London), A, **65**, 773.

RIEZLER, W. and PORSCHEN, W. 1952. Z. Naturforsch. **7A**, 634.

ROBINSON, L. B., MCPHERSON, D., GREENBERG, L. H., KATZ, L., and HASLAM, R. N. H. 1956. Private communication (quoted as Ref. 56R38 in Nuclear Sci. Abstr. **10**, No. 24B, 140).

ROTBLAT, J. 1950. Nature, **165**, 387.

——— 1951. Nature, **167**, 550.

SHER, R., HALPERN, J., and MANN, A. K. 1951. Phys. Rev. **84**, 387.

STEPHENS, F. S. 1955. University of California Radiation Laboratory Report, UCRL-2970.

STOKER, P. H., HEERSCHAP, M., and ONG PING HOK. 1953. Physica, **19**, 433.

WALL, N. S. 1953. Phys. Rev. **91**, 485.

WINSLOW, G. H. 1955. Argonne National Laboratory Report, ANL-5381.

YAGODA, H. 1949. Radioactive measurements with nuclear emulsions (John Wiley and Sons Inc., New York).

LETTERS TO THE EDITOR

Under this heading brief reports of important discoveries in physics may be published. These reports should not exceed 600 words and, for any issue, should be submitted not later than six weeks previous to the first day of the month of issue. No proof will be sent to the authors.

Polarization of Electrons in Forbidden β-Decay*

As a special case of a lengthy calculation of the angular distributions of the electrons and neutrinos and the polarization of the electrons emitted in the arbitrarily forbidden β-decay of an oriented source, an expression for the longitudinal polarization of the electrons from a randomly oriented source has been obtained. Because of the importance and the simplicity of the result, it is believed that immediate publication of this special case may be useful.

The longitudinal polarization is expressed as the quotient of a "modified correction-factor" and the usual correction-factor. The modifications are certain changes in the combinations of coupling constants and in the functions L_ν, M_ν, etc. of Greuling (1942) and Pursey (1951). Let us make the definition $D_{XY} \equiv \mathrm{Re}(C_X C_Y^* + C_X' C_Y'^*)$. X or Y stands for one of the five interactions $SVTAP$; C_X and C_X' are coupling constants as defined by Lee and Yang (1956). The usual correction-factor depends on the coupling constants only through combinations of the type D_{XY}. For the modified correction-factor we shall require $G_{XY} \equiv \mathrm{Re}(C_X' C_Y^* + C_X C_Y'^*)$ and $\Gamma_{XY} \equiv \mathrm{Im}(C_X' C_Y^* + C_X C_Y'^*)$. The modifications in the coupling constant combinations are as follows:

(i) If X and Y both belong to STP, replace D_{XY} by G_{XY}.
(ii) If X and Y both belong to VA, replace D_{XY} by $-G_{XY}$.
(iii) If X belongs to VA and Y to STP, replace D_{XY} by Γ_{XY}.
(iv) If X belongs to STP and Y to VA, replace D_{XY} by $-\Gamma_{XY}$.

Because $\Gamma_{XY} = -\Gamma_{YX}$, cases (iii) and (iv) are equivalent. It is of interest to note that with Pauli's (1957) new β-decay interaction D_{XY} is replaced by the real part of the invariant K_{XY}, G_{XY} and Γ_{XY} by the real and imaginary parts of the invariant L_{XY}.

In addition to the coupling constant changes we must replace the combinations of electron radial wave-functions according to the scheme given in Table I.

TABLE I

TRANSFORMATION OF L_ν, M_ν, ETC.

$L_\nu \to -(p^2F_0\rho^{2\nu})^{-1}g_{-\nu-1}f_{\nu+1}\sin\Omega$	$\doteq \frac{p}{W}L_\nu$
$M_\nu \to (p^2F_0\rho^{2\nu+2})^{-1}g_{\nu+1}f_{-\nu-1}\sin\Omega$	$\doteq \frac{p}{W}M_\nu$
$N_\nu \to (2p^2F_0\rho^{2\nu+1})^{-1}(g_{\nu+1}g_{-\nu-1}-f_{\nu+1}f_{-\nu-1})\sin\Omega$	$\doteq \frac{p}{W}N_\nu$
$P_\nu \to (p^2F_0\rho^{2\nu})^{-1}g_{-\nu-1}f_{\nu+1}\cos\Omega$	$\doteq \frac{-\alpha Z}{\gamma}P_\nu$
$Q_\nu \to (p^2F_0\rho^{2\nu+2})^{-1}g_{\nu+1}f_{-\nu-1}\cos\Omega$	$\doteq \frac{-\alpha Z}{\gamma}Q_\nu$
$R_\nu \to -(2p^2F_0\rho^{2\nu+1})^{-1}(g_{\nu+1}g_{-\nu-1}-f_{\nu+1}f_{-\nu-1})\cos\Omega$	$\doteq \frac{-\alpha Z}{\gamma}R_\nu$

$\gamma^2 = (\nu+1)^2 - \alpha^2Z^2$.

Except for Ω, the notation of Table I is that of Rose, Perry, and Dismuke (1953); $\Omega_\kappa^\xi = \delta^+ - \delta^-$, δ^+ and δ^- being the phase-shifts for angular momentum $j = \nu + \frac{1}{2}$ and for the values $(j+\frac{1}{2})$ and $-(j+\frac{1}{2})$ respectively of the quantum number κ.

*Issued as A.E.C.L. No. 533.

A useful first approximation is to treat the nuclear charge distribution as a point charge and to evaluate the wave-functions to the lowest order in $p\rho$. The expressions in the right-hand column of Table I correspond to this approximation. When these formulae are applied to allowed transitions, agreement with the results of Jackson, Treiman, and Wyld (1957) is obtained. If in addition the two-component neutrino theory (Lee and Yang 1957) is assumed, the longitudinal polarization is $\pm v/c$ for interactions drawn from either STP or VA. If the ratio $C_X'/C_X = \pm 1$ has the same value for each of STP and has the opposite value for each of VA, the polarization is again $\pm v/c$. By demonstrating that the approximate relations of the last column of Table I fail when one retains terms of the next higher order of $p\rho$ in the radial wave-functions, one sees that the formula $\pm v/c$ for the polarization is not exact.

The results given so far apply to negatron decay. For positron decay one must, in addition to changing the sign of Z in Table I, carry out a suitable transformation of the coupling constants. If $C_X{}^+$ and $C_X{}'^+$ refer to positron emission, it is sufficient to take $C_X{}^+ = C_X{}^*$ when X is V or T, $C_X{}^+ = -C_X{}^*$ when X is S, A, or P, and $C_X{}'^+/C_X{}^+ = -C_X{}'^*/C_X{}^*$ for all X.

Greuling, E. 1942. Phys. Rev. **61**, 568.
Jackson, J. D., Treiman, S. B., and Wyld, H. W. 1957. Nuclear Phys. **4**, 206.
Lee, T. D. and Yang, C. N. 1956. Phys. Rev. **104**, 254.
——— 1957. Phys. Rev. **105**, 1671.
Pauli, W. 1957. Nuovo cimento, **6**, 204.
Pursey, D. L. 1951. Phil. Mag. **42**, 1193.
Rose, M. E., Perry, C. L., and Dismuke, N. M. 1953. Oak Ridge National Laboratory Report, ORNL-1459.

Received November 25, 1957.
G. E. Lee-Whiting
Theoretical Physics Branch,
Atomic Energy of Canada Limited,
Chalk River, Ontario.

The Viscosity of Liquid Helium between 0.78° K. and 1.1° K.

The theory of the viscosity of liquid helium II (Landau and Khalatnikov 1949) gives two expressions for the variation of the viscosity η with temperature T:

$$1° \text{ K.} < T < 1.8° \text{ K.}, \qquad \eta = A + BT^{-1/2}e^{\Delta/kT};$$

$$T < 0.8° \text{ K.}, \qquad \eta = A + (CT^{1/2}e^{-\Delta/kT} + DT^{3})^{-1}.$$

A, B, C, and D are constants which can only be estimated, and Δ/k has the value 8.8° K. (Wiebes *et al.* 1957). The viscosity measurements above 1.1° K. made by Heikkila and Hollis Hallett (1955) using a rotating cylinder viscometer were consistent with the theory, but an adequate test can only be made from measurements at lower temperatures.

Another viscometer of the type described by Heikkila and Hollis Hallett has been used to measure the viscosity of liquid helium down to 0.78° K. in a booster cryostat (Atkins *et al.* 1955). The radius and length of the inner cylinder were 0.995 cm. and 3.03 cm. respectively, and the width of the annular gap between the cylinders was 0.60 mm. The suspension for the inner cylinder was immersed in the liquid helium and the deflections of the inner cylinder were determined with the aid of two specially shaped condenser plates, one fixed, and the other attached to the inner cylinder. The measured change in capacity of this condenser was proportional to the angular deflection of the inner cylinder, and the constant of proportionality was determined from viscosity determinations above 1.1° K. assuming that the viscosity values were known (Heikkila and Hollis Hallett). The viscometer was attached to the appendix of a metal dewar of such a size that approximately 300 cm.^{3} of liquid were cooled to 0.78° K. by pumping. Temperatures were measured using a carbon thermometer, which was calibrated against a paramagnetic salt, and are believed to be accurate to 0.01° K. The velocity of the outer cylinder was less than the critical value for this apparatus.

Interpretation of the results was somewhat complicated by the fact that the effective torsion constant of the fiber suddenly increased somewhere between 0.95° K. and 1.00° K. This effect was due in some way to the superconducting state of the aluminum alloy of which the viscometer was made, because the torsion constant, as measured by the period of free oscillation of the inner cylinder, returned to its original value when the superconductivity was destroyed by a magnetic field.

The results are shown in Fig. 1 and include measurements taken with the apparatus in its normal state (i.e. in a magnetic field), and in its superconducting state, corrections being made for the observed change in torsion constant. The curve which has been drawn represents the theoretical variation of η with temperature using the constants A, B, and Δ/k given by Heikkila and Hollis Hallett. (The known slight variation of B with temperature (Khalatnikov

1956) and use of the latest value of Δ/k (with corresponding changes in A and B) do not change the shape of the curve significantly.)

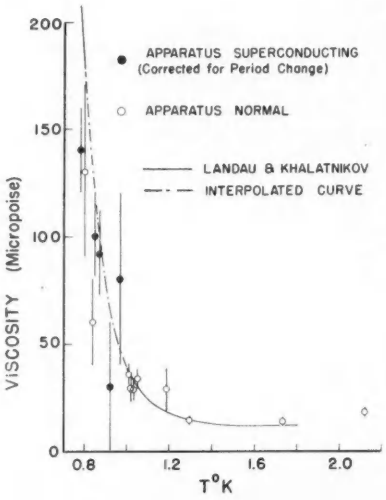

FIG. 1.

The experimental results agree, at least qualitatively, with the predictions of the theory. Quantitatively, the value of 140 ± 30 micropoises for the viscosity at 0.78° K. compares favorably with the value of 173 micropoises at 0.8° K. quoted by Khalatnikov. The measured value at 1.01° K. is 37 ± 7 micropoises. It should be pointed out that the theory does not give specific predictions for the range $0.8° \text{ K.} < T < 1.0° \text{ K.}$; this region can only be covered by interpolation (i.e. the dashed curve in the figure).

These results also agree with the indirect determinations made by Zinov'eva (1956) from measurements of the absorption of second sound down to 0.83° K.

The authors gratefully acknowledge the financial assistance of the National Research Council and the Ontario Research Foundation whose grants in aid of research have made this work possible. One of us (A.D.B.W.) is indebted to the National Research Council for the award of a Studentship.

ATKINS, K. R., EDWARDS, M. H., and PULLAN, G. T. 1955. Rev. Sci. Instr. **26**, 49.
HEIKKILA, W. J. and HOLLIS HALLETT, A. C. 1955. Can. J. Phys. **33**, 420.
KHALATNIKOV, I. M. 1956. Uspekhi Fiz. Nauk, **59**, 673.
LANDAU, L. D. and KHALATNIKOV, I. M. 1949. J. Exptl. Theoret. Phys. (U.S.S.R.), **19**, 637, 709.
WIEBES, J., NIELS-HAKKENBERG, C. G., and KRAMERS, H. C. 1957. Physica, **23**, 625.
ZINOV'EVA, K. 1956. J. Exptl. Theoret. Phys. (U.S.S.R.), **31**, 31. (*Also* Soviet Phys. (J.E.T.P.), **4**, 36 (1957).)

RECEIVED DECEMBER 14, 1957.
DEPARTMENT OF PHYSICS,
UNIVERSITY OF TORONTO,
TORONTO, ONTARIO.

A. D. B. WOODS
A. C. HOLLIS HALLETT

THE PHYSICAL SOCIETY

MEMBERSHIP of the Society is open to all who are interested in Physics.

FELLOWS pay an Entrance fee of £1 1*s*. ($3.00) and an Annual Subscription of £2 2*s*. ($6.00).

STUDENTS: A candidate for Studentship must be between the ages of 18 and 26, and pays an Annual Subscription of 5*s*. ($0.75).

MEETINGS: Fellows and Students may attend all Meetings of the Society including the annual Exhibition of Scientific Instruments and Apparatus.

PUBLICATIONS include the *Proceedings of the Physical Society*, published monthly, and *Reports on Progress in Physics*, published annually. Volume XX, 1957, is now available (price £3 3*s*. ($9.00)). Members are entitled to receive any of the Publications at a reduced rate.

Further information can be obtained from:

THE PHYSICAL SOCIETY
1, LOWTHER GARDENS, PRINCE CONSORT ROAD
LONDON, S.W.7, ENGLAND

CANADIAN JOURNAL OF PHYSICS

Notes to Contributors

Manuscripts

(i) **General.** Manuscripts, in English or French, should be typewritten, double spaced, on paper 8½×11 in. **The original and one copy are to be submitted.** Tables and captions for the figures should be placed at the end of the manuscript. Every sheet of the manuscript should be numbered.

Style, arrangement, spelling, and abbreviations should conform to the usage of recent numbers of this journal. Names of all simple compounds, rather than their formulas, should be used in the text. Greek letters or unusual signs should be written plainly or explained by marginal notes. Superscripts and subscripts must be legible and carefully placed.

Manuscripts and illustrations should be carefully checked before they are submitted. Authors will be charged for unnecessary deviations from the usual format and for changes made in the proof that are considered excessive or unnecessary.

(ii) **Abstract.** An abstract of not more than about 200 words, indicating the scope of the work and the principal findings, is required, except in Notes.

(iii) **References.** References should be listed **alphabetically by authors' names,** unnumbered, and typed after the text. The form of the citations should be that used in current issues of this journal; in references to papers in periodicals, titles should not be given and only initial page numbers are required. The names of periodicals should be abbreviated in the form given in the most recent *List of Periodicals Abstracted by Chemical Abstracts.* All citations should be checked with the original articles and each one referred to in the text by the authors' names and the year.

(iv) **Tables.** Tables should be numbered in roman numerals and each table referred to in the text. Titles should always be given but should be brief; column headings should be brief and descriptive matter in the tables confined to a minimum. Vertical rules should not be used. Numerous small tables should be avoided.

Illustrations

(i) **General.** All figures (including each figure of the plates) should be numbered consecutively from 1 up, in arabic numerals, and each figure referred to in the text. The author's name, title of the paper, and figure number should be written in the lower left corner of the sheets on which the illustrations appear. Captions should not be written on the illustrations (see Manuscripts (i)).

(ii) **Line Drawings.** Drawings should be carefully made with India ink on white drawing paper, blue tracing linen, or co-ordinate paper ruled in blue only; any co-ordinate lines that are to appear in the reproduction should be ruled in black ink. Paper ruled in green, yellow, or red should not be used. All lines should be of sufficient thickness to reproduce well. Decimal points, periods, and stippled dots should be solid black circles large enough to be reduced if necessary. Letters and numerals should be neatly made, preferably with a stencil (**do NOT use typewriting**) and be of such size that the smallest lettering will be not less than 1 mm. high when reproduced in a cut 3 in. wide.

Many drawings are made too large; originals should not be more than 2 or 3 times the size of the desired reproduction. Whenever possible two or more drawings should be grouped to reduce the number of cuts required. In such groups of drawings, or in large drawings, full use of the space available should be made; the ratio of height to width should conform to that of a journal page (4¾×7½ in.), but allowance must be made for the captions.

The original drawings and one set of clear copies (e.g. small photographs) are to be submitted.

(iii) **Photographs.** Prints should be made on glossy paper, with strong contrasts. They should be trimmed so that essential features only are shown and mounted carefully, with rubber cement, on white cardboard, with no space between them. In mounting, full use of the space available should be made to reduce the number of cuts required (see Illustrations (ii)). Photographs or groups of photographs should not be more than 2 or 3 times the size of the desired reproduction.

Photographs are to be submitted in duplicate; if they are to be reproduced in groups one set should be mounted, the duplicate set unmounted.

Reprints

A total of 50 reprints of each paper, without covers, are supplied free. Additional reprints, with or without covers, may be purchased at the time of publication.

Charges for reprints are based on the number of printed pages, which may be calculated approximately by multiplying by 0.6 the number of manuscript pages (double-spaced typewritten sheets, 8½×11 in.) and including the space occupied by illustrations. An additional charge is made for illustrations that appear as coated inserts. Prices and instructions for ordinary reprints are sent out with the galley proof.

Any reprints required in addition to those requested on the author's reprint requisition form must be ordered officially as soon as the paper has been accepted for publication.

Contents

Page

On possible realizations of Mach's program—*F. A. Kaempffer* - - - - 151

Horizontal movements of aurora—*J. S. Kim and B. W. Currie* - - - - 160

Rotational spectra of RbF by the electric resonance method—*H. Lew, D. Morris, F. E. Geiger, Jr., and J. T. Eisinger* - - - - - - - - - - - - 171

Mass spectrometric analysis of some hydrogen oxides. I—*Larkin Kerwin and Maurice Cottin* - - - - - - - - - - - - - - - - - 184

On Volterra's dislocations in a semi-infinite elastic medium—*J. A. Steketee* - 192

Radiation and surface currents from a slot on an infinite conducting cylinder—*F. H. Northover* - - - - - - - - - - - - - - - - 206

High resolution Raman spectroscopy of gases. XI. Spectra of CS_2 and CO_2—*B. P. Stoicheff* - - - - - - - - - - - - - - - - 218

A search for α-particles from the decay of Bi^{209}—*E. P. Hincks and C. H. Millar. With an appendix by G. C. Hanna* - - - - - - - - - - - - 231

Letters to the Editor:

Polarization of electrons in forbidden β-decay—*G. E. Lee-Whiting* - - - 252

The viscosity of liquid helium between 0.78° K. and 1.1° K.—*A. D. B. Woods and A. C. Hollis Hallett* - - - - - - - - - - - - - - 253
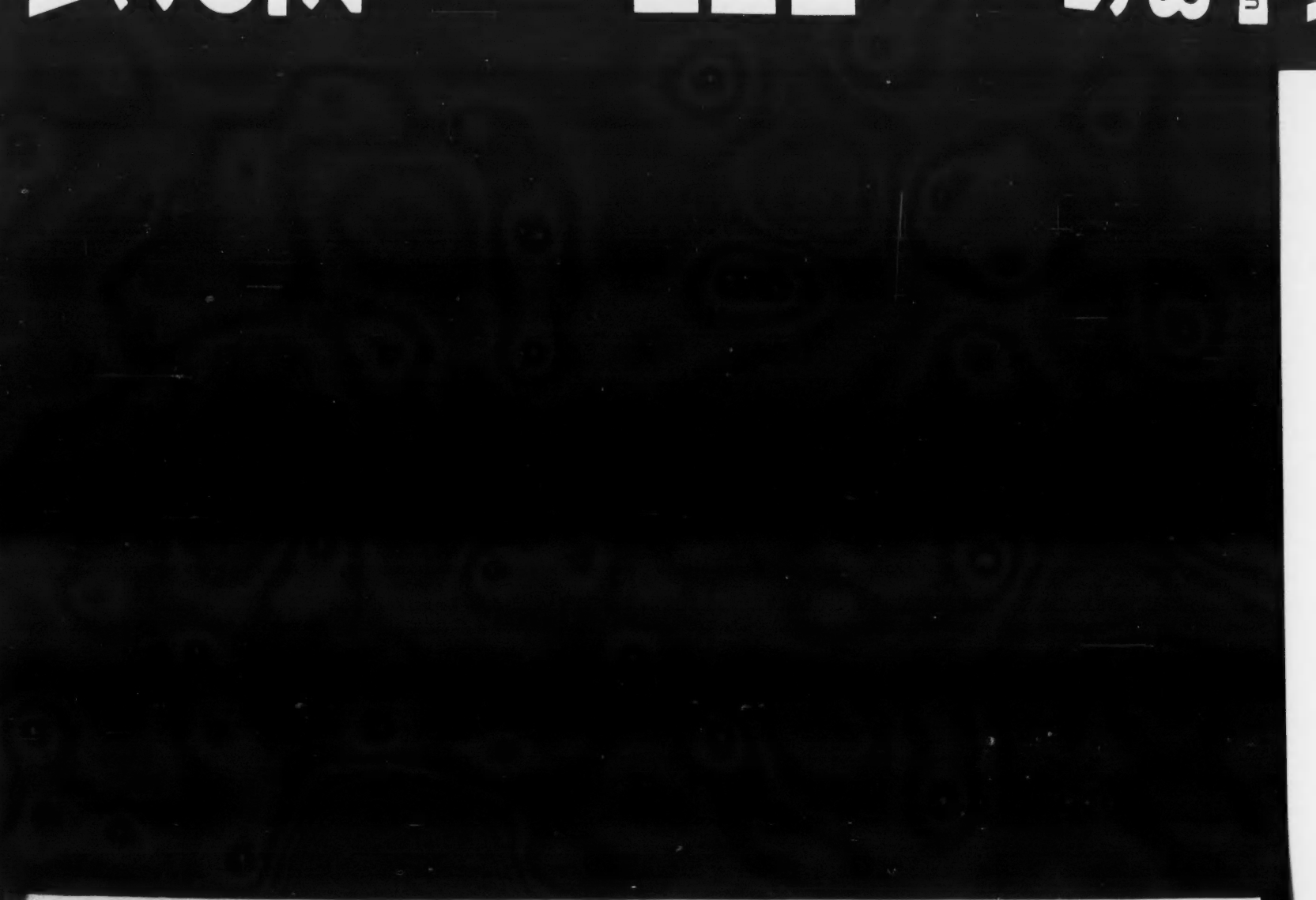
Printed in Canada *by* University of Toronto Press